USING A NOVEL HUMAN NEURAL STEM CELL MODEL OF AGGRESSIVE MEDULLOBLASTOMA TO INVESTIGATE NEW THERAPEUTIC STRATEGIES

by
Allison Rose Hanaford

A dissertation submitted to Johns Hopkins University in conformity with the requirements for the degree of Doctor of Philosophy

Baltimore, MD
March 2017

ABSTRACT

Medulloblastoma is the most common malignant brain tumor in children. Group 3 medulloblastoma is associated with high expression of the MYC oncogene and has the worst clinical prognosis. To investigate the biology of these tumors and develop new therapeutic strategies, we transduced human neural stem and progenitor cells derived from the cerebellar anlage with key oncogenic driver elements associated with aggressive medulloblastoma. Cells transformed with MYC, dominant-negative TP53, constitutively active AKT and hTERT formed brain tumors that histologically, pathologically, and genetically resembled the Group 3 subtype of medulloblastoma. Median survival of these tumor-bearing animals was 117 days. To facilitate rapid screening of a large number of available drugs, we applied a new *in silico* analysis technique named DiSCoVER (Disease-model Signature vs. Compound-Variety Enriched Response) that used the expression profile of the human neural stem cell model and existing drug sensitivity databases to identify novel therapeutic targets. The DiSCoVER analysis predicted MYC-expressing Group 3 medulloblastoma would be sensitive to cyclin-dependent kinase (CDK) inhibitors. We confirmed activity of the CDK4/6 inhibitors palbociclib and flavopiridol in MYC-expressing medulloblastoma. Specifically, palbociclib decreased proliferation of our human neural stem cell model and medulloblastoma cell lines by an average of 62% ($p<0.01$) and increased the percentage of apoptotic cells by an average of 150% ($p< 0.04$). Palbociclib treatment extended the median survival of mice with orthotopic MYC-driven medulloblastoma xenografts by 48% ($p=0.003$). MYC is known to regulate glutamine metabolism, and we also used our neural stem cell model to investigate the hypothesis that MYC-driven medulloblastoma would be sensitive to

inhibition of glutamine metabolism. Treatment with the glutamine analogs Acivicin or 6-diazo-5-oxo-l-norleucine (DON) significantly increased the percentage of apoptotic cells by an average of 290% ($p<0.04$) and 164% ($p<0.04$), respectively. DON therapy increased the median survival of mice with MYC-driven orthotopic medulloblastoma xenografts by up to 246% ($p=0.0018$). In summary, this dissertation presents a novel, genetically accurate human neural stem cell model of aggressive medulloblastoma, and provides preclinical evidence for the use of CDK inhibitors and glutamine analogs in carefully selected medulloblastoma patients.

ACKNOWLEDGEMENTS

Thank you to my high school biology teacher Mrs. Ohta who sparked my interest in science. Under the mentorship of Leona Gagnon at the Summer Student Program at the Jackson Laboratory in Bar Harbor, ME, I learned I loved research and lab work. Without my Jax experience, I never would have applied to grad school. Special acknowledgment to the women who entered the pathobiology program with me in 2011--Rosie Jiang, Corey Porter, Youngran Park, Heidi Hempel, Wan Yee Leong, Meng Su, and Wan Rou Yang. It has been a privilege to go through graduate school with such amazing, intelligent women and an honor to count them as friends. We have supported each other through all manner of challenges in lab and our personal lives, and I hope to continue to count them as friends for decades to come. The other students of the pathobiology program are also a fantastic group of human beings--the parties, social events, and scientific discussions hosted by pathobiology students are some of my favorite memories of grad school. Who knew a bunch of science nerds could have so much fun?

My mentors Dr Eric Raabe and Dr Charles Eberhart deserve much more thanks than I will ever be able to express. They have created a lab environment that manages to be productive, scientifically rigorous, supportive, and fun. I have never been afraid to go to them with any concern, question, or failed experiment. On many occasions I have gone to Eric dispirited, discouraged and disappointed. He never fails to remain positive about my work, and I always leave our conversations more upbeat and excited to keep working. I can only hope that I am someday able to provide the same mentorship to my own students.

I also must thank Eric and Charles for finding such great people to join our lab, because my lab mates have made the long days at the bench and in the tissue culture room enjoyable. So, thank you to labmates, both current and former--Laura Asnaghi, Harpreet Kaur, Jeff Rubens, Sam Semenkow, Brad Poore, Marianne Hutt, Isabella Taylor, Melanie Weingart, Sama Ahsan, Antoinette Price, Ming Yuan, Antje Arnold, Micah Maxwell, Manabu Natsumeda, Ulf Kahlert, and Will Brandt. Isabella and Melanie, two former technicians now in medical school, literally became my right-hand women when I broke my wrist after slipping on black ice and was unable to pipette or write for over a month. Izzy remains a close, wonderful friend, and lab has not been the same since she left. Fellow pathobiology student and labmate Sam has also been a great friend, and I will miss our wide-ranging discussions of books, science, politics, and program gossip. Sama can always be counted on for excellent, un-sugarcoated advice on a wide array of topics. Thanks to Brad for his cheerful disposition his assistance and skills at metabolomics. Without him the metabolic studies in this dissertation would not have been possible. Jesse Alt also provided invaluable assistance on the metabolomics studies.

I am also lucky to remain close with friends from college—Haley Schwalbe, Chelsea Scullion, and Christine Han. None are scientists, but they have listened to my lengthy soliloquies on a wide range of scientific topics for years without complaint and have given me great pep talks over the years. I also treasure my long friendships with Marie Anello, Camilla Moir, Hallie Rane, and Bridget Glenn. Camilla is completing a PhD in physics and I've enjoyed comparing notes on the graduate school experience and talking science. When we see each other, it's like no time has passed.

I also must thank the many administrators who helped me throughout my years here—Nancy Nath, Tracie McElroy, and Stacey Morgan of the pathobiology program, and Barbara Reiss, Charles' assistant. The directors of the pathobiology program, Dr. Noel Rose and Dr. Lee Martin, have also provide a great deal of help and encouragement. I also thank my thesis committee members, Dr Mollie Meffert and Dr Jeff Rothstein, for their advice and patience with the seemingly endless emails it took to get my committee meetings schedule.

Finally, I must thank my family for all their love, support and encouragement. They always made me feel free to follow my own interests and pursuits. Even when my goal was to major in music do a PhD in musicology, they were never anything but encouraging. (Though, I suspect in the end they were happy I decided to go to graduate school for biology, rather than musicology). I have always known they will be there for all the ups and downs in my life and consider myself lucky to have such a solid support system. My parents have also made many trips to visit me in Baltimore, making the long distance easier. They have also flown me home for every Christmas and Thanksgiving, for which I am deeply grateful.

TABLE OF CONTENTS

LIST OF TABLES

LIST OF FIGURES

PART I: DEVELOPMENT OF A HUMAN NUERAL STEM CELL MODEL OF MEDULLOBLSTOMA AND THE IN SILICO DRUG SCREENING TECHNIQUE DISCOVER

CHAPTER 1: INTRODUCTION TO MEDULLOBLASTOMA

1.1 Medulloblastoma Overview

The cerebellar tumor medulloblastoma is the most common malignant pediatric brain tumor (1). Children typically present with symptoms related to increased intracranial pressure and cerebellar dysfunction. Headache, nausea (especially upon waking), dizziness and ataxia are common (2). Standard treatment consists of surgical resection, radiation and chemotherapy. Around 60% of medulloblastoma patients survive for at least 10 years (3). Treatment is associated with high morbidity; medulloblastoma patients often experience cognitive delays and learning disabilities, leading to difficulties in school and social problems. Hearing loss, a side-effect of high-dose chemotherapy and radiation, can also contribute to educational difficulties. (4, 5) Around 25% of medulloblastoma patients will experience cerebellar mutism following surgical resection, a condition associated with ataxia, poor coordination, and irritability in addition to absent speech that can persist from weeks to years (6). Surviving patients are also at increased risk for stroke (4, 7), endocrine problems (8), and development of secondary neoplasms (9). The significant morbidity associated with medulloblastoma indicates a need for better therapies.

Around two-thirds of medulloblastoma patients will survive long-term, but this seemingly good survival rate hides the complexity of this disease. Some patients will respond well to therapy and experience tumor remission without recurrence, while others will experience tumor metastasis, recurrence and the development of therapeutic

resistance and ultimately die from their disease (1). Historically, medulloblastoma was classified based on histologic characteristics. Patients with a desmoplastic/nodular histology were categorized as having good outcomes. Tumors with "classic" histology were considered standard risk, and large/cell anaplastic tumors generally having poor outcomes. Patients with metastatic disease or significant post-operative residual tumor also tended to have poorer outcomes. (10) Genetically, MYC expression is known to correlate with anaplasia and poor outcome (11-14).

1.2 Medulloblastoma Molecular Genetics

Recently RNA expression profiling and DNA methylation studies have subdivided medulloblastoma into four molecular subgroups: WNT, SHH, Group 3, and Group 4 (15, 16). These four subgroups vary in their clinical prognoses and molecular genetics. Some researchers, such as Cho et al (14), identify six molecular subgroups, C1 through C6 (hereafter referred to as the Cho subgroups), which can be nested into the four consensus subgroups. In addition to differing prognoses and genetics, certain subtypes are also more common in certain age groups, perhaps reflecting a difference in cell-of-origin between the groups.

The WNT subgroup (Cho subgroup C6) represents 10% of medulloblastoma tumors (10, 14, 17). This subgroup is characterized by dysregulation of the WNT signaling pathway, most frequently caused by mutations in β-catenin (*CTNNB1*), and loss of one copy of chromosome 6 (15, 16). Most children diagnosed with WNT tumors are school-aged (15). Patients with WNT-group tumors respond well to therapy and have 95% 5-year survival rate (10). Phoenix et al proposed that WNT driven medulloblastoma

is essentially curable because the mutant β-catenin signaling leads to the development a particularly permeable blood-brain barrier within the tumor and its surrounding environment allowing high-levels of chemotherapy to accumulate within the tumor (18). SHH tumors (the other tumor type studied by Phoenix et al) have a more intact blood-brain barrier, allowing lower levels of chemotherapy to accumulate (18). These WNT-tumor patients do so well, it is thought their disease might respond to less therapy than the current standard of care. An open clinical trial is currently testing the efficacy of surgery and chemotherapy without radiation for patients with WNT-positive medulloblastoma tumors (Trial Number: NCT02212574).

Around 30% of medulloblastoma patients have SHH-type tumors (Cho subgroup C3) (10, 14, 17) . This subgroup is characterized by mutations in the SHH pathway (15). Mutations are found at multiple points in the pathway, including *GLI2, PTCH* and *SUFU* (17, 19). *PTCH* mutations can be inherited, resulting in Gorlin Syndrome. Gorlin patients are predisposed to multiple types of cancer, including medulloblastoma (17). A subset of SHH patients have mutations in *TP53* (19). Like *PTCH* mutations, *TP53* mutations can be inherited causing the cancer pre-disposing Li-Fraumeni Syndrome. Li-Fraumeni patients are pre-disposed to developing medulloblastoma in addition to other cancer types. (19) Clinical prognosis varies within the SHH group. Patients with *TP53* mutant tumors tend to do very poorly, while patients without *TP53* and/or *GLI2* mutations have a better clinical outcome (20). Infants, older adolescents, and adults diagnosed with medulloblastoma typically have SHH group tumors (15).

Group 3 and Group 4 tumors are less well characterized than SHH and WNT tumors. These tumor types most commonly occur in school-aged children (15). Group 3

(Cho subgroups C1 and C5) is the most clinically devastating of the subgroups and comprises about 25% of medulloblastoma tumors (10, 14). Group 3 tumors are most commonly associated with amplification or over-expression of the *MYC* oncogene (10, 17). *MYC* overexpression is associated with anaplastic histology—traditionally a sign of poor prognosis (11). These *MYC*-amplified medulloblastoma tumors make up Cho subgroup C1, with the non-MYC amplified Group 3 tumors falling into Cho subgroup C5 (14). In many cases, the increased levels of MYC mRNA are associated with DNA amplicons at this locus (13, 21), but in other tumors the precise cause of MYC upregulation is unclear. Several groups have previously shown that increased MYC expression can promote medulloblastoma formation, growth and an anaplastic tumor phenotype (11, 22, 23). Ultimately, only around 50% of patients with a Group 3 tumor survive long term. About 35 to 40% of these tumors will metastasize to the leptomeningeal space and/or spine. (24) Group 4 tumors (Cho subgroups C2 and C4) comprise about 45% of medulloblastoma tumors (14, 24). In this subgroup, mutations are often found in *NMYC, CDK6,* and *SNCAIP* (19). Around 75% of patients with a Group 4 medulloblastoma tumor will survive long-term. About 40 to 45% of Group 4 tumors ultimately metastasize (24).

Medulloblastoma probably arises from immature embryonal cells in the cerebellum. The developing cerebellum has multiple distinct progenitor cell populations, and research suggests that the distinct molecular subgroups of medulloblastoma arise from these different progenitor populations. WNT medulloblastoma is thought to arise from neural progenitor cells of the dorsal brain stem, while SHH tumors are thought to arise from the cerebellar granule neural progenitors (CGNPs) of the external granule

layer (EGL) and rhombic lib. (24-26) There is less evidence for the cells of origin for Group 3 and Group 4 tumors. Group 3 tumors may arise from the CGNPs of the EGL or the neural progenitors of the ventricular zone in the fourth ventricle. (24) Recent work by Lin et al suggests that the cells of origin for Group 4 medulloblastoma are found in the deep cerebellar nuclei (DCN) of the nuclear transitory zone or possibly DCN progenitors in the upper rhombic lip. (27)

1.3 Medulloblastoma Models

1.3a Cell Culture Models

A variety of tools, each with advantages and drawbacks, exist to study medulloblastoma in the laboratory. There are 44 well established, patient-derived cell lines that have been in continuous use/culture over the past several decades (28). According to a 2016 review, efforts in genetic analysis have sorted less than half (18/44) of these cell lines into the four consensus subgroups, with varying degrees of certainty (28). Of the subgrouped cell-lines, around 60% (11/18) fall into Group 3 due to amplifications in *MYC*. About 20% (4/18) are classified as SHH tumors, with half of those having *TP53* mutations. Two cell lines are considered Group 4 (both derived from the same patient), and only one has been classified as WNT. (28) A subset of these cell lines will form tumors when implanted into immune-deficient mice. The long-term use of some of these cell lines makes them are useful *in vitro* tools because current results and experiments can be compared to past work. However, there are many drawbacks to using cells that have been cultured for long periods of time. Genetic drift over time is a very legitimate concern. As cells adapt to culture conditions, their original genetic

alterations may be lost, or new genetic mutations acquired (29). Additionally, the original patient tissue from which the cell line was derived is often currently unavailable, as many of these cell lines were established decades ago. The accuracy of these long-term cell culture models must be considered when they are used for studies.

Primary, short-term medulloblastoma models can also be used as a model system, albeit with more technical difficulties than long-term culture models. Primary cultures are probably more genetically representative of primary tumors, and the tissue of origin is often available for analysis or comparison. These cultures are also more heterogeneous, containing multiple cell types from the primary sample, not just tumor cells. Primary culture models can only be considered such for a few passages, making them only useable as a "primary" model for the short term.

1.3b Serially Passaged Xenograft Models

In addition to creating primary cell lines *in vitro,* primary patient samples can be immediately injected into the brains or flanks of immune compromised mice. If a tumor forms, it can be passaged into additional animals, creating a patient-derived xenograft model. These models are viewed as being more accurate than *in vitro* cell-culture systems because the tumor is growing in conditions more similar to a human brain and there are not the selective pressures faced by a sample being forced to adapt to culture conditions. Rough 20 serially passaged xenograft medulloblastoma cell lines are available for purchase from the Brain Tumor Resource Laboratory run by Jim Olson at the Fred Hutchinson Cancer Research Center (btrl.org). These lines have been characterized by medulloblastoma subgroup. However, a mouse brain is not a human

brain, and serially passaged xenografts have been shown to experience changes in gene expression as they are passaged (30).

1.3c Mouse Models

In addition to xenografting, several genetically engineered mouse models (GEMM) of medulloblastoma exist. Around 15% of mice heterozygous for *Ptc* (the mouse equivalent of *PTCH*) expression will spontaneously develop a medulloblastoma-like tumor (31). When *Ptc* heterozygosity is combined with *Trp53* (the mouse gene coding for p53) heterozygosity, the incidence of tumor formation increases to 95% (32). *Ptc* heterozygosity combined with various other genetic deficits (including deficiency of *Kip1* and *Ink4c*) also will result in formation of medulloblastoma tumors (33, 34). Initial mouse models featured mice with global *Ptch* heterozygosity. Using Cre-lox technology, *Ptc* can be specifically knocked-out post-natally in granular neural precursor (GNP) cells of the cerebellum resulting in fully penetrant medulloblastoma formation (35). Mice with mutations in the SHH signaling pathway other than *Ptch* (*Sufu* and *Smo)* have also been generated. In total, around 17 different GEMM-models of SHH-medulloblastoma have been created. (36)

Few GEMMs exist for the other subgroups of medulloblastoma. Expressing mutant *Ctnnb1* in the cells of the cerebellar ventricular zone and the lower rhombic lip is not sufficient to induce tumor formation, but when *Tp53* expression is also knocked out, WNT-like tumors form in around 15% of mice (25). Swartling et al created a non-SHH, non-WNT GEMM model of medulloblastoma (called the GTML model) by inducing *MYCN* expression in cells expressing GLT1 (glutamate transporter) (37). Unlike the majority of other mouse models of medulloblastoma, the GTML model forms metastases

(36, 37). The majority of medulloblastoma patients die of metastases and recurrent disease, so there is a critical need to study the biology of medulloblastoma metastasis to develop better therapeutics (36).

There are also multiple non-genetically engineered mouse models of medulloblastoma. If *Shh*-expressing retrovirus is injected into the cerebella of embryonic mice *in utero*, around three-quarters of the injected animals will develop medulloblastoma after birth (38). The *RCAS/tv-a* system can also be used to induce medulloblastoma formation. In this system, RCAS vectors carrying genes of interest were transfected into DF-1 cells, which are then injected into the cerebella of mice that expressed TV-A under the control of the *Nestin* promoter, thus causing TV-A to be expressed in neural progenitor cells. Using this system, it was shown that both *Myc* and *MycN* and *Igf2* can combine with *Ptc* heterozygosity to promote medulloblastoma formation. (39-41).

Two separate groups created models of Group 3 medulloblastoma by implanting previously isolated and transfected mouse neural stem cells into the cerebella of mice. Kawauchi et al transfected granular neural precursor cells isolated from the cerebella of postnatal day 6 *Trp53* null mice with *Myc*. These implanted cells formed tumors that killed mice in a median of 39 days. Genetic analysis indicated that these tumors highly expressed the mouse orthologues of the genes that characterize human Group 3 medulloblastoma tumors (23). Pei et al isolated cells from the cerebella of C57BL/6J mice on the basis of Promin1 (CD133) expression and the lack of expression of neuronal and glial markers. These cells were transfected with *Myc* and dominant-negative *Trp53* retrovirus and transplanted into the cerebella of nude mice. The resulting tumors were

histologically similar to primary Group 3 tumors and reduced the survival of implanted mice to a median of 49 days. Genetic analysis showed these tumors and human Group 3 tumors have similar gene expression profiles. (22)

Modeling medulloblastoma in mice has led to great advances in our understanding of the cell of origin and other biological features of the various molecular subtypes. However, questions can arise when performing cross species comparisons. Murine cells are not always transformed in a fashion equivalent to human ones (42, 43), and expression profiles can be challenging to reconcile between mouse and human. For example, it has been suggested that the MYCN driven murine model may represent a better molecular match for human Group 3 tumors than MYC driven ones, despite the fact that MYCN is most prominent in other medulloblastoma subgroups (44). Thus one of the goals of this dissertation is to show the creation of a human model of MYC-driven medulloblastoma using neurospheres derived from the developing human cerebellum and to use these transformed cells to interrogate new treatments. A human neural stem cell model of medulloblastoma that faithfully recapitulates the overall oncogenic state of these tumors can be a powerful tool. An additional motivation for this strategy is the fact that medulloblastoma tumors are genetically relatively simple, having 5 to 10-fold fewer mutations than adult solid tumors (45), making them an ideal choice for this approach.

CHAPTER 2: RESULTS

2.1 Group 3 primary medulloblastoma tumors express MYC, phospho-AKT, and TP53

To generate a genetically defined model of aggressive medulloblastoma, we began with human neural stem and progenitor cells obtained as described in (46) (Figure 1 A,B). These cells express the stem cell marker CD133 and the neural stem cell markers NESTIN, SOX2, and GFAP (Figure 1C). We used a tissue microarray (TMA) containing 65 primary human medulloblastoma samples that was previously characterized with respect to subgroup (15) to interrogate the expression of oncogenic elements associated with Group 3/C1 medulloblastoma. Group 3 tumors are known to overexpress *MYC* at the mRNA level (12), but MYC protein expression has not been extensively investigated in primary tumors. Immunohistochemical analysis of MYC on our TMA showed that expression was highest in Group 3 tumors (Figure 1D), with 50% expressing MYC, while only 27% of SHH tumors and 6% of Group 4 tumors had detectable MYC protein levels.

In addition to MYC, Group 3 samples had significantly higher expression of TP53 (Figure 1E), indicating dysfunction of the p53 pathway. Among Group 3 tumors, 56% were positive for increased TP53 expression, while only 25% of SHH tumors and 23% of Group 4 tumors were positive for TP53. Our group has demonstrated that anaplastic medulloblastoma tumors have elevated TP53 expression (47, 48), suggesting inactivation of the p53 pathway. We and others have shown that increased TP53 protein levels or TP53 mutations are associated with worse clinical outcomes in a subgroup-dependent fashion (20).

We next investigated the expression of phospho-AKT as an indicator of mTOR status. The mTOR pathway is active in multiple medulloblastoma subgroups, including Group 3 and is associated with increased metastasis (49). We identified increased phospho-AKT staining in all subgroups represented in our TMA. Although there was a trend for increased AKT signaling in Group 3, it did not reach statistical significance (Figure 1F). In addition to MYC, TP53 and phospho-AKT, human telomerase (hTERT) has been identified as being highly expressed in embryonal tumors, and was included as a transforming element (50, 51).

2.2 Neural stem cells transduced with MYC, dominant-negative TP53, hTERT, and AKT form aggressive tumors that phenocopy Group 3 medulloblastoma

The addition of MYC alone or with AKT, DNp53 and hTERT increases proliferation compared to normal neural stem cells and to cells immortalized with SV40 (Figure 2A). The human MYC transformed cells were *ATOH* negative (data not shown), consistent with prior murine models of MYC-driven medulloblastoma (22). Cerebellar derived neural stem and progenitor cells transduced with dominant-negative TP53, MYC, constitutively active (myristolated) AKT, and human telomerase (hTERT) formed aggressive tumors when injected into the brains of nude mice (Figure 2B). Cerebellar stem cells immortalized with SV40 did not form tumors (Figure 1B).

The tumors expressed TP53, MYC, and phospho-AKT, indicating that these oncogenic elements used to drive transformation were maintained (Figure 2C). Tumors formed by cells transduced with all four oncogenic elements also had anaplastic features (Figure 2D i) and could spread to the leptomeningeal space (Figure 2D ii).

Approximately 20% of mice had spinal metastases (Figure 2D iii). Metastasis is associated with Groups 3 and 4, the most aggressive subgroups of medulloblastoma (52). The DN-TP53 hTERT AKT MYC orthotopic xenografts expressed NESTIN and MAP2 and were negative for GFAP (Figure 2E), indicating a primarily progenitor and neuronal phenotype consistent with medulloblastoma. Because no effective antibody exists for hTERT immunohistochemistry, we verified high-level expression of this hallmark in our 4-gene transduced cells by qPCR (data not shown).

2.3 Human neural stem cell models of Group 3 medulloblastoma share mRNA expression profile with human primary tumors

To further confirm that our model replicates Group 3 medulloblastoma, we performed Affymetrix mRNA expression profiling on our human cerebellar neural stem and progenitor cell models and two of our DN-TP53 hTERT AKT MYC tumor orthotopic xenografts. Specifically, we examined the expression of 32 pathways that have been previously associated with each of the six Cho subgroups (53). High expression of a specific subset of each of these 32 pathways is characteristic of each subgroup. We performed single-sample gene-set enrichment analysis (ssGSEA) on our model in culture and as xenografts to obtain an enrichment score for each of the medulloblastoma associated pathways. This analysis was also performed for the primary medulloblastoma tumor dataset of Tamayo *et al.* 2011 (53), allowing us to compare the profiles of our xenografts and cultured cells against human medulloblastoma tumors. The pathway enrichment profile of our cells and xenografts closely matches the profile of C1 primary tumors, the most aggressive subclass of patients within MYC-driven Group 3 (14) (Figure 3A, green boxes). Samples from cells transduced with only MYC expressed

the Group 3 associated mRNAs and corresponding pathway enrichment. The addition of DN-TP53, hTERT and AKT to MYC increased the expression of these Group 3 associated pathways. The orthotopic xenografts of cells transduced with MYC, DN-TP53, hTERT and AKT most highly express the Group 3 associated mRNAs. (Figure 3B)

We also generated an association matrix that compares the pathway enrichment scores of xenografts and cell models against each tumor subtype (Fig. 3C). The association is estimated using the Information Coefficient, an information-theoretical counterpart to the correlation coefficient (see Chapter 4.7 for details). Primary cultures of untransduced cerebellar neural stem and progenitor cells associate most closely with the C6/Wnt subgroup. The sequential addition of MYC, TP53, hTERT and AKT increases the association with the C1 subtype. Growth of these cells as orthotopic xenograft tumors further increases the association with the subtype C1 (Fig 3C).

2.4 Analysis of drug sensitivity databases with a profile created by analyzing the human neural stem cell model of Group 3 medulloblastoma reveals CDK inhibitors as a potential therapeutic target

The human neural stem cell model of medulloblastoma was used as a test subject for a novel computational analysis technique, DiSCoVER (Disease-model Signature vs. Compound-Variety Enriched Response), that we briefly describe here (see Chapter 4.6 for details). We created a gene set called the "hNSC G3 signature" of the 150 most up-regulated genes in the murine xerographs of human neural stem cell line transformed with DNp53, hTERT, constitutively active AKT and MYC (Table 1).We then analyzed the gene expression datasets of two mRNA datasets using single-sample gene set

enrichment analysis (ssGSEA). This analysis allowed us to obtain a hNSC G3 signature enrichment score for each sample in the two mRNA datasets. We then matched the signature enrichment scores against drug sensitivity profiles that have been generated for the same samples. In this way, we identified compounds that killed cells sharing a high hNSC G3 enrichment score. We performed this comparison against three different drug sensitivity datasets and looked for overlaps in the top scoring compounds or their compound varieties. A summary of the procedure is shown in Figure 4A.

In this analysis we focused on the top scoring compounds with False Discovery Rates (FDR) below 0.33. The overlap analysis across datasets revealed that cancer cell lines that highly express the hNSC G3 signature are sensitive to the cyclin-dependent kinase inhibitors (Figure 4B). These inhibitors include the pan-CDK inhibitor Flavopiridol/Alvocidib (PubChem CID: 5287969) (54), CDK 1/2/5/7 inhibitor CGP-60474 that was developed as a PKC inhibitor (PubChem ID: 644215) (55), CDK4 inhibitor CGP-082996 (PubChem CID: 24825971), and the CDK4/6 inhibitor PD-0332991/Palbociclib (PubChem ID: 5330286) (56). MYC expression is known to increase the expression of cyclin-dependent kinases, so CDK inhibition is biologically congruent with the *in silico* screen (57).

2.5 The CDK4/6 inhibitor palbociclib and the pan-CDK inhibitor flavopiridol decrease proliferation in the human neural stem cell model of medulloblastoma and patient-derived medulloblastoma cell lines

Of the CDK inhibitors identified by the DiSCoVER analysis, we decided to test palbociclib (PD-0223991) because of its clinical relevance. Palbociclib is used clinically

for the treatment of recurrent breast cancer. In addition to cerebellar neural stem cells transformed with MYC, DNp53, AKT and hTERT, we used cerebellar neural stem cells transformed with MYC alone and two MYC-expressing, patient-derived medulloblastoma lines (D425Med and D283Med) to test the effects of palbociclib on medulloblastoma. Inhibition of CDK4/6 activity prevents the phosphorylation of the retinoblastoma protein (Rb) (56). Western blotting showed that 5uM palbociclib treatment led to a decrease in phosphorylation of Rb at two different phosphorylation sites (Ser780, and Ser807/811) in all medulloblastoma cell lines test. Phosphorylation at S780 decreased by 96% in cells transformed with MYC alone, by 62% in cells transformed with all four oncogenes, by 24% in D425Med cells, and by 37% in D283Med cells. The phosphorylation at S807/811 decreased by 99% in MYC alone cells, 56% in cells transformed with all four oncogenes, by 33% in D425Med cells and by 43% in D283Med cells. (Figure 5A). Neural stem cells immortalized with SV40 were not tested because SV40 functions through suppression of Rb (58).

Palbociclib treatment caused a significant decrease in proliferation in all four medulloblastoma models, as determined by BrdU incorporation (Figure 5B). 5uM Palbociclib treatment for 72h caused the percentage of BrdU positive cells to decrease from 41% to 3% in cells transformed with MYC alone ($p=0.0000009$ by Student's t-test), from 30% to 13% in cells transformed with all four oncogenic elements ($p=0.02$ by Student's t-test), from 32% to 12% in D425Med ($p=0.000004$ by Student's t-test), and from 40% to 21% in D283Med ($p=0.004$ by Student' t-test). In cells immortalized with SV40, palbociclib caused a modest decrease in BrdU incorporation—34% BrdU positive cells to 24% ($p=0.06$ by Student's t-test) (Figure 5B). The pan-CDK inhibitor

flavopiridol, which was also identified by DiSCoVER, decreased the percentage of BrdU positive cells from 62% to 17% in neural stem cells only transformed with MYC ($p=0.000014$ by Student's t-test), from 27% to 14% in cells transformed with all four oncogenes ($p=0.00055$, by Student's t-test), from 51% to 35% in D425Med cells ($p=0.03$, by Student's T-test) and from 47% to 29% in D283Med cells ($p=0.000008$, by Student's T-test) (Figure 6A).

2.6 Palbociclib and flavopiridol induce apoptosis in human MYC-driven medulloblastoma cells

Palbociclib treatment increased apoptosis in medulloblastoma models that express MYC (Figures 5C and 5D). Treatment with 1uM or 5uM of palbociclib for 24h caused an increase in the expression of cleaved-PARP (as measured by Western blotting), indicating increased levels of apoptosis (Figure 5C). Treatment of our MYC-driven human neural stem cell models of medulloblastoma with 5uM of palbociclib for 72h caused the percentage of cleaved caspase-3 positive cells in to increase from 20% to 70% in cells immortalized with MYC alone ($p=0.0000004$ Student's t-test), from 21% to 45% in cells transformed with all four oncogenic elements ($p=0.000002$ by Student's t-test), from 7% to 21% in D425Med ($p=0.0005$ Student's t-test), and from 3% to 9% in D283Med ($p=0.001$ Student's t-test) (Figure 5D). In SV40 immortalized cells, 5uM palbociclib caused a modest increase in the percentage of cleaved-caspase 3 positive cells—10% to 15%--but this was not statistically significant ($p=0.14$ by Student's t-test) (Figure 5D).

Like palbociclib, flavopiridol also caused an increase in apoptosis as measured by cleaved caspase-3 immunofluorescence (Figure 6B). Treatment with 100nM of flavopiridol increased the percentage of cleaved caspase-3 positive cells from 4% to 62% in human neural stem cells transformed with MYC alone (p=0.00008 by Student's t-test), from 5% to 31% in cells transformed with all four oncogenic elements (p=0.000001 by Student's t-test), from 6% to 23% in D425Med cells (p=0.4 by Student's t-test), and from 2% to 12% in D283Med cells (p=0.02 by Student's test). In SV40 immortalized cells, flavopiridol treatment caused a modest increase in cleaved caspase-3 positive cells—1% to 4%-- and though this change was statistically significant (p=0.005 by Student's t-test) it is unlikely to be biologically meaningful (Figure 6B).

2.7 Palbociclib significantly improves survival of mice with medulloblastoma orthotopic xenografts

We next tested the efficacy of palbociclib as a monotherapy *in vivo*. Palbociclib treatment has been shown to increase survival in a mouse models of brainstem glioma and GBM (59, 60). Palbociclib treatment significantly extended survival of nude mice with D425Med intracranial xenografts by 48%--from 25 to 37 days (p=0.003 by Log-rank test) (Figure 7A). Palbociclib treatment significantly extended the survival of nude mice with DNp53 hT AKT MYC tumors by 22%--from 162 to 197 days (p=0.0322 by Log-rank test). To verify that palbociclib was causing this effect by inhibiting CDK function, we performed IHC for phospho-Rb on D425Med tumors from animals that were given a single dose of vehicle or palbociclib four hours prior to euthanasia. Tumors from mice given palbociclib had a significantly lower percentage of phospho-Rb positive

cells compared to mice given the vehicle control (38% vs 54%, p=0.00025 by Student's t-test), indicating that the drug cross the blood brain barrier and penetrates the tumor (Figure 7C). Images of two tumors from mice given vehicle are in Figure 7D, left. Images of two tumors from mice given palbociclib are in Figure 7D, right. We were unable to conduct any *in vivo* survival studies using flavopiridol due to toxicity in mice.

CHAPTER 3: DISCUSSION

Group 3 medulloblastoma is a highly lethal disease. The human neural stem and progenitor cell model presented here phenotypically, histologically and genetically mimics the C1 component of Group 3, the most lethal sub-group of medulloblastoma (14, 53). Although our model shares MYC activation and p53 pathway inhibition with the murine neural stem cell models created by Pei et al (22) and Kawauchi et al (23), the addition of activated *AKT*, which is a known driver of medulloblastoma metastasis and resistance to therapy as well as *hTERT*, which reflects the high frequency of *TERT* promoter mutations in medulloblastoma, adds a richness to our model (50, 61). The increasing fidelity of our human neural stem cells to Group 3 with the sequential addition of oncogenic elements as demonstrated in Figure 3 highlights this point.

Our model might also serve as a model for recurrent and metastatic disease. The majority of medulloblastoma patients initially respond to therapy. Patients that die of their disease are dying from relapsed, sometimes metastatic, disease, making recurrence and metastatic models critical. Recurrence patterns vary between the four medulloblastoma subgroups; SHH-type tumors are more likely to reoccur locally, while Group 3 and Group 4 tumors are more like to recur as metastases (52). Medulloblastoma tumors retain their subgroup identity when they reoccur, whether or not the recurrence is local or metastatic, suggesting that subgroup-affiliation is determined by cell of origin (52). Though subgroup affiliation remains stable, there are genetic changes at recurrence. Hill et al found that alterations in MYC and the TP53 pathway often occur together in relapsed medulloblastoma of all subtypes (62). These MYC-TP53 altered recurrent tumors were particularly aggressive, with all patients studied in this group rapidly succumbing to their disease (62). Our model expresses high levels of MYC and

alterations in the TP53 pathway, through dominant-negative TP53, and so it could serve as a model of relapsed disease.

This dissertation also presents a novel method for *in silico* prediction of drug sensitivity, which we believe may significantly accelerate the identification of novel therapeutics for rare cancer types. Our DiSCoVER approach differs from existing *in silico* methods such as Connectivity MAP (C-MAP) in that DiSCoVER uses the actual drug response cell viability profiles (e.g. IC50 or AUC) of multiple drug screening datasets involving hundreds of cell lines treated with each drug, rather than the transcriptional changes, such as those detected by 1,000 "landmark" genes, induced by drug perturbations in a few selected cell lines as it is done in CMAP. The drug screening responses are more accurate at representing the effect of a drug in terms of affecting cell viability and not only transcriptional changes that may, or may not, impinge on cell viability.

CMAP matches the gene set representing the disease signature against transcriptional profiles of drug perturbations in a few cell lines using the Kolmogorov-Smirnov enrichment statistic. This is a useful approach in general, but sometimes it does not easily allow the detection of more subtle disease vs. drug associations in a broader context involving a large number and diversity of cellular states. In DiSCoVER we first produced an enrichment score for the disease signature in each cell line (using single-sample GSEA); and then we match the pattern of these scores across hundreds of cell lines, against the drug sensitivity profiles for the same cell lines, using an information-theoretic metric of association. This approach provides a high degree of sensitivity and specificity in finding drug responses that match the disease signature, even when the relationship, i) is restricted to a few cell lines representing a relevant but narrowly

represented biological state, ii) when this relationship is not strictly linear or, iii) when it is very weak. DiSCoVER also repeats the analysis in multiple external datasets and then compares the results across them, considering drug classes, and not only individual instances as occurs in CMAP.

An identified therapeutic target in our *in silico* pre-clinical drug screen was cyclin-dependent kinases (CDKs). MYC plays a significant role in regulating the cell cycle through variety of mechanisms (63), including by directly regulating the expression of CDKs, cyclins, and E2F transcription factors (63). Additionally, MYC induces CDK-activated kinase (CAK) and phosphatases that lead to hyper-activation of cyclin-CDK complexes (63). MYC also antagonizes the activity of cell cycle inhibitors like p21 and p27 (63). MYC-driven murine lymphoma and hepatoblastoma are sensitive to CDK1/2 inhibition, further highlighting CDKs as a potential Achilles' heel in MYC-driven malignancies (64, 65). Other groups have demonstrated the use of CDK inhibitors in treating brain tumors (59, 60). Faria *et al* showed the efficacy of an investigational CDK1/5/GSK3b inhibitor, alsterpaullone, in MYC-driven medulloblastoma cell lines, though much of the tumor suppressing effect was demonstrated to be mediated through mTOR inhibition (66). Palbociclib (under the trade-name Ibrance) is a CDK4/6 inhibitor approved for treatment of advanced estrogen-receptor positive breast cancers (67). Phase I clinical trials in pediatric brain tumor patients—including patients with medulloblastoma--are currently ongoing (NCT02255461). The data presented here provides strong preclinical support for the use of palbociclib in medulloblastoma patients. A study by Whiteway *et al* showing that palbociclib decreased the growth of high-serum medulloblastoma cell lines *in vitro* (68) also provides preclinical support. We chose an *in vivo* dose of palbociclib consistent with that given in other pre-clinical models, 150

mg/kg (56, 59, 60, 69). However, the MTD of pediatric patients has yet to be reported (NCT02255461).

Methotrexate and cytarabine were among other top hits revealed by the DiSCoVER analysis (Tables 2 to 4). These drugs are currently in use in medulloblastoma treatment and are structurally similar to pemetrexed and gemcitabine, which were recently identified as being active in medulloblastoma xenografts (70). The identification of biologically plausible targets and compounds that are being explored by other scientists provides strong validation of our *in silico* strategy of using the hNSC G3 signature to probe available datasets of drug sensitivity data.

Identification of increased apoptosis downstream of palbociclib in our cell lines and neural stem cell models differs from the standard response to CDK inhibitors, which are largely viewed as cytostatic agents in other cancer types (69, 71-74). As we showed in Figure 5A, palbociclib treatment causes decreased phosphorylation of Rb. Phosphorylation of Rb releases Rb's inhibition of E2F transcription factors, allowing transcription of genes necessary for cycle progression (75). De-phosphorylated Rb binds to E2F transcription factors, preventing transcription initiation and cell cycle progression (75). Several studies showed that as a single agent, palbociclib caused cell-cycle arrest, but did not lead to apoptosis (69, 71-74). However, in combination with cytarabine, dexamethasone, and bortezomib, palbociclib enhances cytotoxicity (69, 73, 74). In our model, palbociclib induces apoptosis as a monotherapy, so is possible that we will see synergy and enhanced cell killing when it is used in combination with other cytotoxic agents commonly used to treat in MYC-driven medulloblastoma.

Among the other candidate drugs in the DiSCoVER prediction, mTOR inhibitors occur three times (Tables 2 to 4). mTOR is known to alter cellular metabolism, and

Group 3 medulloblastoma showed increased AKT expression compared to normal brain (Figure 1). mTOR in specific can activate glutamine metabolism by upregulation of glutamine dehydrogenase (GDH). MYC also upregulates glutamine metabolism by activating multiple transporters and genes involved in glutaminolysis, including GLS. Multiple cancers are thought to have aberrant glutamine metabolism (76-81), and inhibiting glutaminase is an attractive therapeutic option in MYC-driven and mTOR-driven medulloblastoma. Glutamine metabolism and its role as a potential therapeutic target in medulloblastoma will be discussed extensively in Part II.

This dissertation presents a novel strategy for creating new models of tumors and for pre-clinical screening of therapeutic targets. This strategy enabled us to create a human neural stem cell model of Group 3 medulloblastoma and to use this model to screen drug sensitivity databases and validate an identified target—palbociclib. The data presented here provides pre-clinical support for the use of palbociclib or other CDK inhibitors in carefully selected medulloblastoma patients. Our overall strategy of using tissue-specific human stem and progenitor cells may be useful for developing models of other tumor types. The DiSCoVER technique could also be applied to other disease states for quick identification of candidate drugs without lengthy *in vitro* experiments.

PART II: GLUTAMINE METABOLISM IS A POTENTIAL THERAPEUTIC TARGET IN AGGRESSIVE MEDULLOBLASTOMA

CHAPTER 4: INTRODUCTION TO CANCER METABOLISM

4.1 The Warburg Effect

It is widely recognized that one of the characteristic "hallmarks" of cancer is altered metabolism (82). Interest in the cellular energetics of cancer began early in the 20th century with Otto Warburg. Warburg observed that even the presence of oxygen, cancer cells performed glycolysis ("aerobic glycolysis") to produce ATP, rather than the more efficient oxidative phosphorylation (83). Warburg believed that metabolic reprogramming to use anaerobic glycolysis to meet energy needs was the fundamental cause of cancer (83), and it is now known as the "Warburg Effect." Modern studies have provided support for the Warburg Effect. Positron Emission Tomography (PET) scans of human cancer patients show that many tumors take up high levels of glucose. This increase in glucose uptake is sometimes facilitated by upregulation of glucose transporters such as GLUT1. (82) Well known oncogenes (like *RAS*, *AKT*, and *MYC*) are involved metabolic reprogramming (84, 85).

Through a series of ten enzymatic reactions, glycolysis breaks down one molecule of glucose into two molecules of pyruvate, generating two molecules of ATP. In differentiated cells under normal oxygen tension, pyruvate is oxidized into acetyl-CoA and funneled into the citric acid (TCA) cycle where it is fully oxidized to carbon dioxide in a process called oxidative phosphorylation. Oxidative phosphorylation generates 36 molecules of ATP. If differentiated cells are under hypoxic (low oxygen) conditions, the pyruvate generated from glycolysis undergoes anaerobic glycolysis (fermentation) to generate lactate and two molecules of ATP. Fermentation allows cells to generate ATP

in low oxygen conditions, but is about 18-fold less efficient than oxidative phosphorylation.

Proliferating normal cells also undergo aerobic glycolysis. It is somewhat counter-intuitive that proliferating cells would perform high levels of aerobic glycolysis because it is so much less efficient at generating ATP when compared to oxidative phosphorylation (82). Warburg hypothesized that cancer cells had a deficiency in mitochondria, which lead to this dependence on glycolysis for ATP production (86, 87). Modern studies have indicated that most cancers do not have mitochondrial deficiencies (87, 88) and proliferating normal cells presumably have normal mitochondrial function. Differentiated, non-proliferating cells use glycolysis for ATP production in anaerobic conditions. Many types of tumors grow hypoxic conditions, perhaps indicating that aerobic glycolysis is an adaptation to survive in this environment. However, cancers that grow in locations with abundant access to oxygen (blood cancers and lung cancers) also undergo aerobic glycolysis, suggesting that the Warburg effect is not merely an adaptation to survive in hypoxic conditions. (84, 87)

Cell proliferation requires more than the generation of ATP. Cellular proliferation requires large quantities of biomolecules like lipids, proteins and nucleotides. A high rate of biosynthesis requires rapid synthesis of biosynthetic precursor molecules. Glycolytic intermediates are a critical source of biosynthetic precursor molecules. (85, 87, 89) The glycolytic intermediate glucose-6-phosphate is converted into 5-phosphoribosyl-α-pyrophosphate (PRPP), which is necessary for the synthesis of nucleotides. Glyceraldeyde-3-phosphate, another glycolytic intermediate, is converted by cells into glycerol-3-phosphote, a critical intermediate in the generation of the phospholipids, sphingolipids, and triacylglycerols that make up the cell membrane.

Pyruvate and 3-phosphoglycerate are precursors for the synthesis of the amino acids alanine and serine, respectively. (89) Glycolytic intermediates are crucial for biosynthesis, and so it is necessary for a dividing cell to have large pools of these intermediates available. Thus, it is now thought that aerobic glycolysis enables proliferating cells to maintain a large supply of the molecules critical for generating the biomass necessary for cell division. (87, 89, 90) Like glycolysis, the TCA cycle serves as a source of biosynthetic intermediates in addition to generating ATP. Citrate is an important substrate for lipid biosynthesis. Oxaloacetate and α-ketoglutarate are used in the synthesis of aspartate and glutamate, respectively. Aspartate can then be converted to asparagine, and proline, arginine and glutamine can be generated from glutamate. (84, 89)

4.2 Glutamine Metabolism in Cancer

In addition to glucose metabolism, glutamine metabolism is essential to the metabolism of both normal cells and cancer cells. Glutamine is the primary source of nitrogen for the synthesis of nucleic acids, other amino acids and hexosamines. Glutamine can be metabolized by cells to replenish the intermediates of the TCA cycle in a process called anaplerosis. In the case of anaplerosis, glutamine is being used as a carbon source for the synthesis of amino acids and lipids. Glutamine is converted to glutamate by the enzyme glutaminase (GLS). Glutamate can then be converted to α-ketoglutarate--a component of the TCA cycle--by glutamate dehydrogenase (GLDH). This α-ketoglutarate can be processed through the TCA cycle into oxaloacetate and citrate, which are key precursors for amino acid and lipid biosynthesis. (89, 91) This

processing of glutamine is sometimes referred to as glutaminolysis (89, 92), and replenishment of the TCA cycle by glutaminolysis can generate ATP. Even when glucose—long thought to be the primary source of ATP--is present, glutamine can be used to generate ATP. (89) For example, glutamine provides 30% of cellular ATP in human fibroblasts cultured with glucose (93).

Many types of cancers uptake large quantities of glutamine, some to the point of becoming "addicted" and being unable to survive without glutamine (77, 78, 81, 94, 95). Glutamine addicted cancer cells experience apoptotic cell death following glutamine withdrawal, most likely due to decreased anaplerosis (77, 96, 97). Some cancers might depend on a TCA cycle run totally independent of glucose (98). Zheng et al, however, suggest that glutamine-withdrawal-induced apoptosis is related to the depletion of the asparagine rather than decreased anaplerosis. Asparagine is synthesized by the addition of a nitrogen from glutamine to aspartate, so decreased cellular access to glutamine results in decreased asparagine levels. In normal situations, depletion of asparagine leads to a signaling cascade that increases translation of the ATF4 transcription factor, which induces expression of asparagine synthetase (ASNS). Increased synthesis of asparagine then leads to decreased levels of ATF4. In the case of glutamine withdrawal however, ATF4 levels remain high, and ATF4 interacts with CHOP and XBP1 to trigger apoptosis (97).

Cellular utilization of glutamine is largely regulated by the oncogene MYC. MYC suppresses the expression of the micro-RNA miR-23a/b which suppresses translation of GLS. High-level expression of MYC effectively "de-represses" GLS and leads to increased GLS expression (76). Expression of the glutamine transporter SLC6A14 may also be regulated through miR-23a/b in a similar manner to GLS (99).

MYC directly up-regulates the expression of two additional glutamine transporters: SLC1A5 (also known as ASCT2) and SLC7A5 (also known as LAT-1) (78, 99). SLC7A5 couples the transport of glutamine and leucine. Glutamine is transported out of the cell and leucine into the cell. This glutamine-leucine exchange activates additional signaling pathways through mTOR (100). The activities of SLC1A5 and SLC7A5 are functionally coupled; the glutamine imported via SLC1A5 is then exchanged for leucine by SLC7A5 and mTOR signaling is activated (99). In both normal cells and cancer, signaling through mTOR is critical for cell growth, proliferation and metabolism. Dysregulation of mTOR signaling is found in multiple types of cancer, including medulloblastoma (101). Additionally, activation of the mTOR pathway stimulates glutamine metabolism by activating GLDH via repression of *SIRT4*, an inhibitor of GDH (102).

MYC also regulates the expression of SLC7A11, which exports glutamate and imports cysteine for the generation of the anti-oxidant molecule glutathione. Glutathione protects cells against oxidative stress, and in the case of cancer, upregulation of SLC7A11 helps prevent apoptosis by increasing glutathione levels, thus reducing oxidative damage. Upregulation of SLC7A11 can facilitate resistance to chemotherapy drugs that generate reactive oxygen species. The glutamate exported by SLC7A11 can activate glutamate receptors on the surface of cells (99), Glutamate receptors regulate the proliferation, migration and survival of neurons during brain development, and glutamate can act as a growth factor in some cancers, including the malignant adult brain tumor GBM (103).

As discussed in Chapter 1.2, Group 3/C1 medulloblastoma tumors express high levels of MYC. MYC is a potent regulator of glutamine metabolism in other cancer

types, it is logical to hypothesize that Group 3/C1 medulloblastoma tumors will also have elevated glutamine metabolism. The role of glutamine metabolism in medulloblastoma is largely under explored, but a study by Wilson et al (104) supports the hypothesis that a subset of medulloblastoma tumors have elevated glutamine metabolism. Wilson et al non-invasively measured glutamate levels in the tumors of medulloblastoma patients using magnetic resonance spectroscopy (MRS). They found that patients with high-levels of glutamate in their tumors had much poorer survival than patients with low glutamate levels. Of the 34 patients in the study, only one had a MYC amplification. This patient was in the high glutamate group and only survived for less than two years after diagnosis (104). The initial step in glutamine metabolism is the conversion of glutamine to glutamate by GLS. High levels of glutamate indicate that glutamine is being metabolized at a high level. Thus, Wilson et al's paper indicates that increased glutamine metabolism is associated with poor-prognosis medulloblastoma.

4.3 Glutamine metabolism utilized for imaging and as a therapeutic target

The high utilization of glutamine by some types of cancer can be exploited for the purposes of imagining. Positron emission tomography (PET) uses a radioactive tracer to image metabolic processes. The most commonly used PET tracer is ^{18}F-fluorodeoxyglucose (^{18}F-FDG), a modified form of glucose. When ^{18}F-FDG is administered, it is taken up by metabolically active tissues, allowing glucose utilizing tissues (such as cancer, if present) to be imaged. Glucose-based PET scanning is commonly used in oncology, and new research suggests utility for glutamine-based PET scanning. Venneti et al created a glutamine-based radioactive tracer—4-^{18}F-(2S,4R)-

fluoroglutamine (^{18}F-FGln) that allows for imaging of glutamine-utilizing tumors. This could prove especially useful in brain tumors where glucose-based PET is impaired by the brain's naturally high level of glucose uptake and utilization (105).

MYC is one of the most highly amplified and overexpressed oncogenes in all types of cancers (106), making it a very attractive therapeutic target. Directly targeting MYC pharmacologically has proven difficult, and no compounds have shown *in vivo* efficacy (107). The downstream targets of MYC may therefore be better options for therapeutic intervention. Inhibition of glutamine metabolism to treat cancer has been explored by a number of different laboratories. The key enzyme GLS is an especially popular target.

Several different small molecule inhibitors of GLS have been reported. BPTES has been shown inhibit the growth of Burkitt lymphoma cells *in vitro* and *in vivo* (98), pancreatic cancer *in vitro* and *in vivo* when used in combination with metformin (108), and triple-negative breast cancer cells *in vitro* when used in combination with cisplatin or etoposide (109). Compound 968 was identified as a glutaminase inhibitor in a screen for compounds that inhibited Rho-GTPase induced transformation (110). Compound 968 decreased the proliferation of breast cancer cells (110), and decreased the proliferation and migration of non-small cell lung cancer cells *in vitro* (111). Ovarian cancer cells were sensitive to treatment with compound 968 alone, and compound 968 treatment sensitized the cells to the chemotherapy agent paclitaxel (112). Compound 968 was effective against GBM cells resistant to mTOR inhibition (113) and non-small cell lung cancer cells resistant to erlotinib (114). CB-839, the GLS inhibitor produced by Calithera Biosciences, demonstrated efficacy against triple-negative breast cancer *in vitro* and *in vivo* (115). CB-839 is currently being tested in a clinical trial (NCT02071862) for

patients with advanced solid tumors, including triple-negative breast cancer, non-small cell lung cancer, and mesothelioma. As of early 2017, the trial is still ongoing, and it is predicted to be completed in September 2017. Unfortunately, CB-839 does not penetrate the blood-brain barrier (115), so it will have no utility in brain tumors such as medulloblastoma.

Less-specific inhibitors of glutamine metabolism also exist in the form of glutamine analogs like 6-diazo-5-oxo-l-norleucine (DON) and Acivicin. DON is a diazo-compound isolated from *Streptomyces* found in Peruvian soil and shown to inhibit the growth of a variety of other bacteria and multiple mouse cancer models (116, 117). DON inhibits the activity of several glutamine utilizing enzymes, including those involved in purine and pyrimidine synthesis (118-120), GLS (118, 119), NAD synthase (118, 121) and asparagine synthetase (118, 122). One research group found that DON treatment disrupted the morphology of the inner mitochondrial membrane in a carcinoid cell line (123). Another group reported DON could cause single-strand DNA breaks in a cell-free setting (124), suggesting DNA damage as possible DON activity. In the mid-1980s and 1990s DON was tested in both adult (125-128) and pediatric (129) clinical trials. These trials were of limited success, most likely because patients were not chosen based on any sort of biomarker expression. Only a few brain tumor patients were included in the trials, and DON was not systematically tested against MYC-expressing cancers.

Acivicin ((2*S*)-Amino[(5*S*)-3-chloro-4,5-dihydro-1,2-oxazol-5-yl]ethanoic acid) was identified in 1978 as a fermentation product from *Streptomyces sviceus* in a screen for anti-metabolic compounds that had anti-cancer activity (130). Like DON, Acivicin can inhibit a number of glutamine utilizing enzymes, including those involved in

pyrimidine and purine synthesis (131, 132), gamma-glutamyl transpeptidase (133, 134), GLS (135), and glutamate synthase (136). Acivicin has also be tested in a number of adult clinical trials, including trials for colorectal carcinoma (137-139), breast cancer (140-142) , mesothelioma (143), non-small cell lung cancer (144-146), and astrocytoma (147). There has been one pediatric clinical trial for patients with refractory solid tumors (148). Like DON, these trials were of limited success, though three brain tumor patients in the pediatric trial showed stable disease at the trial's conclusion (148). Again, patients in these trials were not chose based on any selection criteria that would have predicted response to Acivicin.

There is legitimate concern about neurological side-effects when using brain-penetrant glutamine metabolism inhibiting drugs. Glutamate is the most common excitatory neurotransmitter in the brain, and is generated by the activity of GLS. Inhibition of glutamate generation in the brain could have serious neurological consequences. Adult patients receiving Acivicin did experience CNS toxicities including dizziness, confusion, hallucinations, nightmares, and disorientation. These symptoms resolved after the drug was ceased (137-147, 149-151). Acivicin CNS symptoms could be mitigated by co-administration of an infusion of aminosyn—a solution of electrolytes and amino acids (152). Patients enrolled in the pediatric trial also experienced CNS symptoms—somnolence and nightmares—but these symptoms were less severe than those seen in adults (148). Few CNS toxicities were observed in the adult clinical trials with DON, and those that were reported were mild (127, 128). No CNS toxicities were reported in children, and side-effects were milder over-all. Also worth noting, is that the maximum tolerated dose (MTD) of DON was never reached in children—making it higher than 450mg/m^2 (129).

CHAPTER 5: RESULTS

5.1 Medulloblastoma cell lines expressing MYC are sensitive to glutamine metabolic inhibitors

MYC contributes significantly to the aggressiveness of poor-prognosis Group 3 medulloblastoma (14), and we sought novel mechanisms for targeting MYC and its downstream effectors, in addition to CDK inhibitors and other candidates identified on the DiSCoVER screen. Because MYC regulates the expression of key glutaminolytic enzymes, including glutaminase (GLS), we hypothesized that MYC-expressing medulloblastoma would have abnormal glutamine metabolism (76). Staining our subgrouped-TMA for GLS showed high-level GLS expression (H score >50) in 70% of Group 3 tumors, in 40% of SHH tumors and 37.5% of Group 4 tumors (Figure 8A). MYC amplification and expression is known to be enriched in Group 3 tumors. We found that 100% of tumors on the TMA that expressed MYC by IHC also expressed GLS. In tumors with elevated GLS but low MYC, GLS expression may be regulated by MYCN or in a MYC-independent fashion (153-155). When we investigated the expression of GLS in our cerebellar neural stem cell model of medulloblastoma, we found that MYC transduced cells also expressed GLS. In comparison, SV40-immortalized cerebellar cells did not express GLS (Figure 8B). Two patient-derived medulloblastoma cell lines that express MYC also express GLS (Figure 8C).

To target glutamine metabolism, we used two glutamine analogs: Acivicin and DON, discussed extensively in Chapter 4.3. Both Acivicin and DON have been tested in Phase I clinical trial in children, but never systematically interrogated in MYC-driven malignancies (129, 148). Treatment with 10uM of Acivicin decreased the growth of

D425Med (Figure 9A) and D283Med (Figure 9B) cells as measured by MTS assay. Acivicin treatment significantly decreased proliferation in MYC-transformed neural stem cells as measured by BrdU incorporation. Following 10uM Acivicin treatment, the percentage of BrdU positive cells dropped from 38% to 11% in cells transduced with MYC only ($p=0.002$ by Student's t-test) and from 32% to 7% in cells transduced with dominant negative TP53, hTERT, AKT and MYC ($p=0.016$ by Student's t-test) (Figure 9C). The proliferation of human neural stem cells immortalized with SV40 was not significantly affected by Acivicin treatment (Figure 9C, $p=0.19$ by Student's t-test).

Acivicin increased apoptosis in cells expressing MYC, as measured by cleaved caspase-3 immunofluorescence. Apoptosis increased from 35% to 65% in human neural stem cells transformed with MYC alone ($p=0.09$ by Student's t-test), from 19% to 80% in cells transformed with all four oncogenes ($p=0.001$ by Student's t-test), from 6% to 22% in D425Med cells ($p=0.04$ by Student's t-test), and from 3% to 14% in D283Med cells ($p=0.01$ by Student's t-test) (Figure 9D). Human stem cells immortalized with SV40 were not significantly affected by Acivicin treatment (Figure 9D, $p=0.19$ by Student's t-test).

Treatment with 10uM DON also decreased the growth of D425Med (Figure 10A) and D283Med (Figure 10B) cells as determined by MTS assay. 10uM DON treatment did not decrease proliferation of neural stem cells transformed with MYC, of neural stem cells transformed with all four oncogenes, D425Med or D283Med cells (Figure 10C). Treatment with DON increased apoptosis in the cerebellar stem cells transformed with MYC and in MYC expressing patient-derived cell lines as measured by cleaved caspase-3 immunofluorescence. Apoptosis increased from 21% to 33% in neural stem cells

transformed with only MYC (p=0.01 by Student's t-test), from 11% to 22% in stem cells transformed with all four oncogenes (p=0.006 by Student's t-test), from 6% to 22% in D425Med cells (p=0.004 by Student's t-test), and from 2% to 9% in D283Med cells (p=0.04 by Student's t-test) (Figure 10D). Human neural stem cells immortalized with SV40 did experience significant changes in proliferation (Figure 10C, p=0.99 by Student's t-test) or apoptosis (Figure 10D, p=0.65 by Student's t-test) after treatment with DON.

5.2 Normal human neural stem cells are not sensitive to treatment with glutamine metabolic inhibitors

Glutamine metabolism is crucial to normal brain function, so there is legitimate concern that inhibition could have deleterious effects on patients. Though Acivicin and DON treatment were very well tolerated by pediatric patients and resulted in only minimal neurological side-effects (129, 148), we decided to test the effect of Acivicin and DON therapy on normal, untransformed, un-immortalized human neural stem cells. Neither Acivicin nor DON treatment caused a significant change in proliferation in normal human neural stem cells as measured by BrdU incorporation ($p<0.37$ by Student's t-test, Figure 11A). Neither compound caused apoptosis as measured by cleaved caspase-3 immunofluorescence ($p<0.23$ by Student's t-test Figure 11B). This data suggests that glutamine analog therapy will not cause damage to the normal stem cells of the brain.

5.3 Acivicin therapy decreases the size of medulloblastoma flank tumors but did not extend survival in animals with orthotopic xenografts

We next texted the efficacy of Acivicin as a monotherapy *in vivo*. Treatment four times a week with a 25mg/kg dose of Acivicin did not extend the survival of mice bearing D425Med cerebellar xenografts (p=0.19 by Log-rank test) (Figure 12A). A higher dose of 75mg/kg four times a week also failed to extend survival in mice with D425Med orthotopic xenografts (p=0.78 by Log-rank test) (Figure 12B). The higher dose of Acivicin was able to decrease the size of D283Med flank xenografts by 70% (Figure 12C). That Acivicin can successfully reduce the size of flank tumors but not extend survival of animals with brain tumors suggests the compound is failing to pass the blood-brain barrier. This is surprising because the neurological side effects observed in the Acivicin clinical trials (discussed in Chapter 4.3) suggest that the drug is able to cross the blood-brain barrier. Acivicin is known to have affinity for and is a ligand of the Large Neutral Amino Acid Transporter, which is highly expressed in the blood brain barrier (156-158). There may be difference in the blood brain barrier between humans and mice which could explain Acivicin's failure to increase survival of tumor bearing mice. There is also the possibility that a larger dose of drug is needed. However, the limited commercial availability of Acivicin eliminated the possibility of further *in vivo* studies with this compound.

5.4 DON treatment decreases flank tumor burden and extends survival in mice with medulloblastoma orthotopic xenografts

Once weekly treatment with 30mg/kg of DON dramatically decreased the tumor burden of animals with D425Med flank xenografts. For subcutaneous flank xenograft studies, treatment was started after moderately sized tumors were formed. In control animals, all tumors increased in volume during the course of the experiment (n=19 tumors) and in DON treated individuals all the tumors decreased in volume (n=20 tumors) (Figure 13A). Mice treated with DON experienced an average 94% decrease in flank tumor volume, while control animals experienced a 263% increase in tumor volume ($p=0.0001$, Figure 13B). This dramatic decrease in tumor burden is shown in Figure 13C. In this figure DON treatment began on day 0 (top panel), when all five animals had well-established tumors. After only two weeks (two doses) of treatment, tumor burden was dramatically decreased (middle panel). Four weeks after treatment there are almost no detectable tumors (lower panel).

Weekly DON treatment increased the median survival of mice with orthotopic D425Med by 64 days—an increase of 246% (26 days vehicle treated animals vs 90 days DON treated animals, $p=0.0018$ by Log-rank test) (Figure 13D). We also tested the efficacy of DON therapy in mice bearing serially passaged medulloblastoma xenografts. The Med211 xenograft has been genetically profiled as a Group 3 medulloblastoma tumor. In animals with Med211 orthotopic xenografts, DON therapy improved median survival by 39 days—an increase of 80% (49 days vehicle treated animals vs 88 days DON treated animals, $p=0.0017$ by Log-rank test) (Figure 13E).

5.5 An orally available, pro-drug version of DON extends survival of animals with medulloblastoma orthotopic xenografts

We also tested the efficacy of a DON pro-drug developed by Johns Hopkin Drug Discovery (JHDD). The development of this pro-drug is described in detail in the paper by Rais et al (159). This dual promoeity pro-drug, called JHU-083, has leucine and ethyl groups on DON's carboxylate and amine functionalities to enhance lipophilicity and improve brain penetration (Figure 14A). Unlike unmodified DON, JHU-083 is orally bioavailable. After it is administered, JHU-083 is metabolized into DON. When administered to mice in DON-equivalent doses, JHU-083 delivers DON to the plasma at a slightly reduced C_{max} compared to un-modified DON (Figure 14B). JHU-083 treatment (20mg/kg DON equivalent, 3x week) extends the survival of mice with D425Med orthotopic xenografts by 33%--21 days for vehicle treated mice vs 28 days for pro-drug treated mice ($p=0.006$ by Log-rank test) (Figure 14C). Unmodified DON administered as a 30m/kg bolus dose extends the survival of mice with D425Med orthotopic xenografts by 246% (Figure 13D). JHU-083 cannot be administered as a single 30mg/kg DON equivalent bolus dose due to gut toxicity. It is possible that the dosing of JHU-083 could be increased to 20mg/kg DON equivalent 5x a week, which could possibly increase the survival benefit. It is also possible that the reduced C_{max} of JHU-083 contributes to the decrease survival benefit provided by JHU-083 compared to DON.

5.6 Stable isotope metabolomics suggests that DON inhibits glutamine synthetase

To investigate the mechanism of DON's activity in MYC-driven medulloblastoma tumors, we performed stable isotope labeled metabolic analysis. For this study, nude mice with established D425Med flank tumors were given one 30mg/kg dose of DON or vehicle prior to being injected with uniformly-labeled glucose ($^{13}C_6$-glucose), uniformly labeled glutamine ($^{13}C_5$-$^{15}N_2$-glutamine), or vehicle (PBS). Metabolites extracted from the tumors were analyzed using LC-MS. We predicted that we would find decreased levels of glutamate in tumors from animals treated with DON. Contrary to this predication, we found that glutamate levels remained unchanged in tumors treated with DON, suggesting that DON's primary mechanism of action in D425Med tumors is not inhibiting GLS activity (Figure 17A).

Tumors from animals treated with DON had lower levels of glutamine than tumors from vehicle treated animals (Figure 15B). There are several explanations for this result. DON could be inhibiting a glutamine transporter such as ASCT2, or the activity of glutamine synthetase. In DON treated tumors from animals injected with uniformly labeled glucose, we observe a significant decrease in the amount of M+2 glutamate isotopologue ($p=0.000068$ by Student's t-test, Figure 15C). In the $^{13}C_6$-glucose-labeled tumors, the C13 carbons in the M+2 glutamate isotopologue are coming from glucose entering the TCA cycle in the form of citrate, which is converted to α-ketoglutarate, which is converted to glutamate (Figure 15E). We also observe a significant decrease in the M+2 glutamine isotopologue in tumors from DON treated animals labeled with uniformly-labeled glucose ($p=0.000004$ by Student's t-test, Figure 15D). The M+2 glutamine is generated by the enzyme glutamine synthetase from M+2 glutamate (Figure

15E). The reduction in M+2 glutamate and M+2 glutamine in tumors from animals treated with DON and subjected to stable isotope labeling with $^{13}C_6$-glucose suggests that glutamine synthetase activity is being inhibited by DON.

5.7 Stable isotope labeling suggests that DON is inhibiting asparagine synthetase

Tumors from animals treated with DON had decreased levels of the amino acid asparagine (Figure 16A). Comparing vehicle treated and DON treated tumors from animals labeled $^{13}C_5$-$^{15}N_2$-glutamine revealed a significant decrease in the level of M+1 asparagine compared to tumors from vehicle treated $^{13}C_5$-$^{15}N_2$-glutamine labeled tumors ($p=0.016$ by Student's t-test, Figure 16B). The enzyme asparagine synthetase (ASNS) catalyzes the creation of asparagine by joining a nitrogen donated from glutamine to aspartate and is a known target of DON (118, 122). In tumors labeled with $^{13}C_5$-$^{15}N_2$-glutamine, the M+1 asparagine isotopologue is created when an N15 from $^{13}C_5$-$^{15}N_2$-glutamine is added to aspartate (Figure 16C). The decrease in the M+1 asparagine in DON-treated $^{13}C_5$-$^{15}N_2$-glutamine labeled tumors indicates that ASNS activity is being inhibited by DON.

We also observed a significant reduction in M+2 asparagine isotopologue levels in tumors from animals treated with DON and labeled with $^{13}C_6$-glucose compared to tumors from vehicle treated, $^{13}C_6$-glucose labeled mice ($p=3.7x10^{-9}$ by Student's t-test, Figure 16D), further suggesting that ASNS is being inhibited. In the case of $^{13}C_6$-glucose labeled tumors, the M+2 asparagine isotopologue is generated when the $^{13}C_6$-glucose is broken down into $^{13}C_2$-acetyl co-A and enters the TCA cycle. This $^{13}C_2$-acetyl-CoA is eventually converted to $^{13}C_2$-oxaloacetate, which is converted into $^{13}C_2$-aspartate by the

enzyme aspartate transaminase. The resulting $^{13}C_2$-aspartate is converted into asparagine by ASNS generating M+2 asparagine. (Figure 16E). If asparagine synthesis was being affected at an earlier point, we would expect to observe changes in M+2 aspartate, but there was no difference in the level of M+2 aspartate in DON treated-$^{13}C_6$-glucose labeled tumors and vehicle treated-$^{13}C_6$-glucose labeled tumors ($p=0.40$ by Student's t-test, Figure 16F). Asparagine can also be generated by bypassing the TCA cycle when pyruvate is converted by pyruvate carboxylase into oxaloacetate rather than acetyl-CoA. This oxaloacetate can be converted into aspartate and then asparagine. If this reaction was occurring, we would see M+3 asparagine in $^{13}C_6$-glucose labeled tumors (Figure 16E). There was no detectable M+3 asparagine in either DON or vehicle treated $^{13}C_6$-glucose labeled tumors, indicating low pyruvate carboxylase activity in our tumors.

5.8 DON and asparaginase can be combined for enhanced anti-tumor activity

Since we found that DON depletes asparagine levels in D425Med tumors (Figure 16), we decided to test it in combination with asparaginase. Asparaginase (ASNase) is an enzyme that breaks down asparagine into aspartate. Clinically, it is used to treat acute lymphoblastic leukemia, non-Hodgkin's lymphoma, and other hematologic malignancies (160). In D425Med medulloblastoma cells, a combination of ASNase and DON was more effective at reducing growth than either drug line alone (Figure 17A). The combination of DON and ASNase increased the percentage of cleaved caspase-3 positive cells more than either drug alone in D425Med cells—an average of 6% cleaved caspase-3 positive cells in vehicle treated cells, 16% in DON treated cells, 5% in ASNase treated cells, and 23% in combination treated cells (Figure 17B, vehicle vs combination treated

p=0.015 by Student's t-test). In human neural stem cells transformed wit MYC, the combination treatment increased the percentage of cleaved caspase-3 cells more than either drug alone—an average of 21% in vehicle treated cells, 21% in DON treated cells, 17% in ASNase treated cells and 33% in combination treated cells (Figure 17C). In human neural stem cells transformed with MYC, DNp53, hTERT and AKT the combination therapy was particularly effective. The average percent cleaved caspase-3 positive cells was 9% in vehicle treated cells, 15% in DON treated cells, 15% in ASNase treated cells, and 64% in combination treated cells (Figure 17D, vehicle vs combination treated p=0.00006 by Student's t-test). The increased efficacy of the DON and asparaginase therapy is most likely due to DON and ASNase working in concert to drastically deplete asparagine levels.

CHAPTER 6: DISCUSSION

Another therapeutic target presented in this dissertation is glutamine metabolism. Multiple cancers are thought to have aberrant glutamine metabolism (76-81), and inhibiting glutaminase is an attractive therapeutic option in MYC-driven medulloblastoma. The glutamine analogs DON and Acivicin are known to inhibit a variety of glutamine utilizing enzymes, including GLS and those involved in nucleic acid biosynthesis (118-122, 130-136). Inhibiting glutamine metabolism at multiple levels with either DON or Acivicin may lead to a decreased likelihood of developing resistance. Additionally, these drugs could be used as part of personalized therapy for patients with Group 3 tumors in association with chemotherapy and radiation

Because neurons use GLS to synthesize glutamate for use as a neurotransmitter, there is concern that glutaminase inhibitors may cause neurotoxicity. Phase I pediatric clinical trials of Acivicin reported somnolence and nightmares as a major side effect – however these were moderate and reversible after stopping treatment (148). The lack of toxicity of DON and Acivicin against normal human neural stem cells and SV40-immortalized cells suggests that the normal cells of the pediatric brain would not be harmed by DON or Acivicin treatment and the drugs will selectively kill tumor cells. The most serious side effect in phase I trials of DON and Acivicin was myelosuppression. Other side effects, like nausea and vomiting, were easily managed and all symptoms resolved after the cessation of therapy (129, 148). The maximum tolerated dose for DON was never reached in a pediatric oncology phase I trial, suggesting that there is significant therapeutic index for this drug (129). In the Acivicin

trial, of the eight pediatric patients with brain tumors who were enrolled, three had stable disease at the cessation of the trial (148).

Based on the pre-clinical data presented here, we believe these compounds will be most successful against MYC-dependent cancers. Another concern with systemically delivered drugs is their ability to penetrate the blood-brain barrier. The CNS side-effects of somnolence and nightmares suggest that the drugs successfully penetrate the blood-brain barrier. DON and Acivicin have been shown to have affinity for and are ligands of the Large-neutral Amino Acid Transporter, a transporter highly expressed in the BBB (156-158). This evidence suggests that Acivicin and DON are transported across the blood-brain barrier. Though unmodified DON is capable of crossing the blood brain barrier, Johns Hopkins Drug Discovery has been developing orally available, pro-drug versions of DON that enhance brain delivery (159). The pro-drug form of DON JHU-083 was demonstrated here to have efficacy in medulloblastoma. Pro-drug versions of DON with improved brain penetration could further enhance DON's clinical utility.

Providing additional support for the role of glutamine metabolism in medulloblastoma is the finding that high levels of glutamate in medulloblastoma tumors as measured *in vivo* by magnetic resonance spectroscopy (MRS) are associated with decreased survival (104). Increased levels of glutamate in high risk medulloblastoma suggest activity of and potential sensitivity to glutamine anti-metabolites such as DON or Acivicin. MRI spectroscopy may represent a potential non-invasive method for identifying patients who could benefit from glutamine metabolism inhibition.

Using stable isotope metabolomics we determined that in D425Med medulloblastoma tumors, DON is most likely acting through inhibition of glutamine

synthetase and asparagine synthetase. The enzyme asparaginase reduces asparagine levels by converting asparagine into aspartate and ammonia and is used clinically for hematologic malignancies. We found that the in our medulloblastoma models, the combination of DON and asparaginase increased apoptosis more than either compound alone, presumably because of an even larger decrease in asparagine levels. This data is consistent with previous work by Zhang et al, which showed depletion of asparagine led to increased apoptosis. They found that when asparagine levels are low, the ATF4 protein interacts with CHOP and XBP1 to trigger apoptosis (97). We predict that the combination of DON and asparaginase would increase survival more than either compound alone in animals bearing MYC-driven medulloblastoma tumors. Though the *in vivo* studies have yet be conducted, the *in vitro* data presented here is very encouraging and further investigation into this drug combination is warranted.

In conclusion, this dissertation presents data that shows that glutamine analogs have efficacy in *in vitro* and *in vivo* models of Group 3 medulloblastoma. This data provides preclinical justification for the testing of DON therapy in carefully selected medulloblastoma patients.

CHAPTER 7: METHODS

7.1 Generation of a Cerebellar Neural Stem and Progenitor Cell Model of Group 3/C1 Medulloblastoma

Human cerebellar neural stem cells were derived as described (46). Human neural stem and progenitor cells were obtained in concordance with German law and Ethics Board evaluation. The study was also approved by the Johns Hopkins Institutional Review Board. The cells were obtained by dissecting the cerebellar anlage and then culturing as neurospheres. The neural stem and progenitor neurospheres were transduced using lentiviral and retroviral vectors carrying genetic elements of interest. R248W-TP53 (Addgene plasmid 16437) and MYC (Addgene plasmid 17758) were subcloned into pWPI (Addgene 12254) (161). For hTERT, Addgene plasmid 12245 was used. The SV40 plasmid is described in Raabe et al (162). For constitutively active AKT, the retroviral Addgene plasmid 15294 was used. Lentivirus was produced by transfecting 293T cells with VSV-G envelope plasmid, Δ8.9 gag/pol plasmid and the plasmid containing the gene of interest as described in (162) using FuGene (Roche) per manufacturer's instruction. Retrovirus was produced by transfecting 293T-GP cells with VSV-G plasmid and the plasmid containing the gene of interest. 24 hours post transfection, 293T cells were switched to EGF-FGF media and the supernatant was collected at 48 and 72h. The collected supernatant was filtered with a 0.45 micron filter and stored at -80C until use.

Cerebellar neural stem cells were dissociated using Accutase (Sigma) and gentle trituration, then incubated with viral MYC; SV40; or MYC, hTERT and DNp53 viral supernatants for 24 hours. After approximately one week in culture, spheres were

identified and individually placed into wells of 96-well plates. After visually verifying that only a single sphere was in each well, the spheres were broken into single cells by trituration and expanded. Expression of the introduced oncogenes was verified by western blot and qPCR. Cells successfully transduced with MYC, hTERT and DNp53 were then incubated with AKT viral supernatant for 24 hours. The cells were then placed under puromycin selection for 72 hours, following which sub-clones were generated as described above.

7.2 Cell Culture

The neural stem cell lines grow as neurospheres in media composed of 30% Ham's F12, 70% DMEM, 1% antibiotic antimycotic, 20% B27 supplement, 5ug/mL heparin, 20ng/mL EGF, and 20ng/mL FGF2. Lines transformed with AKT are grown under 0.2ug/mL puromycin selection. The human medulloblastoma cell lines D425Med and D238Med were both established at Duke University (163). D283Med is available through ATCC. Both lines are cultured in MEM media supplemented with 10% FBS. All cells were verified to be mycoplasma free by PCR testing. Cell line identity testing by STR DNA profiling was performed by the Johns Hopkins Genetic Resources Core Facility.

7.3 Histology

Brains were removed from mice immediately following euthanasia and fixed in 10% buffered formalin. The brains were processed and H&E slides prepared by the Johns Hopkins Pathology Reference Lab.

7.4 Immunohistochemistry/Tissue Microarray

IHC was performed on deparaffinized sections of brain xenografts as described (161). The following primary antibodies were used: human specific NESTIN (1:500; Millipore, #MAB5326); GFAP (1:1000; DAKO #Z0334); MAP2 (Santa Cruz #20172); MYC (1:300, Epitomics #14721); phospho-AKT (1:50, Cell Signaling Technologies); TP-53 (Sigma, #BP-5312), and phospho-RB (1:250, Cell Signaling Technologies #D20B12). For the TMA of 65 primary medulloblastoma samples, IHC was performed on deparaffinized arrays followed by antigen retrieval, using MYC, phospho-AKT, and GLS antibodies at dilutions of 1:300, 1:70, and 1:50, respectively. The GLS antibody is from ProteinTech (#12855-1-AP), respectively. The array was stained for TP53 by Johns Hopkins Clinical Pathology following a Ventana F standard protocol. The TMA was scored by intensity (scale of 0 to 2) and percentage stained; an H-score was calculated by multiplying intensity by percentage of cells positive.

7.5 Gene Expression Analysis

RNA was extracted from cells and xenograft tumors using TRIZOL according to manufacturer's directions. RNA was assessed for quality and integrity using a Bioanalyzer (Agilent Technologies) and samples had a RNA Integrity Number score of higher than 8.2 (164). Gene expression data was generated using Affymetrix High Throughput (HT) U1332+ Chip (Santa Clara, CA) according to manufacturer's guidelines. Raw data was processed and analyzed using GenePattern as previously described (14, 165). The dataset is available as dataset GSE77475 at GEO (Gene Expression Omnibus**).**

7.6 DiSCoVER Analysis Method

The main analysis components of DiSCoVER are shown in Figure 18. The murine xerographs of human neural stem cells transformed with DNp53, hTERT, AKT and MYC (hNSC G3) and controls were profiled using Affymetrix arrays (see Gene expression analysis above). The gene probe identifiers were mapped into gene symbols using the *Collapse Dataset* tool ("max probe") of the GSEA software (166). The top 150 up-regulated genes between the murine xenographs of transformed hNSC G3 samples and controls were used to create an hNSC G3 oncogenic transcriptional signature (Table 1). We used this gene set to project two large mRNA expression datasets, The Cancer Cell Line Encyclopedia (CCLE) (167) and the Sanger Dataset (168). This projection is made using single-sample GSEA (169) to produce enrichment profiles of the hNSC G3 signature in each sample of those datasets. Once this projection is completed we match the signature profile vs. drug sensitive profiles corresponding to drug sensitivity datasets: The Cancer Therapeutics Response Portal (CTRP v2) (170), the CCLE Pharmacological Profiling Drug Data (167); and The Genomics of Drug Sensitivity in Cancer (168). Therefore there are three comparisons we performed between the transcriptional profile of the hNSC G3 signature and the drug sensitivity profiles (see Figures 18 and 19, Comparison I, II and III). There are only two mRNA datasets because the CCLE and CTRP v2 sensitivity datasets share the same mRNA samples. The matching scores between the signature, and each drug sensitivity profile, were computed using the Information Coefficient (IC), an information theoretic-measure of association, similar to the measure of association we used in Abazeed *et al.* 2013 (171) to compare radiation sensitivity vs. pathway expression. Once we obtained the matching scores of each drug against the hNSC G3 signature, we performed a permutation test on the signature profile

with 10,000 permutations. These values are used to create an empirical null distribution from which nominal p-values and False Discovery Rates (FDR) (172) are computed.

We focus in the top scoring compounds with FDR below 0.33 in the three comparisons and look for overlaps in compounds or compound classes (Tables 2-4). This is the way we noticed the appearance of CDK inhibitors for each dataset (Figure 4B and Figure 19). In Figure 19 we show that CDK inhibitors are top hits in the 3 drug sensitivity datasets by plotting the Information score (IC) in the y-axis and the correlation coefficient (between signature and drugs) in the x-axis. This comparison of correlation vs. information coefficients provides supplementary information about how linear or non-linear is the relationship between the signature and a given drug. The DiSCoVER method will be made publicly available as an analysis module in GenePattern (www.genepattern.org).

7.7 *In vitro* Drug Treatments

Palbociclib and flavopiridol were purchased from Sellekchem and diluted according to manufacturer's instructions. DON and Acivicin were purchased from Sigma and Bachem and diluted according to manufacturer's instructions.

7.8 BrdU Incorporation Assay

Cells were pulsed with 100 uM of bromodeoxyuridine (BrdU) for the last 6 hours of drug treatment then fixed in cytospin fluid and spun onto glass slides using a cytocentrifuge. Cells were permeabilized in 0.1% Triton X, DNA denatured in 2N HCl, blocked in 5% normal goat serum, and incubated with anti-BrdU antibody diluted 1:500

(Sigma, clone BU-33), followed by secondary antibody conjugated to Cy3 diluted 1:500 (Jackson ImmunoResearch). DAPI was used as a counterstain. Three DAPI and the corresponding Cy3 images were taken for each slide. The number of DAPI and Cy3 positive cells were counted using Adobe® Photoshop®. For each pair of images, the percent of Cy3 positive cells was calculated. The average Cy3 positivity was determined by calculating the average of at least three pairs of images for each treatment. Images were blinded before counting.

7.9 Cleaved Caspase-3 Immunofluorescence

Following drug treatment, cells were fixed in cytospin fluid and spun onto glass slides using a cytocentrifuge. Cells are permeabilized in 0.1% TritonX, blocked in 5% normal goat serum, and incubated with anti-cleaved caspase 3 antibody diluted 1:400 (Cell Signaling Technology®, clone 5A1E), followed by a secondary antibody conjugated to Cy3 diluted 1:500 (Jackson ImmunoResearch). Cells were scored for apoptosis similarly to the method used for BrdU incorporation.

7.10 Western Blot

Protein was extracted by lysing cell pellets with RIPA buffer and quantified using a Bradford Assay. Protein samples were run on 4 to 12% Bis-Tris gels. Antibodies against GAPDH (6C5: sc-32233), Actin (C4: sc-47778) and MYC (9E10: sc-40) were obtained from Santa Cruz Biotechnology®. Antibodies for GFAP (#3670), total Rb (#9309), Phospho-Rb Ser780 (#8180), Phospho-Rb Ser807/811 (#8516), and cleaved-PARP (#5625) are from Cell Signaling Technology. The Nestin (10C2, MAB5326) and

SOX2 antibodies are from Millipore. The GLS antibody is from ProteinTech (#12855-1-AP). The following antibody dilutions were used: GAPDH (1:1000), Actin (1:1000), MYC (1:1000), GFAP (1:2000), Sox2 (1:200), Nestin (1:1000), total Rb (1:1000), phospho-Rb Ser780 (1:1000), phospho-Rb Ser807/811 (1:1000), cleaved-PARP (1:800), GLS (1:1000) Peroxidase labeled secondary antibodies were diluted 1:5000 and are from KPL or Cell Signaling Technologies.

7.11 Metabolomics

Flank tumors were flash frozen in liquid nitrogen immediately after animal euthanasia. Tumors were manually homogenized in liquid nitrogen using a mortar and pestle chilled by dry ice and liquid nitrogen. Tumors and the resulting homogenized powder were kept chilled on dry ice at all times. As the flank tumors were very large, an aliquot of tumor powdered was weighed and the extraction performed on the aliquot. Samples were incubated at -80C with 5 volumes of 80% ice-cold HPLC grade methanol to extract metabolites. Before LC/MS analysis, samples were spun down at top speed in a chilled centrifuge to prevent protein contamination.

After extraction, samples were analyzed using an Agilent 6550 Q-TOF with a Waters Acquity UPLC. Data analysis was performed using MAVEN, an open-source metabolomics software program developed at Princeton (173, 174). Isotopomer distribution was determined as percent incorporation into the entire metabolite pool minus naturally occurring isotopes.

7.12 Quantification of DON

The concentration of DON in plasma was determined as described in Rais et al (159).

7.13 *In vivo* studies

7.13a Orthotopic xenograft procedure

All xenografting was conducted in female nude (Nu/Nu) mice at approximately 6 weeks of age from Charles River Labs. Prior to implantation of cells, animals were anesthetized using a mixture of 10% ketamine and 5% xylazine. For orthotopic xenografts, the scalp was opened with a sterile blade and a burr hole was made in the skull 1mm to the right and 2 mm posterior of the lambdoid suture with an 18 gauge needle. The needle of a Hamilton syringe was inserted 2mm into the brain using a stereotactic guide and 100,000 cells in 2 to 5uL of media were injected into the cerebellum. After the cells were injected, the scalp incision was closed with sutures.

7.13b Flank xenograft procedure

All xenografting was conducted in female nude (Nu/Nu) mice at approximately 6 weeks of age from Charles River Labs. Prior to injection, animals were anesthetized with a mixture of 10% ketamine and 5% xylazine. One million cells suspended in 200uL of a 50:50 mix of Matrigel (Corning) and media were injected for each flank tumor. Cells were injected using an 18 gauge needle. One tumor was implanted behind each limb, so each mouse carried four flank tumors. All animals were monitored daily. Flank tumors were measured while mice were lightly anesthetized using digital calipers and tumor volume calculated using the formula $width^2 \times length \times 0.52$ (11).

7.13c Drug treatments

Palbociclib was prepared in a pH 4.0 50mM sodium lactate solution and administered by oral gavage in a 100uL bolus. Animals received a 150mg/kg dose 5x a week, which is a widely used dosing schedule in pre-clinical murine xenograft models (56, 59, 60, 69). DON and Acivicin were obtained from Sigma and Bachem, prepared in PBS and administered as a 300uL IP injection. For DON, animals received 30mg/kg dose once per week. For Acivicin, animals received 25 or 75mg/kg doses four times a week. All animals were monitored daily. Symptomatic animals were euthanized and their brains or flank tumors removed and fixed in formalin.

7.13d Stable isotope labeling procedure

One hour prior to labeling, animals were give a single 30mg/kg dose of DON. Uniformly labeled glutamine was prepared at a 100uM concentration in PBS and uniformly labeled glucose was prepared as a 20% solution in PBS. Animals were given three 100uL IP injections of isotope spaced 15 minutes apart. Euthanasia occurred two hours after second isotope injection. At the time of euthanasia blood was collected by cardiac puncture. Tumors were immediately removed and flash frozen in liquid nitrogen. The final blood sample was spun down in a chilled (4C) centrifuge at 3,500g for 15 minutes to separate red blood cells from plasma. The plasma was flash frozen in liquid nitrogen. All uniformly labeled isotopes were obtained from Cambridge Isotope Labs.

7.13e Study Approval

For animal care and anesthesia, "Principles of laboratory animal care" (NIH publication No. 8623, revised 1985) was followed, using a protocol approved by the Johns Hopkins

Animal Care and Use Committee, in compliance with the United States Animal Welfare Act regulations and Public Health Service Policy

REFERENCES

References

1. Ward EP, DeSantis CMPH, Robbins AMDP, Kohler BMPH, Jemal ADVMP. Childhood and adolescent cancer statistics, 2014. Ca : a Cancer Journal for Clinicians. 2014; 64: 83.

2. Adamski J, Ramaswamy V, Huang A, Bouffet E. Advances in managing medulloblastoma and intracranial primitive neuro-ectodermal tumors. F1000Prime Rep. 2014; 6: 56.

3. Weil AG, Wang AC, Westwick HJ, Ibrahim GM, Ariani RT, Crevier L, et al. Survival in pediatric medulloblastoma: a population-based observational study to improve prognostication. J Neurooncol. 2016;

4. King AA, Seidel K, Di C, Leisenring WM, Perkins SM, Krull KR, et al. Long-term neurologic health and psychosocial function of adult survivors of childhood medulloblastoma/PNET: a report from the Childhood Cancer Survivor Study. Neuro Oncol. 2016;

5. Ellenberg L, Liu Q, Gioia G, Yasui Y, Packer RJ, Mertens A, et al. Neurocognitive status in long-term survivors of childhood CNS malignancies: a report from the Childhood Cancer Survivor Study. Neuropsychology. 2009; 23: 705-17.

6. Wells EM, Khademian ZP, Walsh KS, Vezina G, Sposto R, Keating RF, et al. Postoperative cerebellar mutism syndrome following treatment of medulloblastoma: neuroradiographic features and origin. J Neurosurg Pediatr. 2010; 5: 329-34.

7. Bowers DC, Liu Y, Leisenring W, McNeil E, Stovall M, Gurney JG, et al. Late-occurring stroke among long-term survivors of childhood leukemia and brain tumors: a report from the Childhood Cancer Survivor Study. J Clin Oncol. 2006; 24: 5277-82.

8. Ricardi U, Corrias A, Einaudi S, Genitori L, Sandri A, di Montezemolo LC, et al. Thyroid dysfunction as a late effect in childhood medulloblastoma: a comparison of hyperfractionated versus conventionally fractionated craniospinal radiotherapy. Int J Radiat Oncol Biol Phys. 2001; 50: 1287-94.

9. Friedman DL, Whitton J, Leisenring W, Mertens AC, Hammond S, Stovall M, et al. Subsequent neoplasms in 5-year survivors of childhood cancer: the Childhood Cancer Survivor Study. J Natl Cancer Inst. 2010; 102: 1083-95.

10. Northcott PA, Korshunov A, Pfister SM, Taylor MD. The clinical implications of medulloblastoma subgroups. Nat Rev Neurol. 2012; 8: 340-51.

11. Stearns D, Chaudhry A, Abel TW, Burger PC, Dang CV, Eberhart CG. c-myc overexpression causes anaplasia in medulloblastoma. Cancer Res. 2006; 66: 673-81.

12. Eberhart CG, Kratz J, Wang Y, Summers K, Stearns D, Cohen K, et al. Histopathological and molecular prognostic markers in medulloblastoma: c-myc, N-myc, TrkC, and anaplasia. J Neuropathol Exp Neurol. 2004; 63: 441-9.

13. Pfister S, Remke M, Benner A, Mendrzyk F, Toedt G, Felsberg J, et al. Outcome prediction in pediatric medulloblastoma based on DNA copy-number aberrations of chromosomes 6q and 17q and the MYC and MYCN loci. J Clin Oncol. 2009; 27: 1627-36.

14. Cho YJ, Tsherniak A, Tamayo P, Santagata S, Ligon A, Greulich H, et al. Integrative genomic analysis of medulloblastoma identifies a molecular subgroup that drives poor clinical outcome. J Clin Oncol. 2011; 29: 1424-30.

15. Northcott PA, Korshunov A, Witt H, Hielscher T, Eberhart CG, Mack S, et al. Medulloblastoma comprises four distinct molecular variants. J Clin Oncol. 2011; 29: 1408-14.

16. Kool M, Korshunov A, Remke M, Jones DT, Schlanstein M, Northcott PA, et al. Molecular subgroups of medulloblastoma: an international meta-analysis of transcriptome, genetic aberrations, and clinical data of WNT, SHH, Group 3, and Group 4 medulloblastomas. Acta Neuropathol. 2012; 123: 473-84.

17. Northcott PA, Jones DT, Kool M, Robinson GW, Gilbertson RJ, Cho YJ, et al. Medulloblastomics: the end of the beginning. Nat Rev Cancer. 2012; 12: 818-34.

18. Phoenix TN, Patmore DM, Boop S, Boulos N, Jacus MO, Patel YT, et al. Medulloblastoma Genotype Dictates Blood Brain Barrier Phenotype. Cancer Cell. 2016; 29: 508-22.

19. Northcott PA, Shih DJ, Peacock J, Garzia L, Morrissy AS, Zichner T, et al. Subgroup-specific structural variation across 1,000 medulloblastoma genomes. Nature. 2012; 488: 49-56.

20. Zhukova N, Ramaswamy V, Remke M, Pfaff E, Shih DJ, Martin DC, et al. Subgroup-specific prognostic implications of TP53 mutation in medulloblastoma. J Clin Oncol. 2013; 31: 2927-35.

21. Badiali M, Pession A, Basso G, Andreini L, Rigobello L, Galassi E, et al. N-myc and c-myc oncogenes amplification in medulloblastomas. Evidence of particularly aggressive behavior of a tumor with c-myc amplification. Tumori. 1991; 77: 118-21.

22. Pei Y, Moore CE, Wang J, Tewari AK, Eroshkin A, Cho YJ, et al. An animal model of MYC-driven medulloblastoma. Cancer Cell. 2012; 21: 155-67.

23. Kawauchi D, Robinson G, Uziel T, Gibson P, Rehg J, Gao C, et al. A mouse model of the most aggressive subgroup of human medulloblastoma. Cancer Cell. 2012; 21: 168-80.

24. Rusert JM, Wu X, Eberhart CG, Taylor MD, Wechsler-Reya RJ. SnapShot: Medulloblastoma. Cancer Cell. 2014; 26: 940- e1.

25. Gibson P, Tong Y, Robinson G, Thompson MC, Currle DS, Eden C, et al. Subtypes of medulloblastoma have distinct developmental origins. Nature. 2010; 468: 1095-9.

26. Gilbertson RJ, Ellison DW. The origins of medulloblastoma subtypes. Annu Rev Pathol. 2008; 3: 341-65.

27. Lin CY, Erkek S, Tong Y, Yin L, Federation AJ, Zapatka M, et al. Active medulloblastoma enhancers reveal subgroup-specific cellular origins. Nature. 2016; 530: 57-62.

28. Ivanov DP, Coyle B, Walker DA, Grabowska AM. In vitro models of medulloblastoma: Choosing the right tool for the job. J Biotechnol. 2016; 236: 10-25.

29. Lee J, Kotliarova S, Kotliarov Y, Li A, Su Q, Donin NM, et al. Tumor stem cells derived from glioblastomas cultured in bFGF and EGF more closely mirror the phenotype and genotype of primary tumors than do serum-cultured cell lines. Cancer Cell. 2006; 9: 391-403.

30. Zhao X, Liu Z, Yu L, Zhang Y, Baxter P, Voicu H, et al. Global gene expression profiling confirms the molecular fidelity of primary tumor-based orthotopic xenograft mouse models of medulloblastoma. Neuro Oncol. 2012; 14: 574-83.

31. Goodrich LV, Milenkovic L, Higgins KM, Scott MP. Altered neural cell fates and medulloblastoma in mouse patched mutants. Science. 1997; 277: 1109-13.

32. Wetmore C, Eberhart DE, Curran T. Loss of p53 but not ARF accelerates medulloblastoma in mice heterozygous for patched. Cancer Res. 2001; 61: 513-6.

33. Ayrault O, Zindy F, Rehg J, Sherr CJ, Roussel MF. Two tumor suppressors, p27Kip1 and patched-1, collaborate to prevent medulloblastoma. Mol Cancer Res. 2009; 7: 33-40.

34. Uziel T, Zindy F, Xie S, Lee Y, Forget A, Magdaleno S, et al. The tumor suppressors Ink4c and p53 collaborate independently with Patched to suppress medulloblastoma formation. Genes Dev. 2005; 19: 2656-67.

35. Yang ZJ, Ellis T, Markant SL, Read TA, Kessler JD, Bourboulas M, et al. Medulloblastoma can be initiated by deletion of Patched in lineage-restricted progenitors or stem cells. Cancer Cell. 2008; 14: 135-45.

36. Wu X, Northcott PA, Croul S, Taylor MD. Mouse models of medulloblastoma. Chin J Cancer. 2011; 30: 442-9.

37. Swartling FJ, Savov V, Persson AI, Chen J, Hackett CS, Northcott PA, et al. Distinct neural stem cell populations give rise to disparate brain tumors in response to N-MYC. Cancer Cell. 2012; 21: 601-13.

38. Weiner HL, Bakst R, Hurlbert MS, Ruggiero J, Ahn E, Lee WS, et al. Induction of medulloblastomas in mice by sonic hedgehog, independent of Gli1. Cancer Res. 2002; 62: 6385-9.

39. Rao G, Pedone CA, Del Valle L, Reiss K, Holland EC, Fults DW. Sonic hedgehog and insulin-like growth factor signaling synergize to induce medulloblastoma formation from nestin-expressing neural progenitors in mice. Oncogene. 2004; 23: 6156-62.

40. Browd SR, Kenney AM, Gottfried ON, Yoon JW, Walterhouse D, Pedone CA, et al. N-myc can substitute for insulin-like growth factor signaling in a mouse model of sonic hedgehog-induced medulloblastoma. Cancer Res. 2006; 66: 2666-72.

41. Rao G, Pedone CA, Coffin CM, Holland EC, Fults DW. c-Myc enhances sonic hedgehog-induced medulloblastoma formation from nestin-expressing neural progenitors in mice. Neoplasia. 2003; 5: 198-204.

42. Hamad NM, Elconin JH, Karnoub AE, Bai W, Rich JN, Abraham RT, et al. Distinct requirements for Ras oncogenesis in human versus mouse cells. Genes Dev. 2002; 16: 2045-57.

43. Boehm JS, Hession MT, Bulmer SE, Hahn WC. Transformation of human and murine fibroblasts without viral oncoproteins. Mol Cell Biol. 2005; 25: 6464-74.

44. Poschl J, Stark S, Neumann P, Grobner S, Kawauchi D, Jones DT, et al. Genomic and transcriptomic analyses match medulloblastoma mouse models to their human counterparts. Acta Neuropathol. 2014; 128: 123-36.

45. Parsons DW, Li M, Zhang X, Jones S, Leary RJ, Lin JC, et al. The genetic landscape of the childhood cancer medulloblastoma. Science. 2011; 331: 435-9.

46. Lopez WO, Nikkhah G, Kahlert UD, Maciaczyk D, Bogiel T, Moellers S, et al. Clinical neurotransplantation protocol for Huntington's and Parkinson's disease. Restor Neurol Neurosci. 2013; 31: 579-95.

47. Frank AJ, Hernan R, Hollander A, Lindsey JC, Lusher ME, Fuller CE, et al. The TP53-ARF tumor suppressor pathway is frequently disrupted in large/cell anaplastic medulloblastoma. Brain Res Mol Brain Res. 2004; 121: 137-40.

48. Eberhart CG, Chaudhry A, Daniel RW, Khaki L, Shah KV, Gravitt PE. Increased p53 immunopositivity in anaplastic medulloblastoma and supratentorial PNET is not caused by JC virus. BMC Cancer. 2005; 5: 19.

49. Mumert M, Dubuc A, Wu X, Northcott PA, Chin SS, Pedone CA, et al. Functional genomics identifies drivers of medulloblastoma dissemination. Cancer Res. 2012; 72: 4944-53.

50. Fan X, Wang Y, Kratz J, Brat DJ, Robitaille Y, Moghrabi A, et al. hTERT gene amplification and increased mRNA expression in central nervous system embryonal tumors. Am J Pathol. 2003; 162: 1763-9.

51. Killela PJ, Reitman ZJ, Jiao Y, Bettegowda C, Agrawal N, Diaz LA, Jr., et al. TERT promoter mutations occur frequently in gliomas and a subset of tumors derived from cells with low rates of self-renewal. Proc Natl Acad Sci U S A. 2013; 110: 6021-6.

52. Ramaswamy V, Remke M, Bouffet E, Faria CC, Perreault S, Cho YJ, et al. Recurrence patterns across medulloblastoma subgroups: an integrated clinical and molecular analysis. Lancet Oncol. 2013; 14: 1200-7.

53. Tamayo P, Cho YJ, Tsherniak A, Greulich H, Ambrogio L, Schouten-van Meeteren N, et al. Predicting relapse in patients with medulloblastoma by integrating evidence from clinical and genomic features. J Clin Oncol. 2011; 29: 1415-23.

54. Kaur G, Stetler-Stevenson M, Sebers S, Worland P, Sedlacek H, Myers C, et al. Growth inhibition with reversible cell cycle arrest of carcinoma cells by flavone L86-8275. J Natl Cancer Inst. 1992; 84: 1736-40.

55. Stanetty P, Hattinger G, Schnurch M, Mihovilovic MD. Novel and efficient access to phenylamino-pyrimidine type protein kinase C inhibitors utilizing a Negishi cross-coupling strategy. J Org Chem. 2005; 70: 5215-20.

56. Fry DW, Harvey PJ, Keller PR, Elliott WL, Meade M, Trachet E, et al. Specific inhibition of cyclin-dependent kinase 4/6 by PD 0332991 and associated antitumor activity in human tumor xenografts. Mol Cancer Ther. 2004; 3: 1427-38.

57. Mateyak MK, Obaya AJ, Sedivy JM. c-Myc regulates cyclin D-Cdk4 and -Cdk6 activity but affects cell cycle progression at multiple independent points. Mol Cell Biol. 1999; 19: 4672-83.

58. Ahuja D, Saenz-Robles MT, Pipas JM. SV40 large T antigen targets multiple cellular pathways to elicit cellular transformation. Oncogene. 2005; 24: 7729-45.

59. Barton KL, Misuraca K, Cordero F, Dobrikova E, Min HD, Gromeier M, et al. PD-0332991, a CDK4/6 inhibitor, significantly prolongs survival in a genetically engineered mouse model of brainstem glioma. PLoS One. 2013; 8: e77639.

60. Michaud K, Solomon DA, Oermann E, Kim JS, Zhong WZ, Prados MD, et al. Pharmacologic inhibition of cyclin-dependent kinases 4 and 6 arrests the growth of glioblastoma multiforme intracranial xenografts. Cancer Res. 2010; 70: 3228-38.

61. Weeraratne SD, Amani V, Teider N, Pierre-Francois J, Winter D, Kye MJ, et al. Pleiotropic effects of miR-183~96~182 converge to regulate cell survival, proliferation and migration in medulloblastoma. Acta Neuropathol. 2012; 123: 539-52.

62. Hill RM, Kuijper S, Lindsey JC, Petrie K, Schwalbe EC, Barker K, et al. Combined MYC and P53 defects emerge at medulloblastoma relapse and define rapidly progressive, therapeutically targetable disease. Cancer Cell. 2015; 27: 72-84.

63. Bretones G, Delgado MD, Leon J. Myc and cell cycle control. Biochim Biophys Acta. 2015; 1849: 506-16.

64. Goga A, Yang D, Tward AD, Morgan DO, Bishop JM. Inhibition of CDK1 as a potential therapy for tumors over-expressing MYC. Nat Med. 2007; 13: 820-7.

65. Campaner S, Doni M, Hydbring P, Verrecchia A, Bianchi L, Sardella D, et al. Cdk2 suppresses cellular senescence induced by the c-myc oncogene. Nat Cell Biol. 2010; 12: 54-9; sup pp 1-14.

66. Faria CC, Agnihotri S, Mack SC, Golbourn BJ, Diaz RJ, Olsen S, et al. Identification of alsterpaullone as a novel small molecule inhibitor to target group 3 medulloblastoma. Oncotarget. 2015; 6: 21718-29.

67. Turner NC, Ro J, Andre F, Loi S, Verma S, Iwata H, et al. Palbociclib in Hormone-Receptor-Positive Advanced Breast Cancer. N Engl J Med. 2015; 373: 209-19.

68. Whiteway SL, Harris PS, Venkataraman S, Alimova I, Birks DK, Donson AM, et al. Inhibition of cyclin-dependent kinase 6 suppresses cell proliferation and enhances radiation sensitivity in medulloblastoma cells. J Neurooncol. 2013; 111: 113-21.

69. Menu E, Garcia J, Huang X, Di Liberto M, Toogood PL, Chen I, et al. A novel therapeutic combination using PD 0332991 and bortezomib: study in the 5T33MM myeloma model. Cancer Res. 2008; 68: 5519-23.

70. Morfouace M, Shelat A, Jacus M, Freeman BB, 3rd, Turner D, Robinson S, et al. Pemetrexed and gemcitabine as combination therapy for the treatment of Group3 medulloblastoma. Cancer Cell. 2014; 25: 516-29.

71. Dean JL, McClendon AK, Knudsen ES. Modification of the DNA damage response by therapeutic CDK4/6 inhibition. J Biol Chem. 2012; 287: 29075-87.

72. Finn RS, Dering J, Conklin D, Kalous O, Cohen DJ, Desai AJ, et al. PD 0332991, a selective cyclin D kinase 4/6 inhibitor, preferentially inhibits proliferation of luminal estrogen receptor-positive human breast cancer cell lines in vitro. Breast Cancer Res. 2009; 11: R77.

73. Baughn LB, Di Liberto M, Wu K, Toogood PL, Louie T, Gottschalk R, et al. A novel orally active small molecule potently induces G1 arrest in primary myeloma cells and prevents tumor growth by specific inhibition of cyclin-dependent kinase 4/6. Cancer Res. 2006; 66: 7661-7.

74. Yang C, Boyson CA, Di Liberto M, Huang X, Hannah J, Dorn DC, et al. CDK4/6 Inhibitor PD 0332991 Sensitizes Acute Myeloid Leukemia to Cytarabine-Mediated Cytotoxicity. Cancer Res. 2015; 75: 1838-45.

75. Indovina P, Pentimalli F, Casini N, Vocca I, Giordano A. RB1 dual role in proliferation and apoptosis: cell fate control and implications for cancer therapy. Oncotarget. 2015; 6: 17873-90.

76. Gao P, Tchernyshyov I, Chang TC, Lee YS, Kita K, Ochi T, et al. c-Myc suppression of miR-23a/b enhances mitochondrial glutaminase expression and glutamine metabolism. Nature. 2009; 458: 762-5.

77. Wise DR, DeBerardinis RJ, Mancuso A, Sayed N, Zhang XY, Pfeiffer HK, et al. Myc regulates a transcriptional program that stimulates mitochondrial glutaminolysis and leads to glutamine addiction. Proc Natl Acad Sci U S A. 2008; 105: 18782-7.

78. Wise DR, Thompson CB. Glutamine addiction: a new therapeutic target in cancer. Trends Biochem Sci. 2010; 35: 427-33.

79. Dang CV. MYC, microRNAs and glutamine addiction in cancers. Cell Cycle. 2009; 8: 3243-5.

80. Dang CV. Therapeutic targeting of Myc-reprogrammed cancer cell metabolism. Cold Spring Harb Symp Quant Biol. 2011; 76: 369-74.

81. Dang CV, Hamaker M, Sun P, Le A, Gao P. Therapeutic targeting of cancer cell metabolism. J Mol Med (Berl). 2011; 89: 205-12.

82. Hanahan D, Weinberg RA. Hallmarks of cancer: the next generation. Cell. 2011; 144: 646-74.

83. Warburg O. On the origin of cancer cells. Science. 1956; 123: 309-14.

84. DeBerardinis RJ, Lum JJ, Hatzivassiliou G, Thompson CB. The biology of cancer: metabolic reprogramming fuels cell growth and proliferation. Cell Metab. 2008; 7: 11-20.

85. DeBerardinis RJ. Is cancer a disease of abnormal cellular metabolism? New angles on an old idea. Genet Med. 2008; 10: 767-77.

86. Warburg O. On respiratory impairment in cancer cells. Science. 1956; 124: 269-70.

87. Vander Heiden MG, Cantley LC, Thompson CB. Understanding the Warburg effect: the metabolic requirements of cell proliferation. Science. 2009; 324: 1029-33.

88. Ward PS, Thompson CB. Metabolic reprogramming: a cancer hallmark even warburg did not anticipate. Cancer Cell. 2012; 21: 297-308.

89. Lunt SY, Vander Heiden MG. Aerobic glycolysis: meeting the metabolic requirements of cell proliferation. Annu Rev Cell Dev Biol. 2011; 27: 441-64.

90. Hume DA, Weidemann MJ. Role and regulation of glucose metabolism in proliferating cells. J Natl Cancer Inst. 1979; 62: 3-8.

91. Daye D, Wellen KE. Metabolic reprogramming in cancer: unraveling the role of glutamine in tumorigenesis. Semin Cell Dev Biol. 2012; 23: 362-9.

92. McKeehan WL. Glycolysis, glutaminolysis and cell proliferation. Cell Biol Int Rep. 1982; 6: 635-50.

93. Zielke HR, Ozand PT, Tildon JT, Sevdalian DA, Cornblath M. Reciprocal regulation of glucose and glutamine utilization by cultured human diploid fibroblasts. J Cell Physiol. 1978; 95: 41-8.

94. DeBerardinis RJ, Mancuso A, Daikhin E, Nissim I, Yudkoff M, Wehrli S, et al. Beyond aerobic glycolysis: transformed cells can engage in glutamine metabolism that exceeds the requirement for protein and nucleotide synthesis. Proc Natl Acad Sci U S A. 2007; 104: 19345-50.

95. Liu W, Le A, Hancock C, Lane AN, Dang CV, Fan TW, et al. Reprogramming of proline and glutamine metabolism contributes to the proliferative and metabolic responses regulated by oncogenic transcription factor c-MYC. Proc Natl Acad Sci U S A. 2012; 109: 8983-8.

96. Yuneva M, Zamboni N, Oefner P, Sachidanandam R, Lazebnik Y. Deficiency in glutamine but not glucose induces MYC-dependent apoptosis in human cells. J Cell Biol. 2007; 178: 93-105.

97. Zhang J, Fan J, Venneti S, Cross JR, Takagi T, Bhinder B, et al. Asparagine plays a critical role in regulating cellular adaptation to glutamine depletion. Mol Cell. 2014; 56: 205-18.

98. Le A, Lane AN, Hamaker M, Bose S, Gouw A, Barbi J, et al. Glucose-independent glutamine metabolism via TCA cycling for proliferation and survival in B cells. Cell Metab. 2012; 15: 110-21.

99. Bhutia YD, Babu E, Ramachandran S, Ganapathy V. Amino Acid transporters in cancer and their relevance to "glutamine addiction": novel targets for the design of a new class of anticancer drugs. Cancer Res. 2015; 75: 1782-8.

100. Nicklin P, Bergman P, Zhang B, Triantafellow E, Wang H, Nyfeler B, et al. Bidirectional transport of amino acids regulates mTOR and autophagy. Cell. 2009; 136: 521-34.

101. Dimitrova V, Arcaro A. Targeting the PI3K/AKT/mTOR signaling pathway in medulloblastoma. Curr Mol Med. 2015; 15: 82-93.

102. Csibi A, Fendt SM, Li C, Poulogiannis G, Choo AY, Chapski DJ, et al. The mTORC1 pathway stimulates glutamine metabolism and cell proliferation by repressing SIRT4. Cell. 2013; 153: 840-54.

103. Stepulak A, Rola R, Polberg K, Ikonomidou C. Glutamate and its receptors in cancer. J Neural Transm (Vienna). 2014; 121: 933-44.

104. Wilson M, Gill SK, MacPherson L, English M, Arvanitis TN, Peet AC. Non-invasive detection of glutamate predicts survival in pediatric medulloblastoma. Clin Cancer Res. 2014;

105. Venneti S, Dunphy MP, Zhang H, Pitter KL, Zanzonico P, Campos C, et al. Glutamine-based PET imaging facilitates enhanced metabolic evaluation of gliomas in vivo. Sci Transl Med. 2015; 7: 274ra17.

106. Beroukhim R, Mermel CH, Porter D, Wei G, Raychaudhuri S, Donovan J, et al. The landscape of somatic copy-number alteration across human cancers. Nature. 2010; 463: 899-905.

107. Dang CV. MYC on the path to cancer. Cell. 2012; 149: 22-35.

108. Elgogary A, Xu Q, Poore B, Alt J, Zimmermann SC, Zhao L, et al. Combination therapy with BPTES nanoparticles and metformin targets the metabolic heterogeneity of pancreatic cancer. Proc Natl Acad Sci U S A. 2016; 113: E5328-36.

109. Chen L, Cui H, Fang J, Deng H, Kuang P, Guo H, et al. Glutamine deprivation plus BPTES alters etoposide- and cisplatin-induced apoptosis in triple negative breast cancer cells. Oncotarget. 2016; 7: 54691-701.

110. Wang JB, Erickson JW, Fuji R, Ramachandran S, Gao P, Dinavahi R, et al. Targeting mitochondrial glutaminase activity inhibits oncogenic transformation. Cancer Cell. 2010; 18: 207-19.

111. Han T, Guo M, Zhang T, Gan M, Xie C, Wang JB. A novel glutaminase inhibitor-968 inhibits the migration and proliferation of non-small cell lung cancer cells by targeting EGFR/ERK signaling pathway. Oncotarget. 2016;

112. Yuan L, Sheng X, Clark LH, Zhang L, Guo H, Jones HM, et al. Glutaminase inhibitor compound 968 inhibits cell proliferation and sensitizes paclitaxel in ovarian cancer. Am J Transl Res. 2016; 8: 4265-77.

113. Tanaka K, Sasayama T, Irino Y, Takata K, Nagashima H, Satoh N, et al. Compensatory glutamine metabolism promotes glioblastoma resistance to mTOR inhibitor treatment. J Clin Invest. 2015; 125: 1591-602.

114. Xie C, Jin J, Bao X, Zhan WH, Han TY, Gan M, et al. Inhibition of mitochondrial glutaminase activity reverses acquired erlotinib resistance in non-small cell lung cancer. Oncotarget. 2016; 7: 610-21.

115. Gross MI, Demo SD, Dennison JB, Chen L, Chernov-Rogan T, Goyal B, et al. Antitumor activity of the glutaminase inhibitor CB-839 in triple-negative breast cancer. Mol Cancer Ther. 2014; 13: 890-901.

116. Coffey GL, Ehrlich J, Fisher MW, Hillegas AB, Kohberger DL, Machamer HE, et al. 6-Diazo-5-oxo-L-norleucine, a new tumor-inhibitory substance. I. Biologic studies. Antibiot Chemother (Northfield Ill). 1956; 6: 487-97.

117. Dion HW, Fusari SA, Jakubowski ZL, Zora JG, Bartz QR. 6-Diazo-5-Oxo-L-Norleucine, a New Tumor-Inhibitory Substance .2. Isolation and Characterization. J Am Chem Soc. 1956; 78: 3075-7.

118. Pinkus LM. Glutamine binding sites. Methods Enzymol. 1977; 46: 414-27.

119. Levenberg B, Melnick I, Buchanan JM. Biosynthesis of the purines. XV. The effect of aza-L-serine and 6-diazo-5-oxo-L-norleucine on inosinic acid biosynthesis de novo. J Biol Chem. 1957; 225: 163-76.

120. Eidinoff ML, Knoll JE, Marano B, Cheong L. Pyrimidine Studies .1. Effect of Don (6-Diazo-5-Oxo-L-Norleucine) on Incorporation of Precursors into Nucleic Acid Pyrimidines. Cancer Res. 1958; 18: 105-9.

121. Barclay RK, Phillipps MA. Effects of 6-diazo-5-oxol-norleucine and other tumor inhibitors on the biosynthesis of nicotinamide adenine dinucleotide in mice. Cancer Res. 1966; 26: 282-6.

122. Rosenbluth RJ, Cooney DA, Jayaram HN, Milman HA, Homan ER. DON, CONV and DONV-II. Inhibition of L-'asparagine synthetase in vivo. Biochem Pharmacol. 1976; 25: 1851-8.

123. Wu F, Lukinius A, Bergstrom M, Eriksson B, Watanabe Y, Langstrom B. A mechanism behind the antitumour effect of 6-diazo-5-oxo-L-norleucine (DON): disruption of mitochondria. Eur J Cancer. 1999; 35: 1155-61.

124. Hiramoto K, Fujino T, Kikugawa K. DNA strand cleavage by tumor-inhibiting antibiotic 6-diazo-5-oxo-L-norleucine. Mutat Res. 1996; 360: 95-100.

125. Rahman A, Smith FP, Luc PT, Woolley PV. Phase I study and clinical pharmacology of 6-diazo-5-oxo-L-norleucine (DON). Invest New Drugs. 1985; 3: 369-74.

126. Earhart RH, Koeller JM, Davis HL. Phase I trial of 6-diazo-5-oxo-L-norleucine (DON) administered by 5-day courses. Cancer Treat Rep. 1982; 66: 1215-7.

127. Lynch G, Kemeny N, Casper E. Phase II evaluation of DON (6-diazo-5-oxo-L-norleucine) in patients with advanced colorectal carcinoma. Am J Clin Oncol. 1982; 5: 541-3.

128. Earhart RH, Amato DJ, Chang AY, Borden EC, Shiraki M, Dowd ME, et al. Phase II trial of 6-diazo-5-oxo-L-norleucine versus aclacinomycin-A in advanced sarcomas and mesotheliomas. Invest New Drugs. 1990; 8: 113-9.

129. Sullivan MP, Nelson JA, Feldman S, Van Nguyen B. Pharmacokinetic and phase I study of intravenous DON (6-diazo-5-oxo-L-norleucine) in children. Cancer Chemother Pharmacol. 1988; 21: 78-84.

130. Neil GL, Berger AE, Bhuyan BK, Blowers CL, Kuentzel SL. Studies of the biochemical pharmacology of the fermentation-derived antitumor agent, (alpha S, 5S)-alpha-amino-3-chloro-4,5-dihydro-5-isoxazoleacetic acid (AT-125). Adv Enzyme Regul. 1978; 17: 375-98.

131. Neil GL, Berger AE, McPartland RP, Grindey GB, Bloch A. Biochemical and pharmacological effects of the fermentation-derived antitumor agent, (alphaS,5S)-alpha-amino-3-chloro-4,5-dihydro-5-isoxazoleacetic acid (AT-125). Cancer Res. 1979; 39: 852-6.

132. Poster DS, Bruno S, Penta J, Neil GL, McGovren JP. Acivicin. An antitumor antibiotic. Cancer Clin Trials. 1981; 4: 327-30.

133. Allen L, Meck R, Yunis A. The inhibition of gamma-glutamyl transpeptidase from human pancreatic carcinoma cells by (alpha S,5S)-alpha-amino-3-chloro-4,5-dihydro-5-isoxazoleacetic acid (AT-125; NSC-163501). Res Commun Chem Pathol Pharmacol. 1980; 27: 175-82.

134. Reed DJ, Ellis WW, Meck RA. The inhibition of gamma-glutamyl transpeptidase and glutathione metabolism of isolated rat kidney cells by L-(alpha S, 5S)-alpha-amino-3-chloro-4, 5-dihydro-5-isoxazoleacetic acid (AT-125; NSC-163501). Biochem Biophys Res Commun. 1980; 94: 1273-7.

135. Shapiro RA, Curthoys NP. Differential effect of AT-125 on rat renal glutaminase activities. FEBS Lett. 1981; 133: 131-4.

136. Tso JY, Bower SG, Zalkin H. Mechanism of inactivation of glutamine amidotransferases by the antitumor drug L-(alpha S, 5S)-alpha-amino-3-chloro-4,5-dihydro-5-isoxazoleacetic acid (AT-125). J Biol Chem. 1980; 255: 6734-8.

137. Maroun JA, Fields AL, Pater JL, Stewart DJ, Cripps C, Eisenhauer E. Phase II study of acivicin in colorectal carcinoma: a National Cancer Institute of Canada study. Cancer Treat Rep. 1984; 68: 1121-3.

138. Adolphson CC, Ajani JA, Stroehlein JR, Barlogie B, Bodey GP, Korinek J, et al. Phase II trial of acivicin in patients with advanced colorectal carcinoma. Am J Clin Oncol. 1986; 9: 189-91.

139. Eisenhauer EA, Maroun JA, Fields AL, Walde PL. Phase II study of acivicin as a 72-hr continuous infusion in patients with untreated colorectal cancer. A National Cancer Institute of Canada Clinical Trials Group Study. Invest New Drugs. 1987; 5: 375-8.

140. Fleishman G, Yap HY, Murphy WK, Bodey G. Phase II trial of acivicin in advanced metastatic breast cancer. Cancer Treat Rep. 1983; 67: 843-4.

141. Booth BW, Korzun AH, Weiss RB, Ellison RR, Budman D, Khojasteh A, et al. Phase II trial of acivicin in advanced breast carcinoma: a Cancer and Leukemia Group B Study. Cancer Treat Rep. 1986; 70: 1247-8.

142. Willson JK, Knuiman MW, Skeel RT, Wolter JM, Pandya KJ, Falkson G, et al. Phase II clinical trial of acivicin in advanced breast cancer: an Eastern Cooperative Oncology Group Study. Cancer Treat Rep. 1986; 70: 1237-8.

143. Falkson G, Vorobiof DA, Simson IW, Borden EC. Phase II trial of acivicin in malignant mesothelioma. Cancer Treat Rep. 1987; 71: 545-6.

144. Maroun JA, Maksymiuk A, Eisenhauer E, Stewart DJ, Young V, Pater J. Phase II study of acivicin in non-small cell lung cancer: a National Cancer Institute of Canada Study. Cancer Treat Rep. 1986; 70: 1327-8.

145. Bonomi P, Finkelstein D, Chang A. Phase II trial of acivicin versus etoposide-cisplatin in non-small cell lung cancer. An Eastern Cooperative Oncology Group study. Am J Clin Oncol. 1994; 17: 215-7.

146. Maroun JA, Stewart DJ, Verma S, Evans WK, Eisenhauer E. Phase I study of acivicin and cisplatin in non-small-cell lung cancer. A National Cancer Institute of Canada study. Am J Clin Oncol. 1990; 13: 401-4.

147. Olver IN, Green M, Millward MJ, Bishop JF. Phase II study of acivicin in patients with recurrent high grade astrocytoma. J Clin Neurosci. 1998; 5: 46-8.

148. Baruchel S, Bernstein M, Whitehead VM, Devine S, Bell B, Dubowy R, et al. A phase I study of acivicin in refractory pediatric solid tumors. A Pediatric Oncology Group study. Invest New Drugs. 1995; 13: 211-6.

149. Weiss GR, McGovren JP, Schade D, Kufe DW. Phase I and pharmacological study of acivicin by 24-hour continuous infusion. Cancer Res. 1982; 42: 3892-5.

150. Earhart RH, Koeller JM, Davis TE, Borden EC, McGovren JP, Davis HL, et al. Phase I trial and pharmacokinetics of acivicin administered by 72-hour infusion. Cancer Treat Rep. 1983; 67: 683-92.

151. Taylor S, Belt RJ, Joseph U, Haas CD, Hoogstraten B. Phase I evaluation of AT-125 single dose every three weeks. Invest New Drugs. 1984; 2: 311-4.

152. Williams MG, Earhart RH, Bailey H, McGovren JP. Prevention of central nervous system toxicity of the antitumor antibiotic acivicin by concomitant infusion of an amino acid mixture. Cancer Res. 1990; 50: 5475-80.

153. Rathore MG, Saumet A, Rossi JF, de Bettignies C, Tempe D, Lecellier CH, et al. The NF-kappaB member p65 controls glutamine metabolism through miR-23a. Int J Biochem Cell Biol. 2012; 44: 1448-56.

154. Qie S, Chu C, Li W, Wang C, Sang N. ErbB2 activation upregulates glutaminase 1 expression which promotes breast cancer cell proliferation. J Cell Biochem. 2014; 115: 498-509.

155. Sun RC, Denko NC. Hypoxic regulation of glutamine metabolism through HIF1 and SIAH2 supports lipid synthesis that is necessary for tumor growth. Cell Metab. 2014; 19: 285-92.

156. Geier EG, Schlessinger A, Fan H, Gable JE, Irwin JJ, Sali A, et al. Structure-based ligand discovery for the Large-neutral Amino Acid Transporter 1, LAT-1. Proc Natl Acad Sci U S A. 2013; 110: 5480-5.

157. Takada Y, Greig NH, Vistica DT, Rapoport SI, Smith QR. Affinity of antineoplastic amino acid drugs for the large neutral amino acid transporter of the blood-brain barrier. Cancer Chemother Pharmacol. 1991; 29: 89-94.

158. Chikhale EG, Chikhale PJ, Borchardt RT. Carrier-mediated transport of the antitumor agent acivicin across the blood-brain barrier. Biochem Pharmacol. 1995; 49: 941-5.

159. Rais R, Jancarik A, Tenora L, Nedelcovych M, Alt J, Englert J, et al. Discovery of 6-Diazo-5-oxo-l-norleucine (DON) Prodrugs with Enhanced CSF Delivery in Monkeys: A Potential Treatment for Glioblastoma. J Med Chem. 2016; 59: 8621-33.

160. van den Berg H. Asparaginase revisited. Leuk Lymphoma. 2011; 52: 168-78.

161. Mao XG, Hutt-Cabezas M, Orr BA, Weingart M, Taylor I, Rajan AK, et al. LIN28A facilitates the transformation of human neural stem cells and promotes glioblastoma tumorigenesis through a pro-invasive genetic program. Oncotarget. 2013; 4: 1050-64.

162. Raabe EH, Lim KS, Kim JM, Meeker A, Mao XG, Nikkhah G, et al. BRAF activation induces transformation and then senescence in human neural stem cells: a pilocytic astrocytoma model. Clin Cancer Res. 2011; 17: 3590-9.

163. Bigner SH, Friedman HS, Vogelstein B, Oakes WJ, Bigner DD. Amplification of the c-myc gene in human medulloblastoma cell lines and xenografts. Cancer Res. 1990; 50: 2347-50.

164. Schroeder A, Mueller O, Stocker S, Salowsky R, Leiber M, Gassmann M, et al. The RIN: an RNA integrity number for assigning integrity values to RNA measurements. BMC Mol Biol. 2006; 7: 3.

165. Subramanian A, Tamayo P, Mootha VK, Mukherjee S, Ebert BL, Gillette MA, et al. Gene set enrichment analysis: a knowledge-based approach for interpreting genome-wide expression profiles. Proc Natl Acad Sci U S A. 2005; 102: 15545-50.

166. Subramanian A, Kuehn H, Gould J, Tamayo P, Mesirov JP. GSEA-P: a desktop application for Gene Set Enrichment Analysis. Bioinformatics. 2007; 23: 3251-3.

167. Barretina J, Caponigro G, Stransky N, Venkatesan K, Margolin AA, Kim S, et al. The Cancer Cell Line Encyclopedia enables predictive modelling of anticancer drug sensitivity. Nature. 2012; 483: 603-7.

168. Yang W, Soares J, Greninger P, Edelman EJ, Lightfoot H, Forbes S, et al. Genomics of Drug Sensitivity in Cancer (GDSC): a resource for therapeutic biomarker discovery in cancer cells. Nucleic Acids Res. 2013; 41: D955-61.

169. Barbie DA, Tamayo P, Boehm JS, Kim SY, Moody SE, Dunn IF, et al. Systematic RNA interference reveals that oncogenic KRAS-driven cancers require TBK1. Nature. 2009; 462: 108-12.

170. Seashore-Ludlow B, Rees MG, Cheah JH, Cokol M, Price EV, Coletti ME, et al. Harnessing Connectivity in a Large-Scale Small-Molecule Sensitivity Dataset. Cancer Discov. 2015; 5: 1210-23.

171. Abazeed ME, Adams DJ, Hurov KE, Tamayo P, Creighton CJ, Sonkin D, et al. Integrative radiogenomic profiling of squamous cell lung cancer. Cancer Res. 2013; 73: 6289-98.

172. Benjamini YaH, Y. Controlling the False Discovery Rate: A Practical and Powerful Approach to Multiple Testing. Journal of the Royal Statistical Society Series B (Methodological). 1995; 57: 289–300.

173. Melamud E, Vastag L, Rabinowitz JD. Metabolomic analysis and visualization engine for LC-MS data. Anal Chem. 2010; 82: 9818-26.

174. Clasquin MF, Melamud E, Rabinowitz JD. LC-MS data processing with MAVEN: a metabolomic analysis and visualization engine. Curr Protoc Bioinformatics. 2012; Chapter 14: Unit14 1.

Table 1: The 150 genes that make up the hNSC G3 signature

C11ORF70	SPEN	C20ORF117	TEAD4
RPLP1	DCUN1D5	RPL30	FLJ90086
ZNF207	B3GNT3	SH3RF2	RPS18
WNT10B	MTRR	HECTD1	LRRC57
KIAA1598	TRMT1	USP54	BXDC5
TCERG1	ANAPC10	LOC285346	ATP5O
OSGEPL1	PAK1	ZNF511	NARS2
THBS2	IKBKAP	LOC440087	CD3EAP
LOC196264	CHCHD2	PARVB	PSMD12
RCOR2	HSF1	PSMA6	TYW3
BDP1	KIAA1875	EIF2S2	ITLN1
FUSIP1	ALPK3	C4ORF15	MGC12965
BANF1	LOC390874	DEPDC6	PGRMC1
ZF	RPL5	CCDC45	ZNF544
UCHL3	MYL9	RELN	TCHP
PDCD2	SKIV2L2	ARS2	NAT10
MECR	MRPL45	ACSL4	ORC2L
C12ORF52	SAE1	MRPL9	INTS1
C1ORF67	SLC22A18AS	DYRK2	ST6GALNAC1
C1ORF37	HISPPD1	SLC19A1	CD48
PEF1	KLHL21	MARK2	MYSM1
UBE2M	RAB3IL1	EXOSC5	LOC388796
KAZALD1	LOC221711	ACSL5	GJA3
GSR	LOC285627	TMEM123	ADRB3
HDAC1	BMPR1B	LOC340178	C1ORF109
B4GALT3	NCOA6IP	WDR35	LOC340061
NUP50	RNF168	NUP160	PEBP1
MID1IP1	CXCL13	DKC1	ZBTB48
AHSG	RPP25	KIAA1333	HEATR2
SPATA5L1	C4ORF14	PAWR	ZNF529
DOCK9	FLJ39779	ST6GAL1	RPL7A
TTF2	BNIP2	IQCA	FLJ43944
FAM58A	CDK4	CCDC99	GCN5L2
DEPDC1B	FLJ44606	SP4	RAB3A
CALML4	C15ORF45	MEF2C	SLC5A10
PTGER2	EXOSC8	C9ORF105	SELI
AHI1	KCNH3	AMBN	NOL11
ZCCHC7	LOC144097		

Table 2: The top 30 hits from the DiSCoVER analysis of the Cancer Therapeutics Response Portal (CTRP v2) database. Cyclin Dependent Kinase inhibitors are highlighted.

DATASET	RANK	Compound	Target, Mechanism or Activity	Information Coeff. [IC]	Nominal p-value	False Discovery Rate [FDR]	Significant at 0.33 FDR
Cancer Therapeutics Response Portal (CTRP v2)	1	BRD-K30748066	inhibitor of CDK9	0.421	0.00178	0.227	*
	2	linsitinib	inhibitor of insulin-like growth factor 1 receptor and insulin receptor (IGF1R;INSR)	0.419	0.00194	0.227	*
	3	BRD-K42260513	inhibitor of enhancer of zeste polycomb repressive complex 2 subunit (EZH2)	0.414	0.00245	0.227	*
	4	BRD-K01737880	-	0.411	0.00275	0.227	*
	5	BRD-K09344309	-	0.411	0.00278	0.227	*
	6	GSK-J4	inhibitor of lysine-specific demethylases (KDM6A;KDM6B)	0.411	0.00283	0.227	*
	7	sotrastaurin	inhibitor of protein kinase C beta (PRKCB)	0.404	0.00379	0.261	*
	8	BRD-K88742110	inhibitor of HDAC8 (HDAC8)	0.397	0.00502	0.294	*
	9	Compound 1541A	activators of executioner procaspases 3, 6, and 7 (CASP3/6/7)	0.393	0.00595	0.294	*
	10	dabrafenib	inhibitor of BRAF	0.388	0.00719	0.294	*
	11	brivanib	inhibitor of VEGFR 1/2 (FLT1;KDR)	0.387	0.00732	0.294	*
	12	SR8278	antagonist of Rev-ErbAalpha (NR1D1)	0.386	0.0078	0.294	*
	13	Mdivi-1	inhibitor of dynamin 1; inhibitor of mitrochondrial division inhibitor (DNM1)	0.382	0.00904	0.294	*
	14	QS-11	inhibitor of GTPase activating protein of ARF 1 (ARFGAP1)	0.376	0.011	0.294	*
	15	alvocidib	inhibitor of cyclin-dependent kinases (CDK1/2/4/6)	0.375	0.0115	0.294	*
	16	BRD-K02251932	product of diversity oriented synthesis	0.375	0.0117	0.294	*
	17	cytarabine hydrochloride	inducer of DNA damage	0.374	0.012	0.294	*
	18	chlorambucil	DNA alkylator	0.373	0.0124	0.294	*
	19	BRD-K13999467	product of diversity oriented synthesis	0.373	0.0125	0.294	*
	20	IU1	inhibitor of the deubiquitinase activity of USP14	0.369	0.0141	0.294	*
	21	GSK461364	inhibitor of polo-like kinase 1 (PLK1)	0.369	0.0143	0.294	*
	22	methotrexate	inhibitor of dihydrofolate reductase (DHFR)	0.369	0.0143	0.294	*
	23	necrostatin-7	inhibitor of necroptosis	0.368	0.0144	0.294	*
	24	docetaxel	inhibitor of microtubule assembly	0.367	0.0152	0.294	*
	25	leptomycin B	inhibitor of exportin 1 (XPO1)	0.366	0.0155	0.294	*
	26	imatinib	inhibitor of BCR-ABL1 and c-KIT (ABL1;BCR;KIT)	0.365	0.0159	0.294	*
	27	BMS-195614	antagonist of retinoic acid receptors (RARA;RARB;RARG)	0.364	0.0166	0.296	*
	28	SCH-79797	antagonist of proteinase-activated receptor 1 (PAR1) (F2R)	0.363	0.0174	0.299	*
	29	VX-680	inhibitor of aurora kinases (AURKA;AURKB;AURKC)	0.361	0.0183	0.303	*
	30	dinaciclib	inhibitor of cyclin-dependent kinases (CDK1/2/5/9)	0.358	0.0205	0.329	*

Table 3: The top 24 hits from the DiSCoVER analysis of the Pharmacological Profiling Drug Data (CCLE) database. Cyclin Dependent Kinase inhibitors are highlighted.

DATASET	Rank	Compound	Target, Mechanism or Activity	Information Coeff. [IC]	Nominal p-value	False Discovery Rate [FDR]	Significant at 0.33 FDR
Pharmacological Profiling Drug Data (CCLE)	1	Paclitaxel	Microtubule-Stabilizing Agent	0.38	0.0116	0.181	*
	2	Irinotecan	DNA Topoisomerase I Inhibitor	0.364	0.0199	0.181	*
	3	Topotecan	DNA Topoisomerase I Inhibitor	0.355	0.0255	0.181	*
	4	PD-0332991	inhibitor of cyclin-dependent kinases (CDK1/2/4/6)	0.341	0.0365	0.181	*
	5	PF2341066	c-MET and ALK Inhibitor	0.339	0.0378	0.181	*
	6	PHA-665752	c-MET Inhibitor	0.321	0.06	0.24	*
	7	L-685458	gamma-Secretase Inhibitor	0.31	0.0776	0.266	*
	8	17-AAG	Heat Shock Protein 90 (hsp90) Inhibitor	0.291	0.116	0.348	
	9	Panobinostat	Histone Deacetylase (HDAC) Inhibitor	0.283	0.134	0.359	
	10	AZD6244	MEK1 and MEK2 Inhibitor	0.254	0.203	0.473	
	11	PD-0325901	MEK1 and MEK2 Inhibitor	0.245	0.227	0.473	
	12	Sorafenib	Multi-kinase inhibitor	0.239	0.243	0.473	
	13	TAE684	ALK Inhibitor	0.229	0.272	0.473	
	14	TKI258	Multi-kinase inhibitor	0.227	0.28	0.473	
	15	RAF265	Raf kinase B and KDR Inhibitor	0.22	0.301	0.473	
	16	AEW541	IGF-1R Inhibitor	0.217	0.316	0.473	
	17	Nilotinib	Abl Inhibitor	-0.219	0.309	0.181	
	18	Nutlin-3	MDM2 Inhibitor	-0.275	0.154	0.181	
	19	AZD0530	Src and Abl inhibitor	-0.275	0.154	0.181	
	20	ZD-6474	Multi-kinase inhibitor	-0.277	0.151	0.181	
	21	Lapatinib	EGFR and HER2 Inhibitor	-0.29	0.12	0.181	
	22	LBW242	Inhibitor of Apoptosis Proteins (IAP) Inhibitor	-0.343	0.0355	0.181	
	23	Erlotinib	EGFR Inhibitor	-0.352	0.0279	0.181	
	24	PLX4720	Raf kinase B Inhibitor	-0.391	0.00823	0.181	

Table 4: The top 30 hits from the DiSCoVER analysis of the Genomics of Drug Sensitivity Cancer (Sanger) database. Cyclin Dependent Kinase inhibitors are highlighted.

Dataset	Rank	Compound	Target, Mechanism or Activity	Information Coeff. [IC]	Nominal p-value	False Discovery Rate [FDR]	Significant at 0.33 FDR
Geonmics of Drug Sensitivity in Cancer (Sanger)	1	Methotrexate_ALPHA	inhibitor of dihydrofolate reductase (DHFR)	0.607	7.85E-06	0.012	*
	2	JW-7-52-1_D	inhibitor of MTOR	0.572	5.41E-05	0.0282	*
	3	Z-LLNle-CHO_B	inhibitor of g-secretase	0.568	6.48E-05	0.0282	*
	4	BMS-509744_B	inhibitor of ITK	0.556	0.000114	0.0282	*
	5	A-443654_B	inhibitor of AKT	0.554	0.000127	0.0282	*
	6	Paclitaxel_B	microtubule inhibitor	0.546	0.000174	0.0282	*
	7	GNF-2_B	inhibitor of BCR-ABL	0.542	0.000207	0.0282	*
	8	BCR-ABL_B	inhibitor of ABL, SRC, KIT, PDGFR	0.542	0.000211	0.0282	*
	9	CGP-082996_B	inhibitor of cyclin-dependent kinase (CDK4)	0.541	0.00022	0.0282	*
	10	CGP-60474_B	nhibitor of cyclin-dependent kinases (CDK2/4/5/7/9)	0.541	0.000221	0.0282	*
	11	WH-4-023_B	inhibitor of SRC family, ABL	0.538	0.000244	0.0282	*
	12	Sunitinib_B	inhibitor of PDGFRA, PDGFRB, KDR, KIT, FLT3	0.537	0.000254	0.0282	*
	13	JW-7-52-1_B	inhibitor of MTOR	0.536	0.000265	0.0282	*
	14	AZD-0530_ALPHA	inhibitor of SRC, ABL1	0.535	0.000277	0.0282	*
	15	BI-2536_B	inhibitor of PLK1, PLK2, PLK3	0.533	0.000291	0.0282	*
	16	WZ-1-84_B	inhibitor of BMX	0.533	0.000295	0.0282	*
	17	A-770041_B	inhibitor of SRC family	0.531	0.000315	0.0282	*
	18	BMS-536924_B	inhibitor of IGF1R	0.53	0.000331	0.0282	*
	19	Doxorubicin_D	DNA intercalating	0.526	0.000375	0.0284	*
	20	BMS-754807_D	inhibitor of IGF1R	0.525	0.000403	0.0284	*
	21	VX-680_B	inhibitor of Aurora A/B/C, FLT3, ABL1, JAK2	0.524	0.000413	0.0284	*
	22	AP-24534_ALPHA	inhibitor of ABL	0.523	0.000423	0.0284	*
	23	S-Trityl-L-cysteine_B	inhibitor of KIF11	0.523	0.000427	0.0284	*
	24	XMD8-85_B	inhibitor of ERK5 (MK07)	0.513	0.000611	0.0374	*
	25	CMK_B	inhibitor of RSK	0.512	0.000633	0.0374	*
	26	Lapatinib_B	inhibitor of EGFR, ERBB2	0.512	0.000645	0.0374	*
	27	AP-24534_B	inhibitor of ABL	0.511	0.00066	0.0374	*
	28	GW843682X_B	inhibitor of PLK1	0.51	0.000687	0.0374	*
	29	Vinorelbine_B	microtubule inhibitor	0.508	0.00074	0.0374	*
	30	AZD-0530_B	inhibitor of SRC, ABL1	0.507	0.00077	0.0374	*

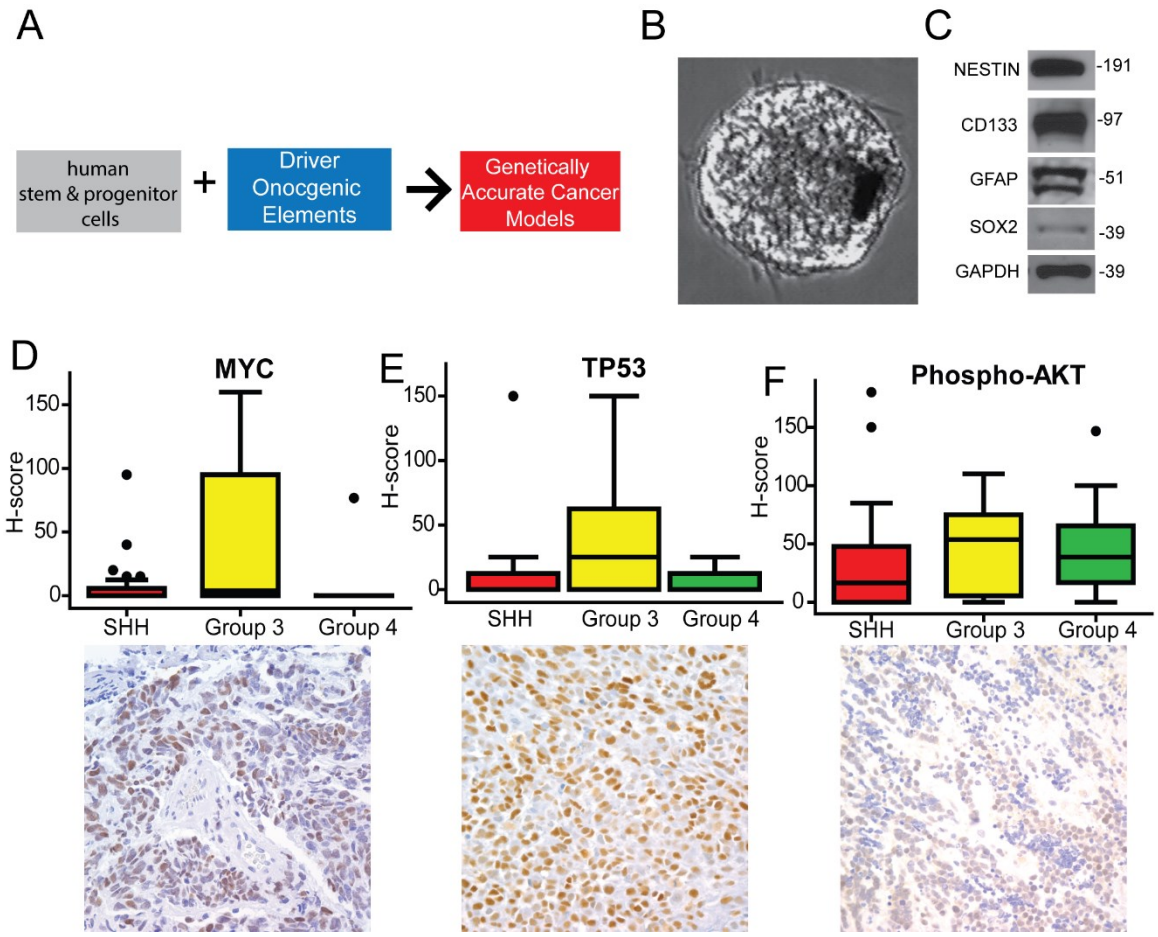

Figure 1: Creation of a human neural stem cell model of medulloblastoma

A) Diagram illustrating the creation of novel cancer models using human stem cells and oncogenic elements of interest. B) Human cerebellar neurosphere. C) Western blot indicating the expression of stem cell markers in the human cerebellar neural stem and progenitor cells. D) 65-sample medulloblastoma tissue microarray (TMA) reveals that Group 3 samples have the highest MYC expression. Lower panel: an example of MYC staining in a Group 3 sample. E) Staining the TMA reveals that Group 3 samples also have the highest expression of TP53, indicating inactivation of this pathway. Lower Panel: an example of TP53 staining in a Group 3 sample. F) Phospho-AKT, which indicates activation of AKT, is expressed in all three subgroups present on the array. Lower panel: an example of Phospho-AKT staining in a Group 3 sample. Magnification of all TMA images 400x.

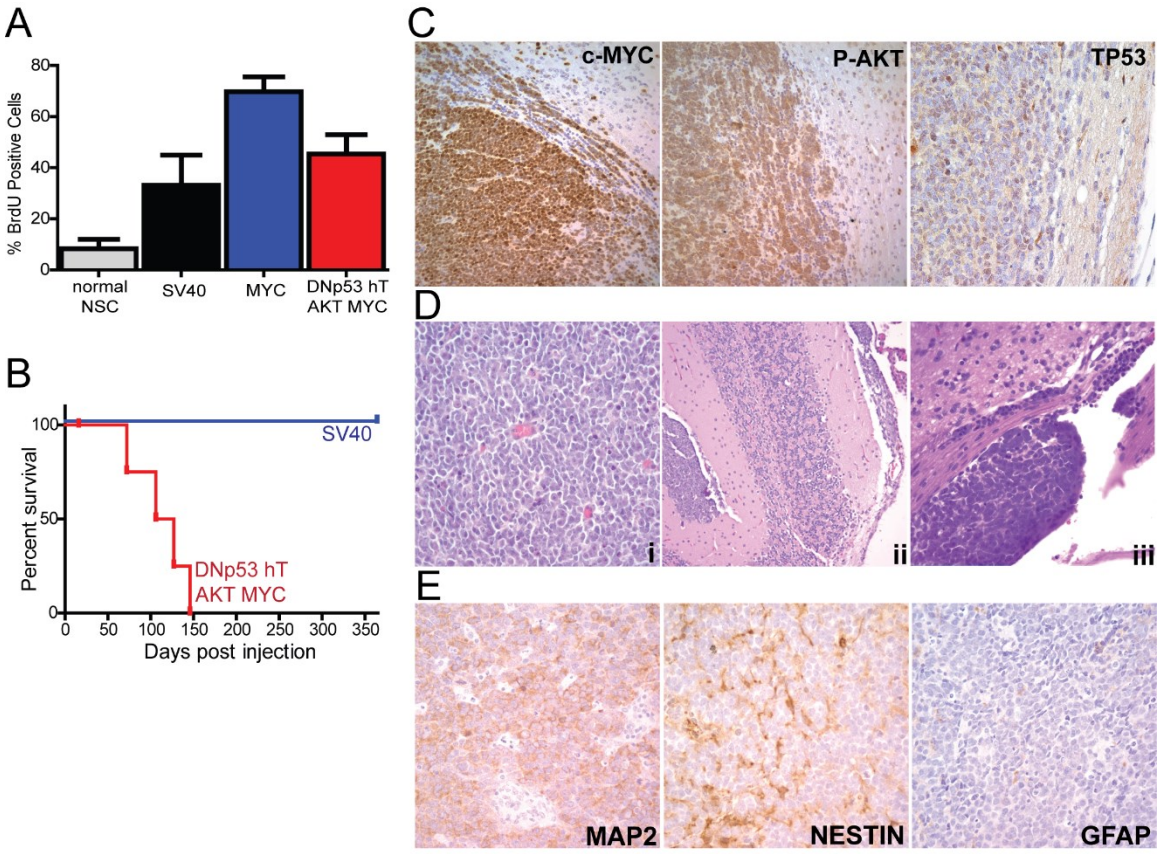

Figure 2: Human neural stem cells transformed with oncogenes associated with aggressive medulloblastoma form tumors that resemble primary human medulloblastoma

A) Stem cells transduced with MYC have increased proliferation compared to untransduced neural stem cells and those immortalized with SV40. B) Cerebellar neural stem cells transduced with DN-TP53 hT AKT and MYC form tumors that kill mice in 117 days. Cells transduced with SV40 alone do not form tumors. C) These tumors express the introduced oncogenes. Images show tumor adjacent to normal brain. 200x magnification. D) Tumors formed from cerebellar neural stem cells transduced with all four oncogenes form aggressive, anaplastic tumors (i, 400x) that spread to the leptomeninges (ii, 200x) and metastasize to the spine (iii, 200x). E) The tumors are positive for MAP2 and NESTIN expression and negative for GFAP expression (400x magnification).

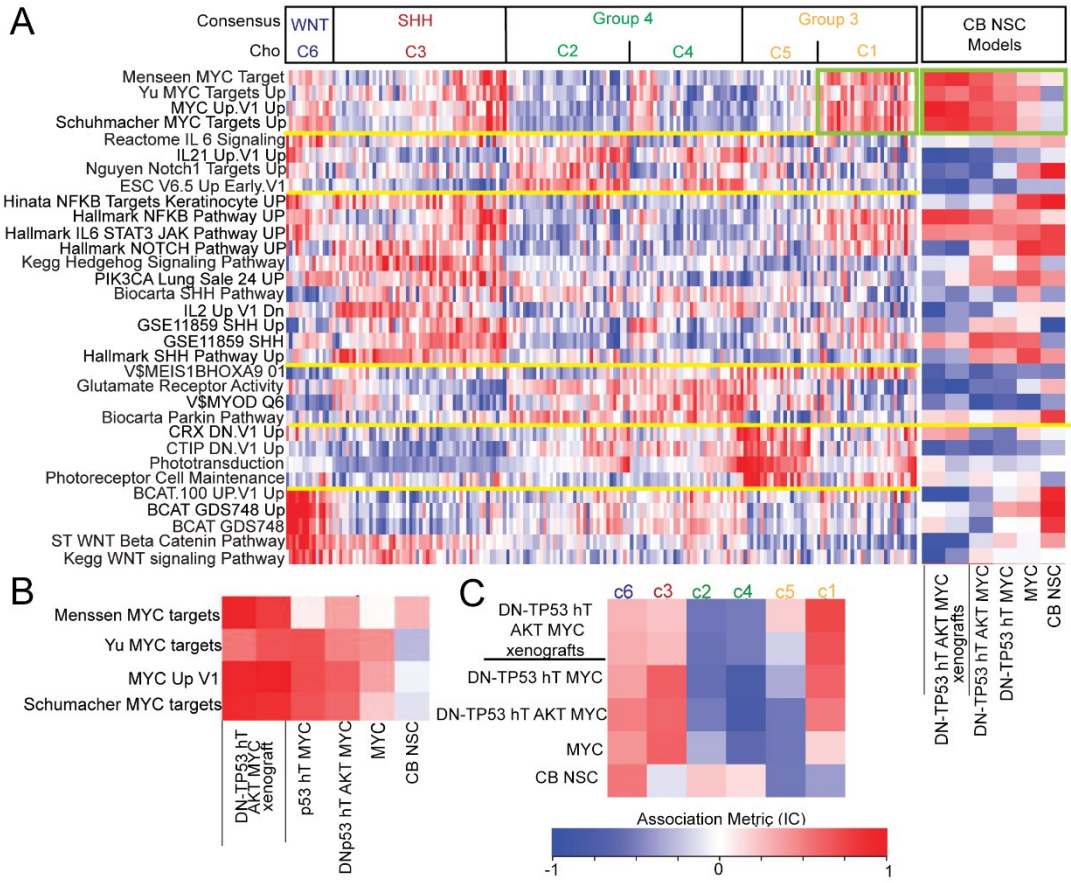

Figure 3: Human neural stem cell models of medulloblastoma are genetically similar to Group 3 medulloblastoma tumors

Human neural stem cell models of medulloblastoma have similar expression profiles to the aggressive C1 component of Group 3. Red indicates high expression and blue indicates low expression of curated gene sets in A, B. A) C1 samples have high levels of the gene sets indicated by the green box. Subtype specific gene sets are separated by yellow lines. Patient expression from data from Cho et al, 2011 (11). B) A close up of the human neural stem cell heat man indicates that increasing the number of oncogenes increases the expression of C1 associated gene sets. The samples most highly expressing C1-associated gene sets are from intracranial xenografts. C) An association metric compares the pathway enrichment subtypes (columns) to xenografts and cell models (rows). Metric is scored using Information Coefficient (IC) with red indicating higher correlation.

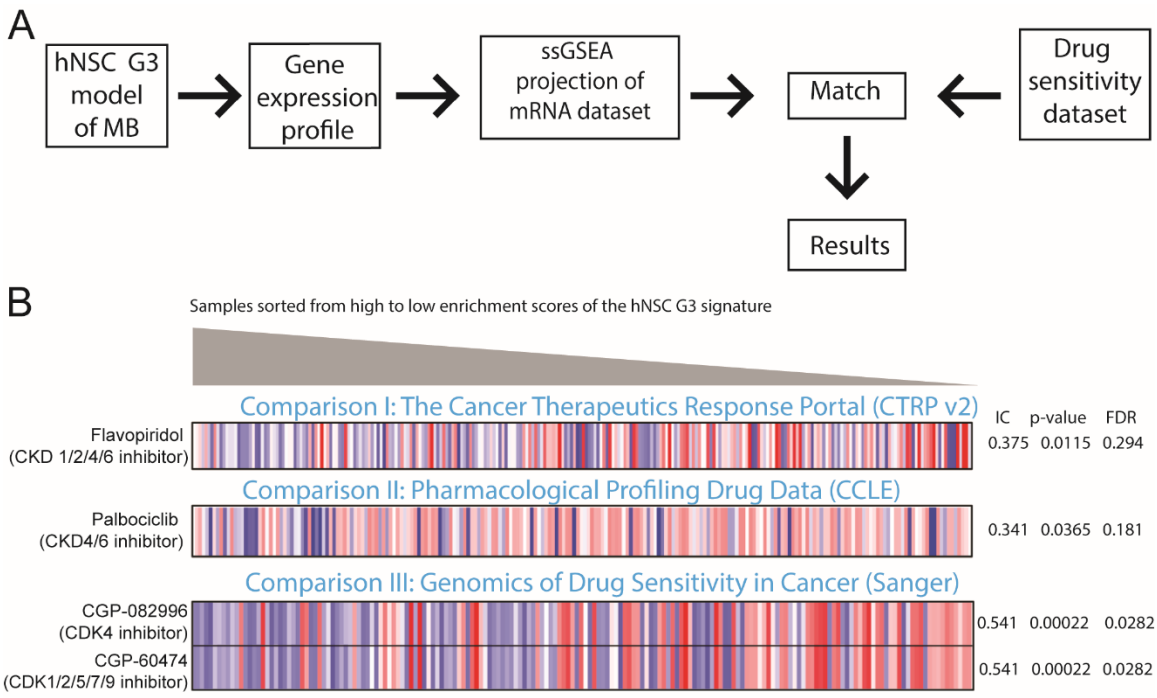

Figure 4: The DiSCoVER technique reveals CDKs as a potential therapeutic target for Group 3 medulloblastoma

A) Diagram showing a summary of the most important steps in the DiSCoVER analysis method. B) Selected cyclin-dependent kinase inhibitor results from the three drug sensitivity datasets. The samples are sorted from high to low enrichment scores of the hNSC G3 signature as indicated by the grey bar. The heatmaps indicate relative viability, and thus sensitivity, with blue indicating sensitivity to the indicated drug (less viable) and red indicating resistance to the indicated drug (more viable). Cells expressing a high level of the hNSC G3 signature tend to be more sensitive to these compounds. Values on the right show Information Coefficient (IC), the nominal p-value and the False Discovery Rate (FDR).

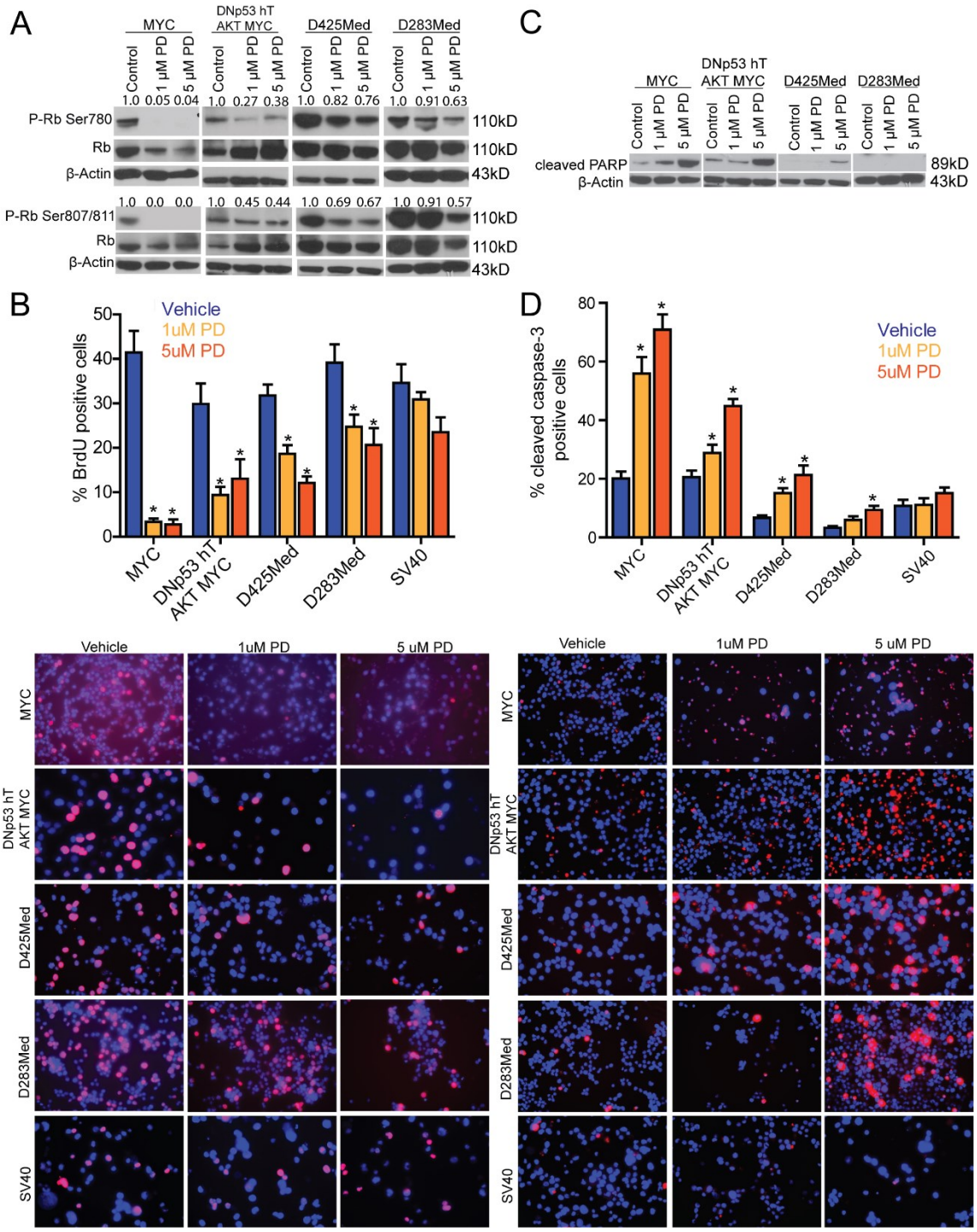

Figure 5: Medulloblastoma cells expressing MYC are sensitive to palbociclib treatment

A) 24h treatment with palbociclib (PD) causes decreased phosphorylation of Rb in D425Med, D283Med, cerebellar derived human neural stem cells transformed with four oncogenes and neural stem cells transformed with only MYC. SV40 immortalized cells were not included because Rb function is disabled by the large T antigen. Numbers represent the level of Rb phosphorylation as a percentage of total Rb normalized to the

control. All values were also normalized to Actin. Quantification performed in ImageJ. B) 72h treatment with PD causes decreased proliferation in MYC-expressing medulloblastoma cell lines as determined by BrdU incorporation. BrdU incorporation was determined by immunofluorescence. Results are from three independent experiments. Bars show mean and SEM. *P<0.05 by Student's t-test. Lower panel shows representative images. Red cells are positive for BrdU. All cells were counterstained with DAPI (blue). C) 24h PD treatment causes increased expression of cleaved-PARP, indicating cell death by apoptosis. D) PD treatment (72h) induces apoptosis. Apoptosis was determined by immunofluorescent staining for cleaved caspase-3. Results are from three independent experiments. Bars show mean and SEM. *P<0.05 by Student's t-test. Lower panel shows representative images. Red cells are positive for cleaved caspase-3. All cells were counterstained with DAPI (blue).

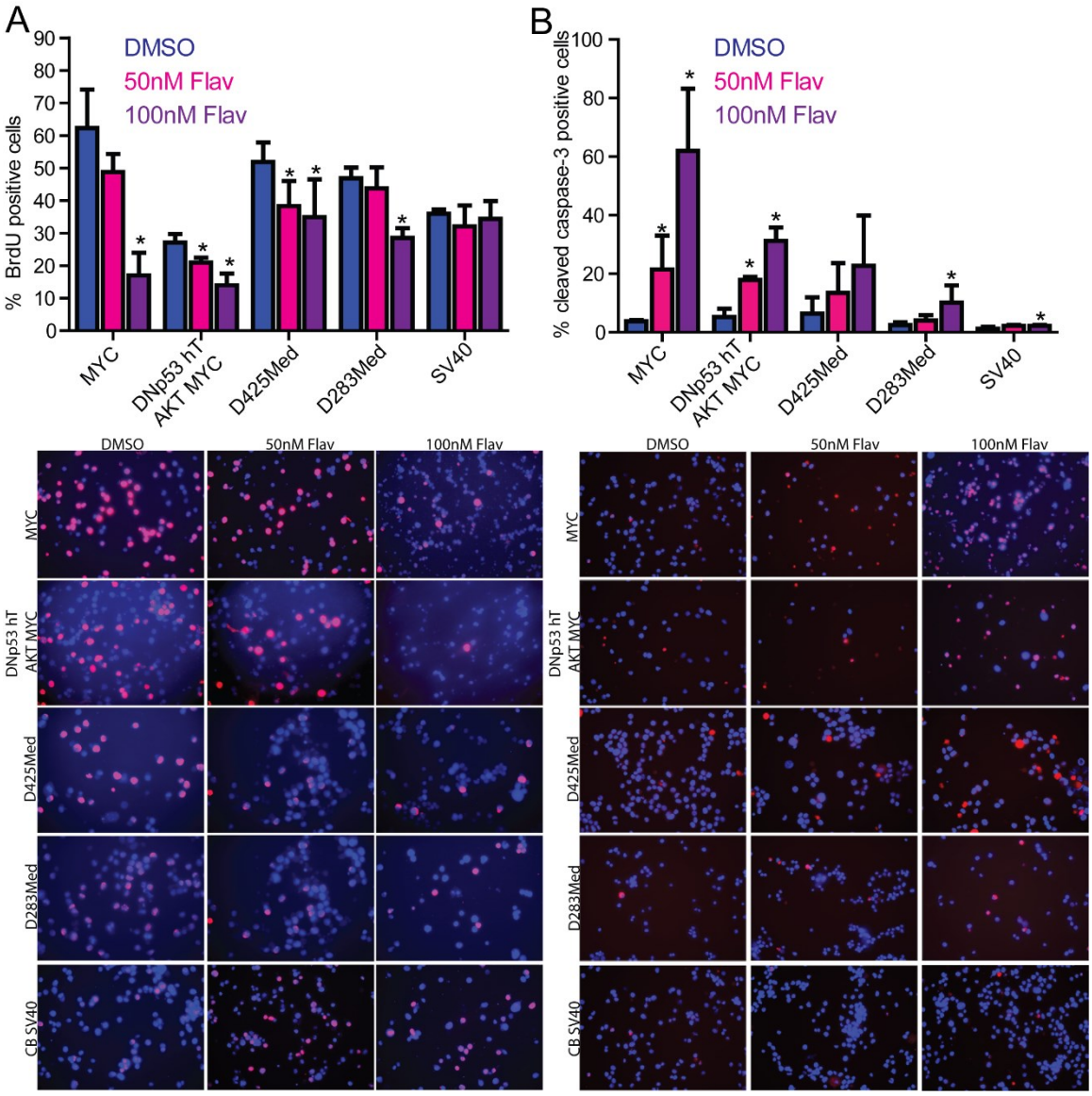

Figure 6: Medulloblastoma cells expressing MYC are sensitive to flavopiridol

72h treatment with the pan-CDK inhibitor flavopiridol causes decreased proliferation in MYC-expressing medulloblastoma cell lines as determined by BrdU incorporation. BrdU incorporation was determined by immunofluorescence. Results are from three independent experiments. Bars show mean and SEM *P<0.05 by Student's t-test. The lower panel shows representative images. Red cells are positive for BrdU. All cells were counterstained with DAPI (blue). B) Flavopiridol treatment (72h) induces apoptosis. Apoptosis was determined by immunofluorescence staining for cleaved caspase-3. Results are from three independent experiments. Bars show mean and SEM. *P<0.05 by Student's t-test. Lower panel shows representative images. Red cells are positive for cleaved caspase-3. All cells were counterstained with DAPI (blue).

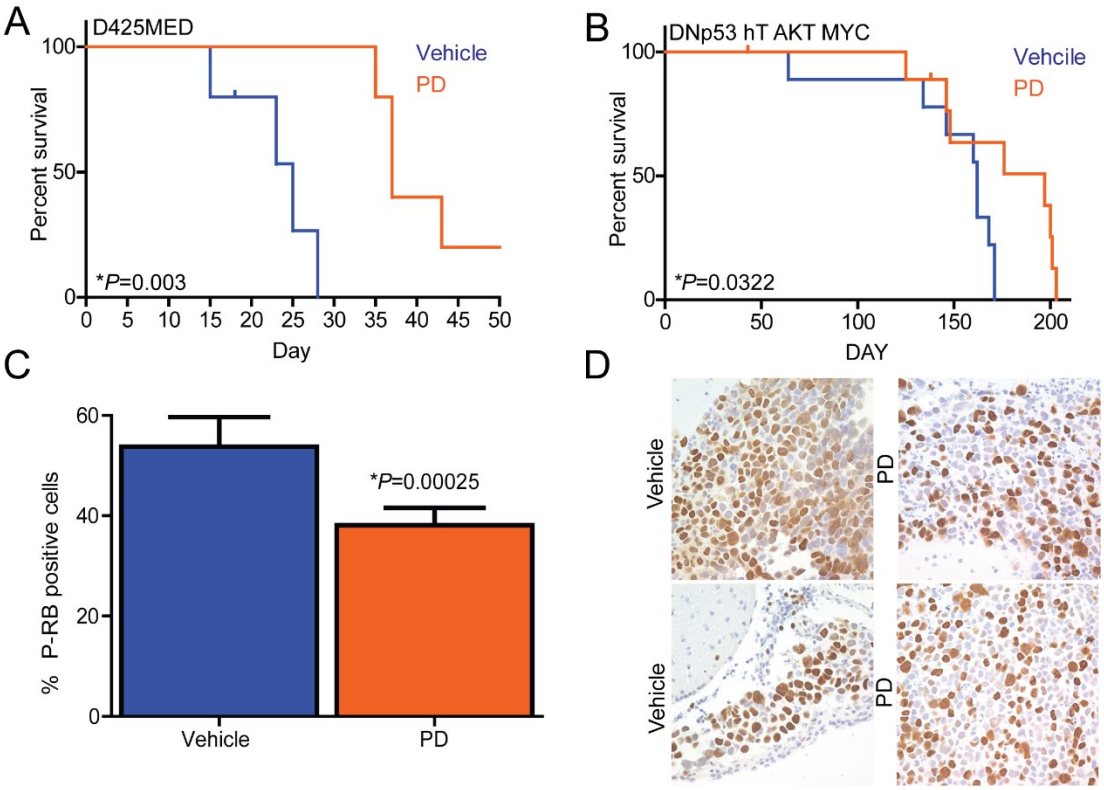

Figure 7: Palbociclib treatment extends the survival of animals with medulloblastoma orthotopic xenografts

A) Palbociclib treatment (150mg/kg 5x per week) significantly increases survival of mice with D425Med orthotopic xenografts. **P*=0.003 by Log-rank Test. B) Palbociclib treatment (150mg/kg 5x per week) significantly increases survival of mice with DNp53 hT AKT MYC orthotopic xenografts (**P*=0.0322 by Log-rank Test). C) One 150 mg/kg dose of palbociclib deceased the percentage 4h prior to euthanasia of phospho-Rb positive cells in D425Med xenografts from 53% to 38% (**P*=0.00025 by Student's t-test). Mice were euthanized 4h post dosing. C) IHC for phospho-Rb. Left column shows tumors from two separate animals treated with vehicle. Right column shows tumors from two separate animals treated with a single dose of 150mg/kg 4h prior to euthanasia. Magnification = 400X.

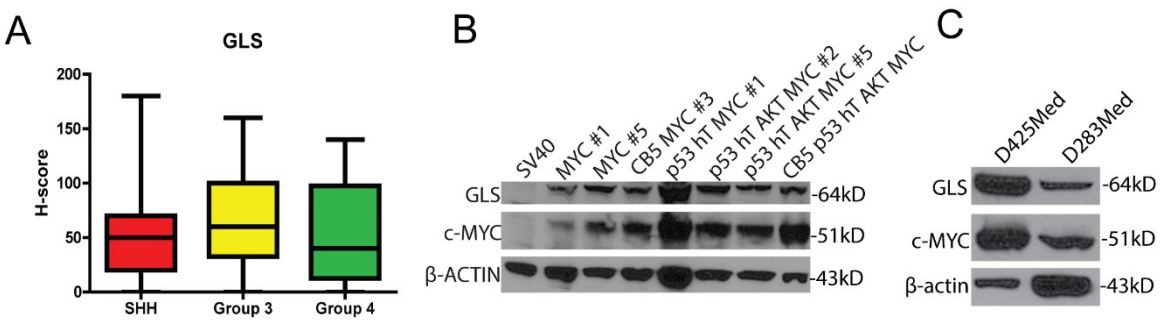

Figure 8: Medulloblastoma tumors and cell lines express GLS

A) Staining a 65-sample, subgrouped medulloblastoma tissue microarray (TMA) reveals that all subgroups present on the array have samples that express GLS. B) Human neural stem cells immortalized with SV40—not MYC—do not express GLS. Stem cells transformed with MYC also express GLS. C) The patient-derived medulloblastoma cell lines D425Med and D283Med express MYC and GLS.

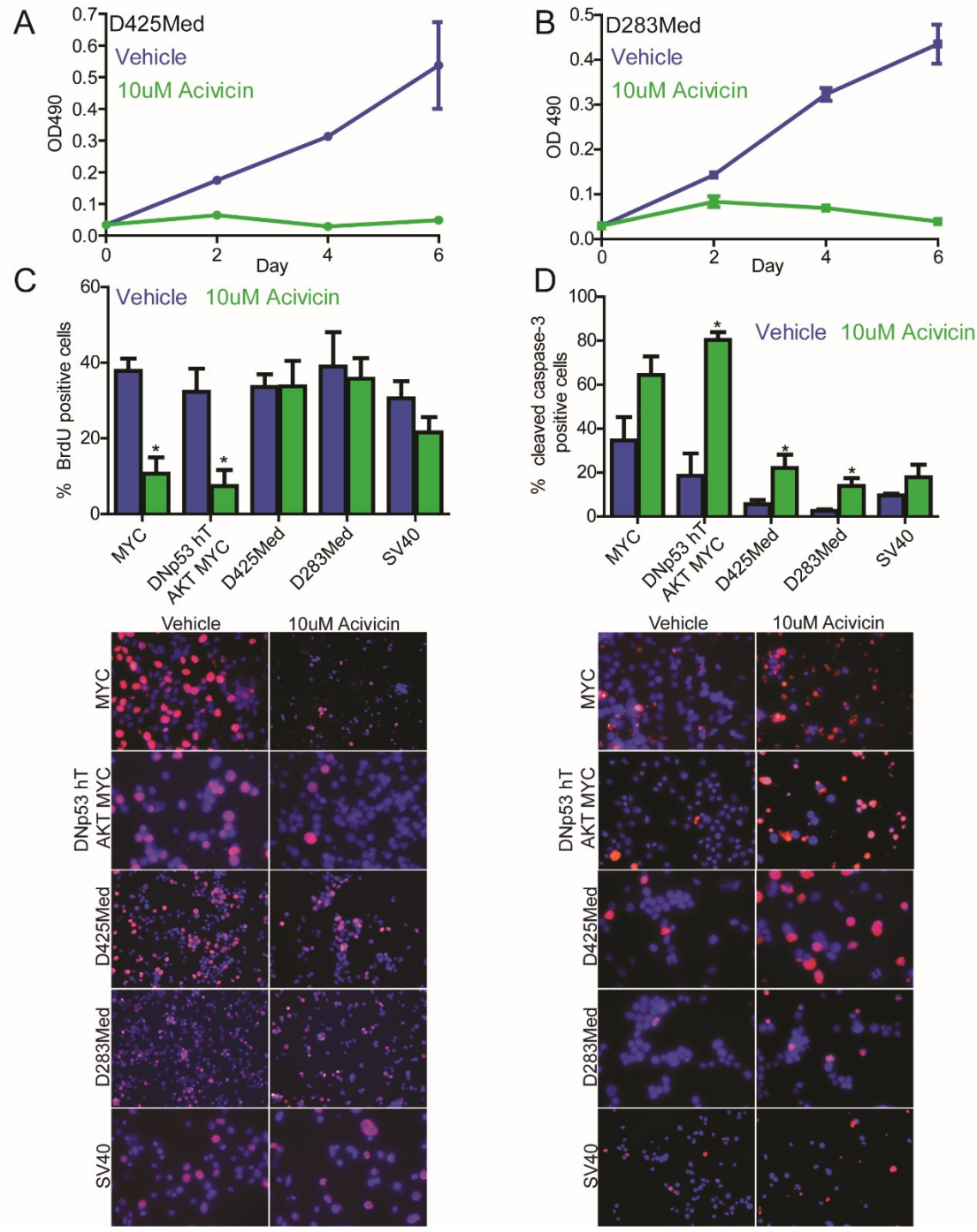

Figure 9: Medulloblastoma cells expressing MYC are sensitive to Acivicin

A, B) 10uM Acivicin treatment decreases the growth of D425Med and D283Med cells as measured by MTS assay. C) 10uM Acivicin treatment significantly decreases the proliferation of human neural stem cells transformed by MYC or by DNp53, hTERT, AKT and MYC as measured by BrdU incorporation immunofluorescent staining. Bars show mean and error bars indicate SEM. (n= 4 to 2 biological replicates. *P<0.05 by

Student's t-test). Lower panel shows representative images. Red cells are positive for BrdU. All cells counterstained with DAPI (blue). D) 10uM Acivicin treatment significantly increased the percentage of cells expressing cleaved caspase-3, an indicator of apoptosis, as measured by immunofluorescence staining for cleaved caspase-3. Bars show mean and error bars indicate SEM. (n=2 to 4 biological replicates. *P<0.05 by Student's t-test). Lower panel shows representative images. Red cells are positive for cleaved caspase-3. All cells counterstained with DAPI (blue).

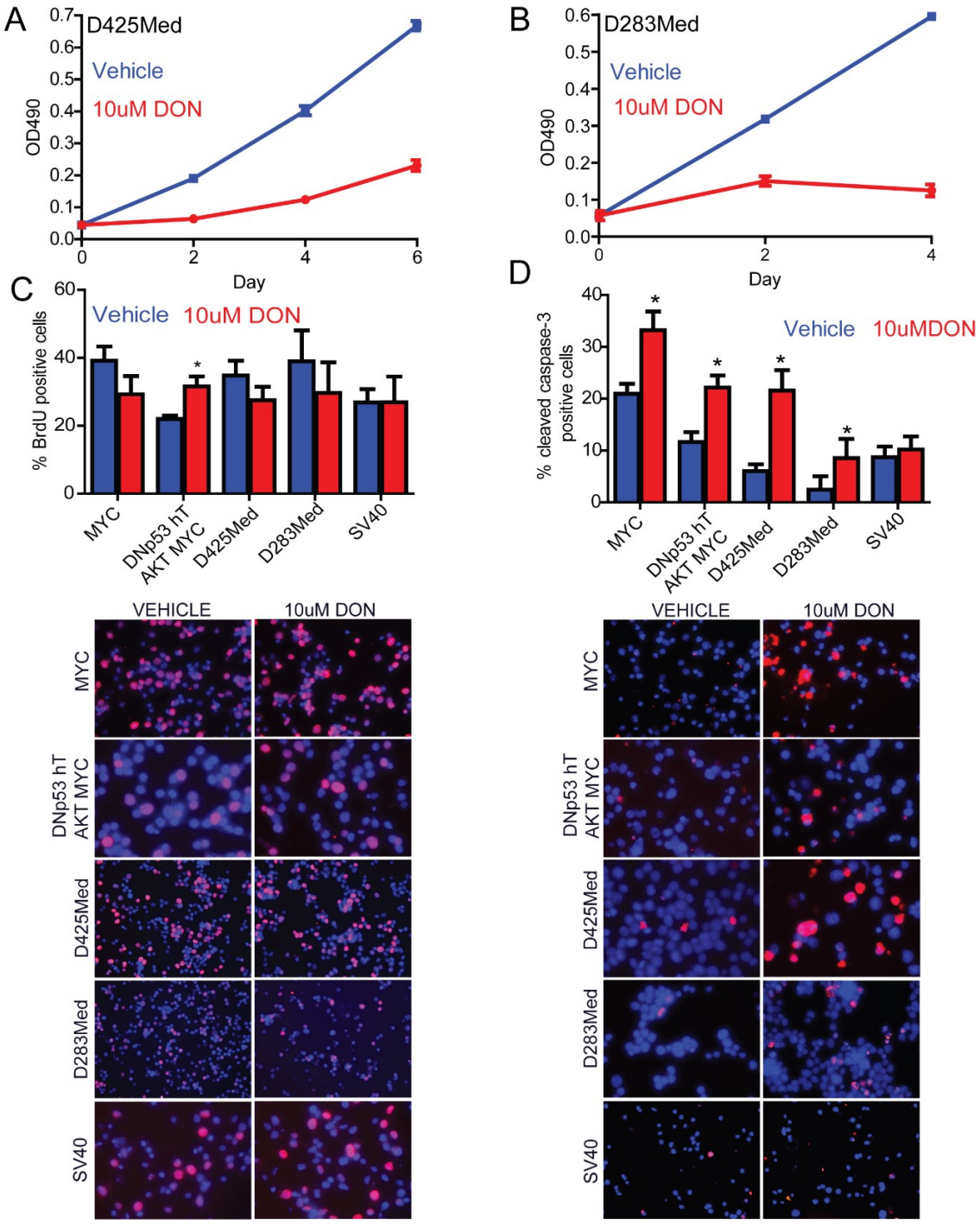

Figure 10: DON increases apoptosis in medulloblastoma cells expressing MYC

A,B) Treatment with 10uM DON decreases the growth of D425Med and D283Med cells as measured by MTS assay. C) 10uMDON does not significantly decrease the proliferation of medulloblastoma cell lines as measured by BrdU incorporation. Bars show mean and error bars indicate SEM. (n=3 to 6 biological replicates. *P<0.05 by

Student's t-test). Lower panel shows representative images. Red indicates cells positive for BrdU incorporation. All cells counterstained with DAPI (blue). D) 10uM DON treatment increases apoptosis in medulloblastoma cell lines as measured by immunofluorescence staining for cleaved caspase-3. Bars show mean and error bars indicate SEM. n=2 to 6 biological replicates. *$P<0.05$ by Student's t-test. Lower panel shows representative images. Red cells are positive for cleaved caspase-3. All cells are counterstained with DAPI (blue).

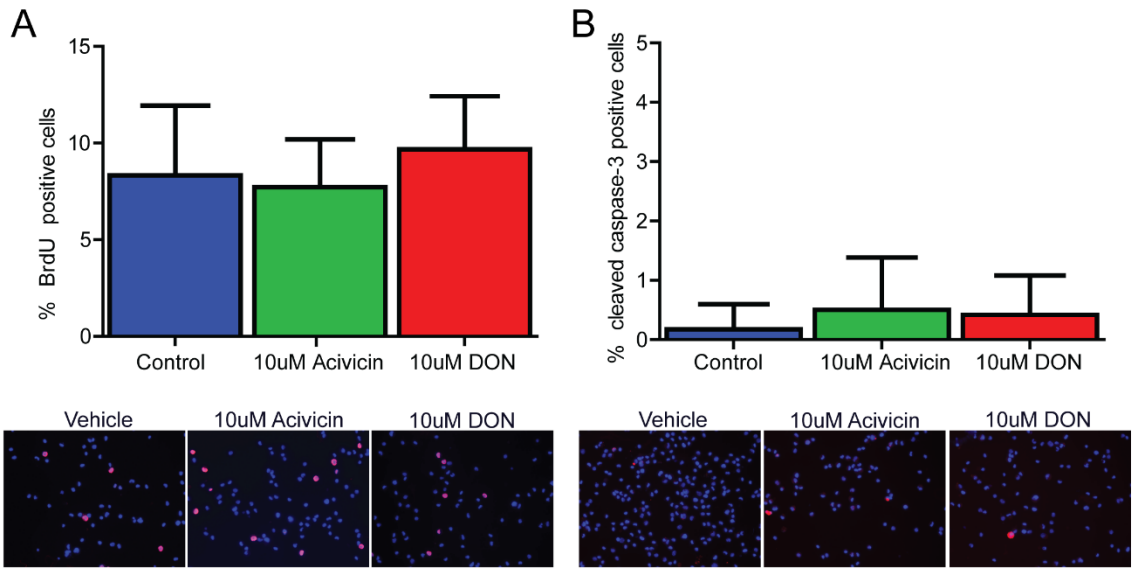

Figure 11: Normal human neural stem and progenitor cells are resistant to treatment with glutamine analogs

A) The proliferation of normal human neural stem cells is not affected by 72h treatment with 10uM Acivicin or 10uM DON as measured by BrdU incorporation. The lower panel shows representative images. Red cells are positive for BrdU and all cells were counterstained with DAPI (blue). B) Treatment with 10uM Acivicin or 10uM DON did not significantly increase apoptosis in normal human neural stem cells as measured by cleaved caspase-3 immunofluorescence. The lower panel shows representative images. Red cells are positive for cleaved caspase-3. Cells were counterstained with DAPI (blue).

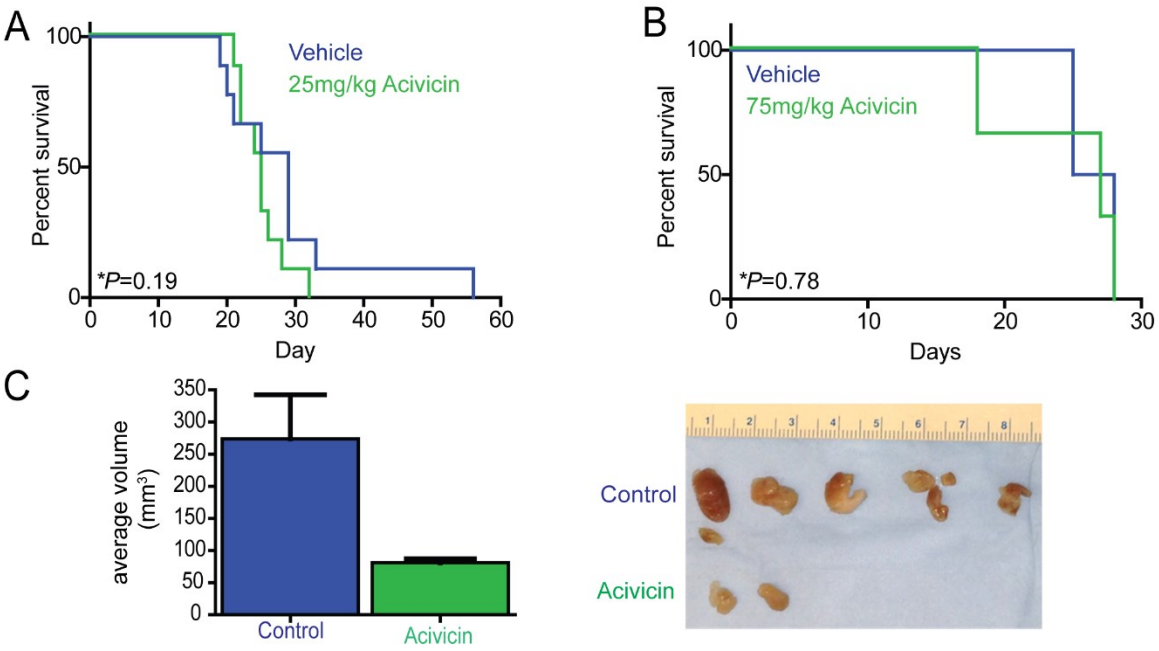

Figure 12: Acivicin treatment does not improve survival in mice with orthotopic medulloblastoma tumors

A) 25mg/kg of Acivicin 4x a week did not significantly increase the survival of mice with orthotopic D425Med xenografts (*P=0.19 by Log-rank Test). B) Increasing the dose of Acivicin to 75mg/kg 4x a week did not significantly increase survival of mice with D425Med orthotopic xenografts (*P=0.78 by Log-rank test). C) 75m/kg 4x a week of Acivicin reduced the average volume of D283Med flank tumors. D) Photograph of tumors measured for C. Ruler shows centimeters.

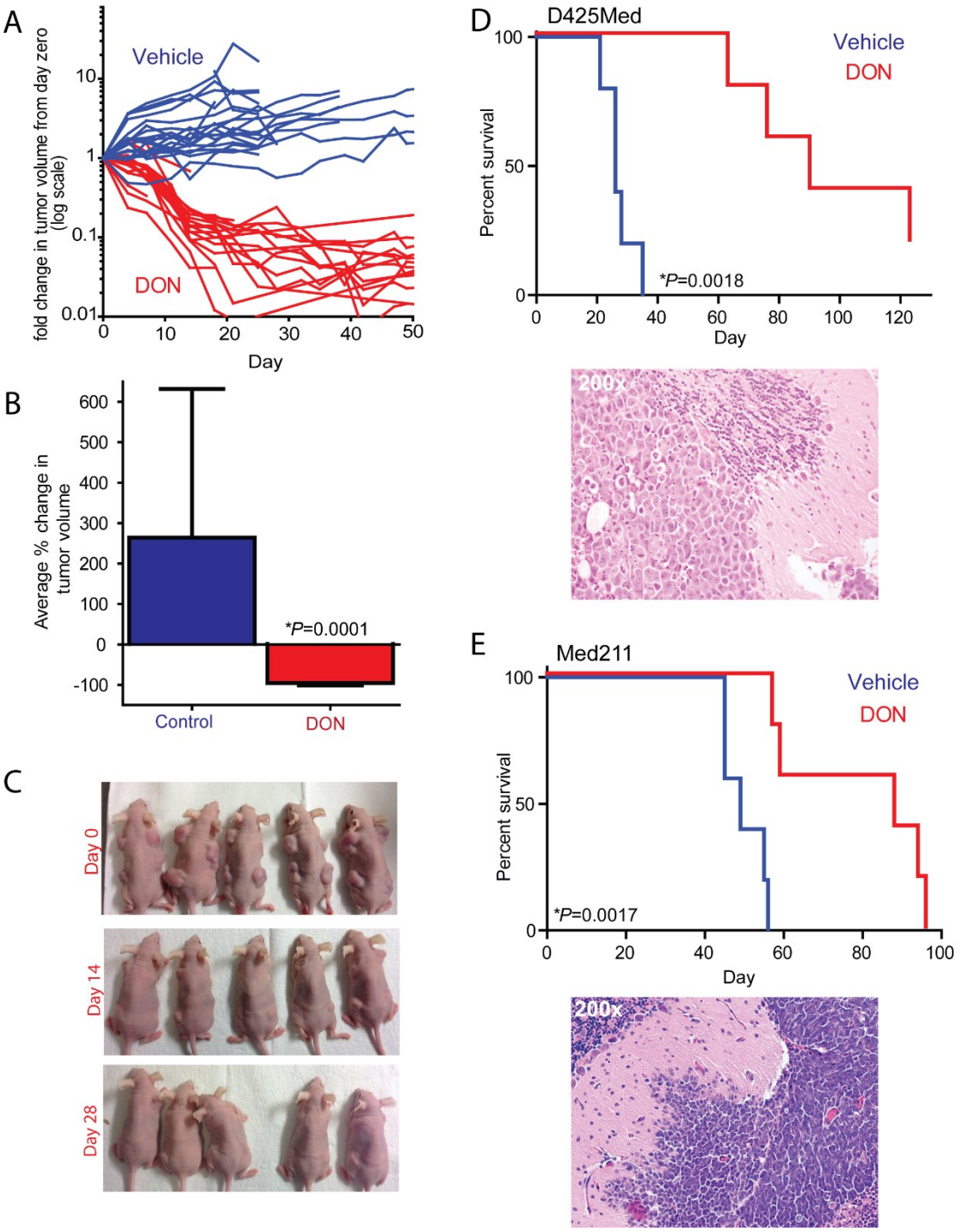

Figure 13: DON therapy dramatically decreases tumor burden and improves survival in mice with medulloblastoma flank and orthotopic xenograft tumors.

A) Once weekly 30mg/kg DON treatment significantly decreased the tumor burden of mice with D425Med flank xenografts. Each line in the graph is one individual tumor. Tumor volume was normalized to day zero. B) The average tumor volume in mice treated with DON decreased significantly, while tumors in animals treated with vehicle

increased in volume. Bars show mean and error bars SD. n=19 control tumors n=20 DON tumors (*P=0.001 by Student's t-test.) C) Pictures of animals treated with 30mg/kg of DON 1x week. The first dose of DON was administered on day 0. D) Treatment 30mg/kg DON once weekly significantly increased the survival of mice with D425Med orthotopic xenografts (*P=0.0018 by Log-rank test). Lower panel shows H&E stain of D425Med mouse brain tumor. E) Once weekly 30mg/kg DON therapy increased the survival of mice with Med211 orthotopic xenografts (*P=0.0017 by Log-rank test). Med211 is a serially passaged Group 3 medulloblastoma xenograft.

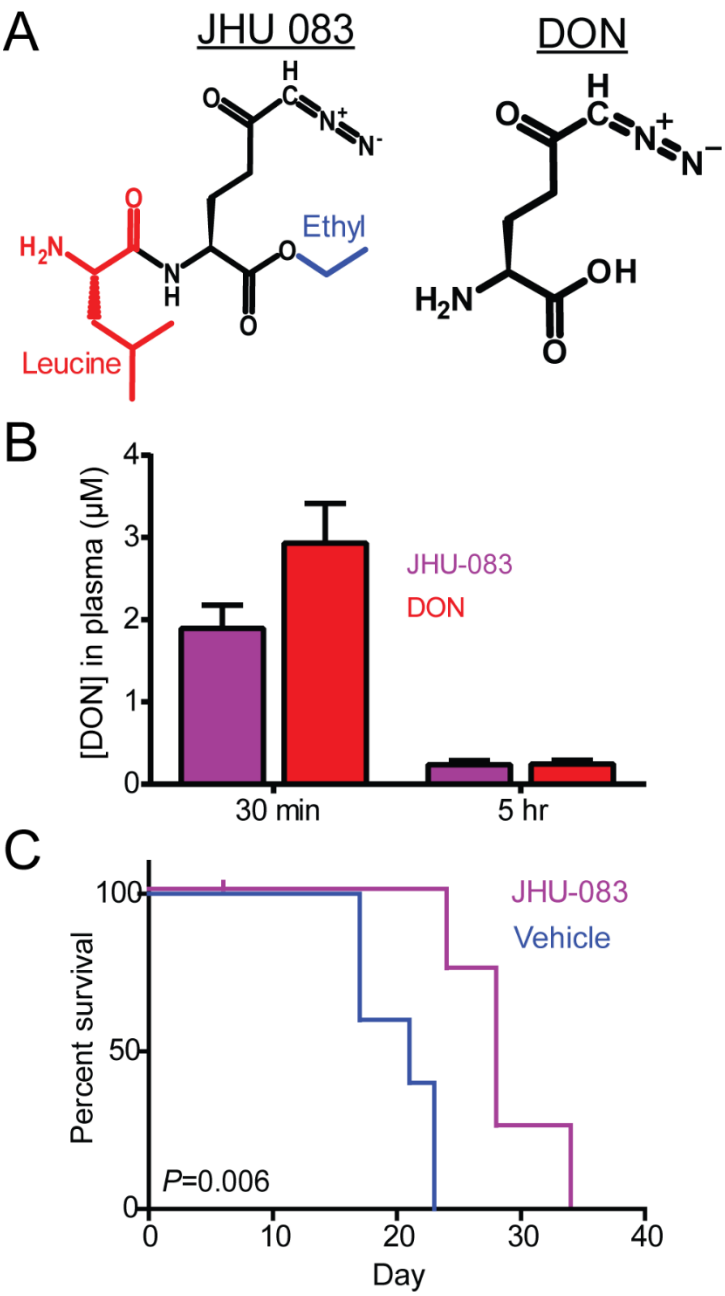

Figure 14: The DON pro-drug JHU-083 increases survival in mice with D425Med orthotopic xenografts

A) The chemical structures of JHU-083 and DON. B) JHU-083 delivers DON to the plasma with a reduced C_{max}. C) Treatment with 20mg/kg JHU-083 (DON equivalent dose) 3x week significantly improved the survival of mice with D425Med orthotopic xenografts (*P=0.006 by Log-rank test).

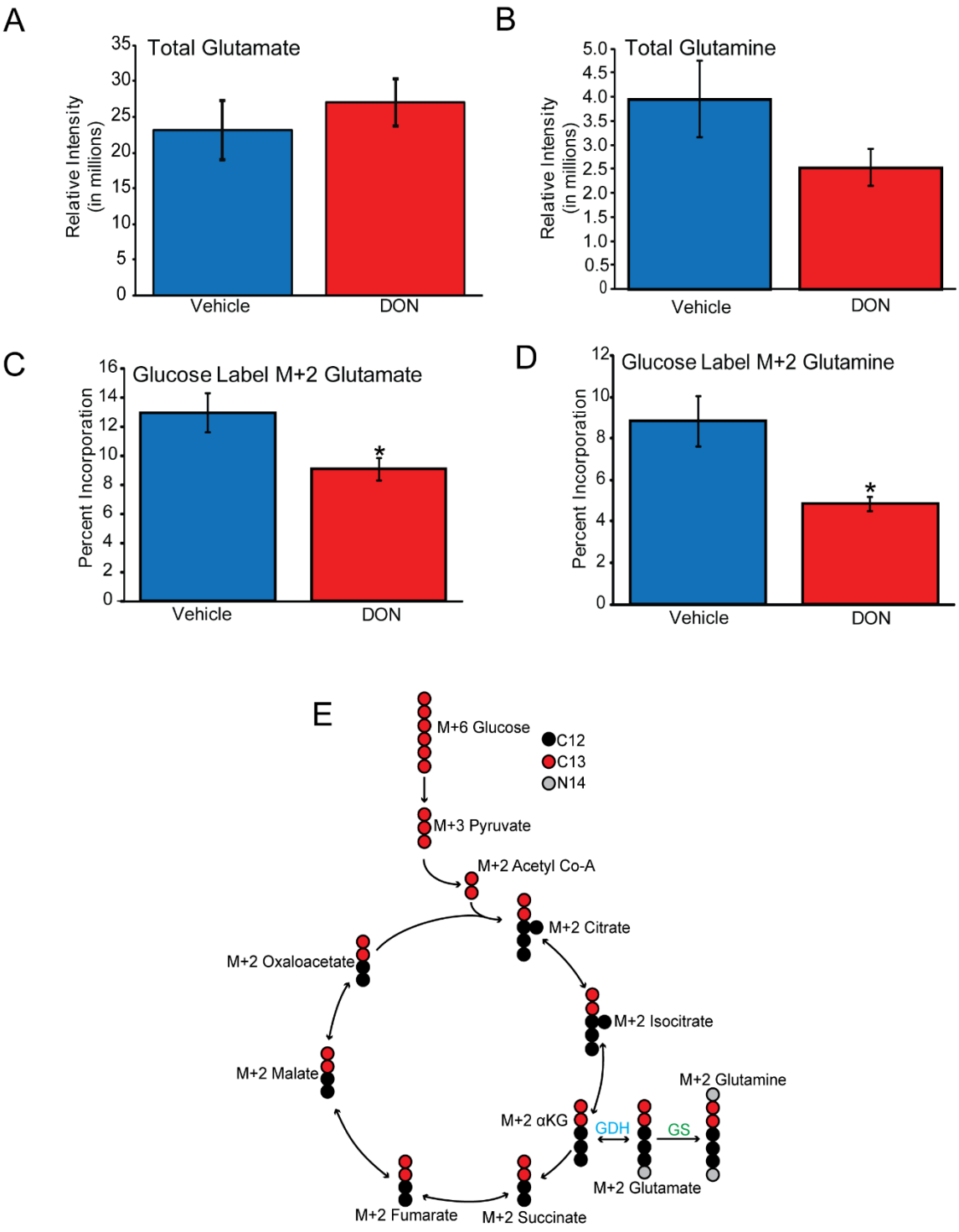

Figure 15: DON inhibits glutamine synthetase

A) DON treatment did not reduce the total amount of glutamate in D425Med tumors (n=16 vehicle tumors, n=19 DON tumors). B) Tumors from animals treated with DON had lower levels of glutamine compared to tumors from vehicle treated animals. (n=16

vehicle tumors, n=19 DON tumors). C, D) Stable isotope metabolomics revealed that DON treated tumors had significantly lower amounts of the glutamate M+2 and glutamine M+2 isotoplogues than vehicle treated tumors (*P<0.00007, by Student's t-test). For C and D animals were labeled with $^{13}C_6$-glucose (uniformly labeled glucose). Reduction in M+2 glutamate and glutamine suggests that DON is inhibiting of glutamine synthetase. (n=4 vehicle tumors, n=8 DON tumors) E) Simplified diagram of a single turn of the TCA cycle and the resulting isotopologues when uniformly $^{13}C_6$-glucose is injected into the system. Glutamate dehydrogenase (GDH) is in blue. Glutamine synthetase (GS) is indicated in green.

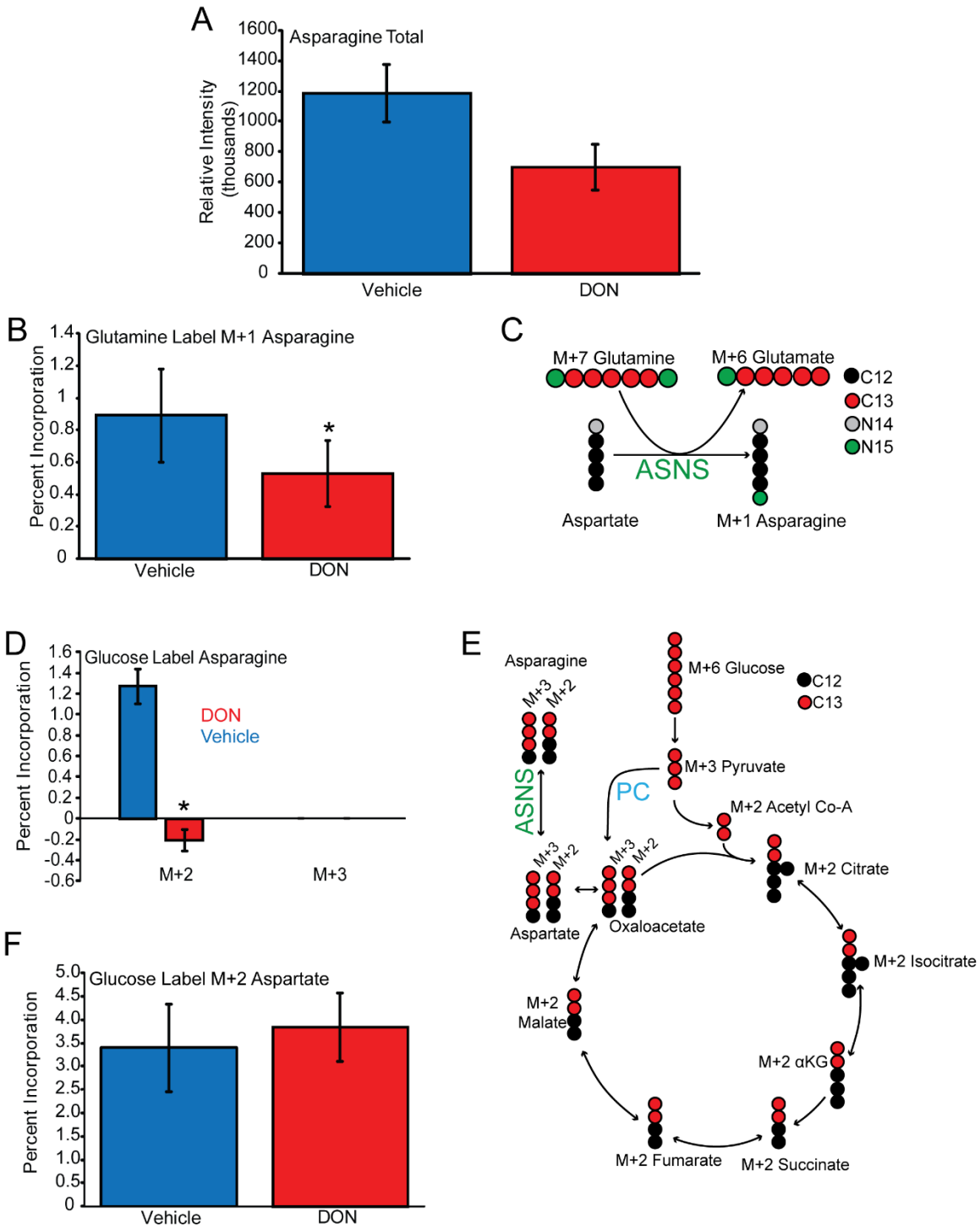

Figure 16: DON inhibits asparagine synthetase

A) D425Med tumors from animals treated with DON have less asparagine than tumors from vehicle treated animals. (n=16 vehicle tumors, n=19 DON tumors). B) M+1 asparagine levels in DON treated tumors are significantly lower than tumors from vehicle treated animals. (*P=0.016 by Student's T-test). Animals in this experiment were

injected with $^{13}C_6$-$^{14}N_2$-glutamine. (n=8 vehicle tumors, n=8 DON tumors). C) Diagram showing how M+1 asparagine is synthesized by asparaginase (ASNS) adding a ^{14}N from $^{13}C_6$-$^{14}N_2$-glutamine to aspartate. D) In $^{13}C_6$-glucose labeled tumors, those treated with DON had significantly lower levels of M+2 asparagine than vehicle treated tumors (*P=3.7x10^{-9} by Student's t-test). M+3 asparagine was not detected. (n=4 vehicle tumors n=8 DON tumors). E) Simplified diagram of the TCA cycle when the system is injected with $^{13}C_6$-glucose. M+2 asparagine is synthesized by M+2 acetyl CoA entering the TCA cycle and being converted to M+2 oxaloacetate, then M+2 aspartate and finally M+2 asparagine by asparagine synthetase (ASNS, green). M+3 asparagine is generated by the activity of pyruvate carboxylase (PC, blue) converting M+3 pyruvate to M+3 oxaloacetate then M+3 aspartate then finally M+3 asparagine. As no M+3 asparagine was detected (D), D425Med tumors likely have little pyruvate carboxylate activity. F) In $^{13}C_6$-glucose labeled tumors there was no difference in M+2 aspartate levels in tumors from DON vs vehicle treated mice (*P=0.40 by Student's t-test) suggesting that DON inhibits ASNS. (n=4 vehicle tumors, n=8 DON tumors).

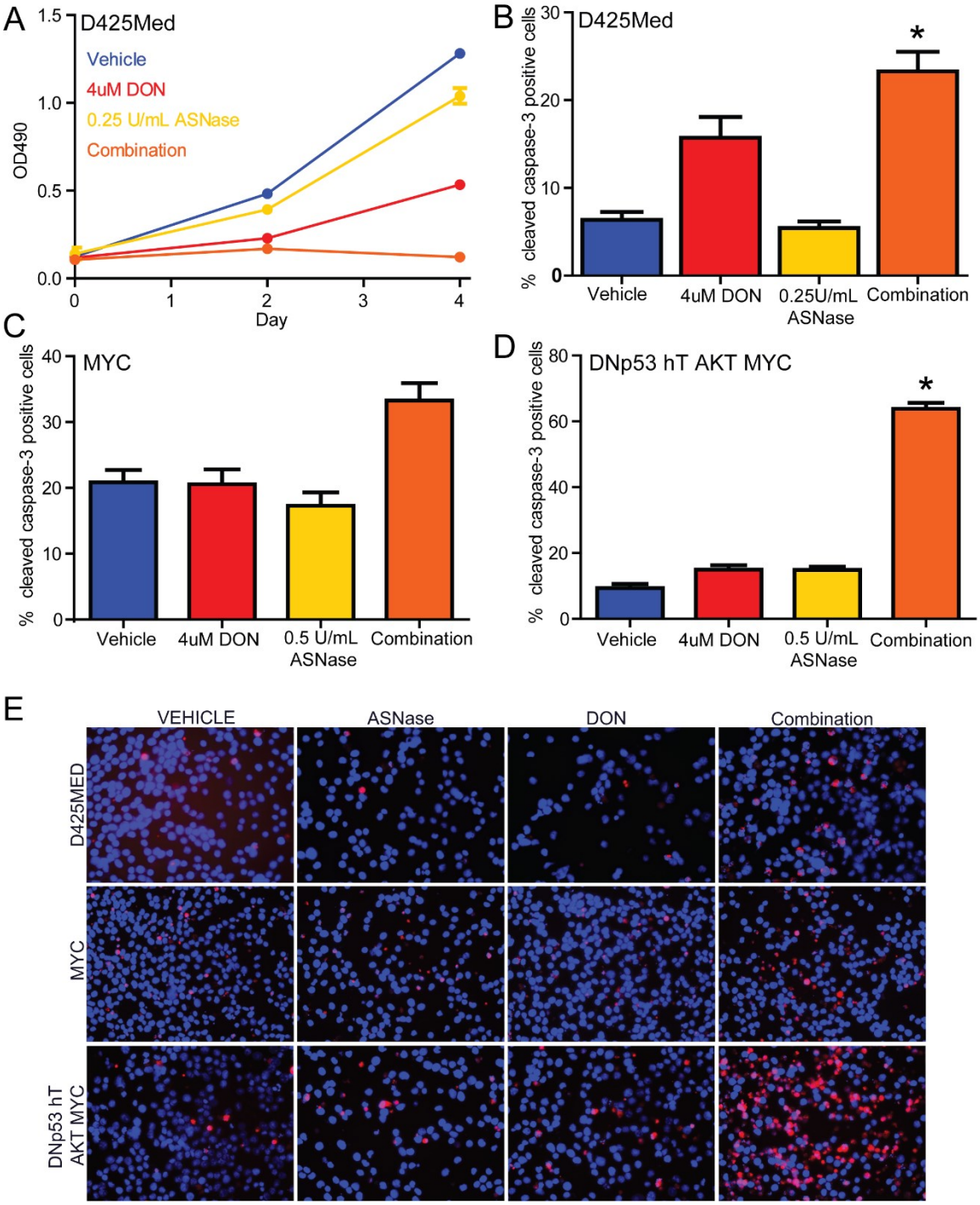

Figure 17: DON and ASNase in combination are more effective at killing medulloblastoma cells than either drug alone.

A) The growth of D425Med cells was slightly decreased by growth in 0.25 U/mL ASNase and partially decreased by growth in 4uM DON. Growth was completely inhibited by the combination of 4uM DON and 0.25 U/mL. B) The combination of 4uM

DON and 0.25 U/mL ASNase increased the percentage of cleaved caspase-3 positive cells more than either drug alone as measured by cleaved caspase-3 immunofluorescence. Bars show means and SEM. (*P<0.05 by Student's t-test. n=3 biological replicates). C, D) The combination of 4uM DON and 0.5 U/mL ASNase increased the percentage of cleaved caspase-3 positive cells more than either drug alone. Bars show mean and SEM (*P<0.05 by Student's t-test. n=3 biological replicates). E) Representative images. D425Med cells were grown in 0.25 U/mL ASNase, while human neural stem cells transformed with MYC or DNp53 hT AKT MYC were grown in 0.5 U/mL ASNase. Cells positive for cleaved caspase-3 are red. All cells were counterstained with DAPI (blue).

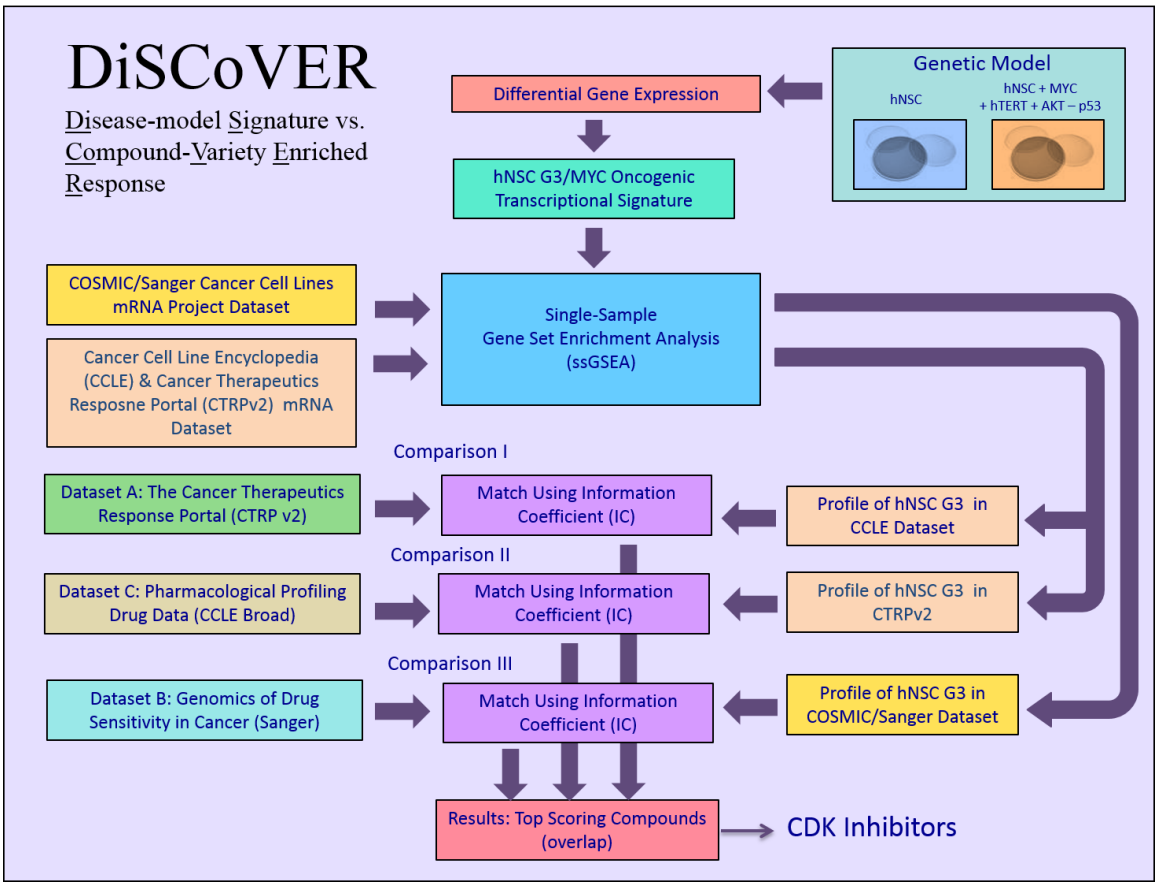

Figure 18: Detailed diagram of the DiSCoVER method

Schematic diagram showing the main analysis components and datasets that are part of the DisCoVER method. Note that there are only two mRNA datasets asthe CCLE and the CTRP v2 share the same mRNA samples.

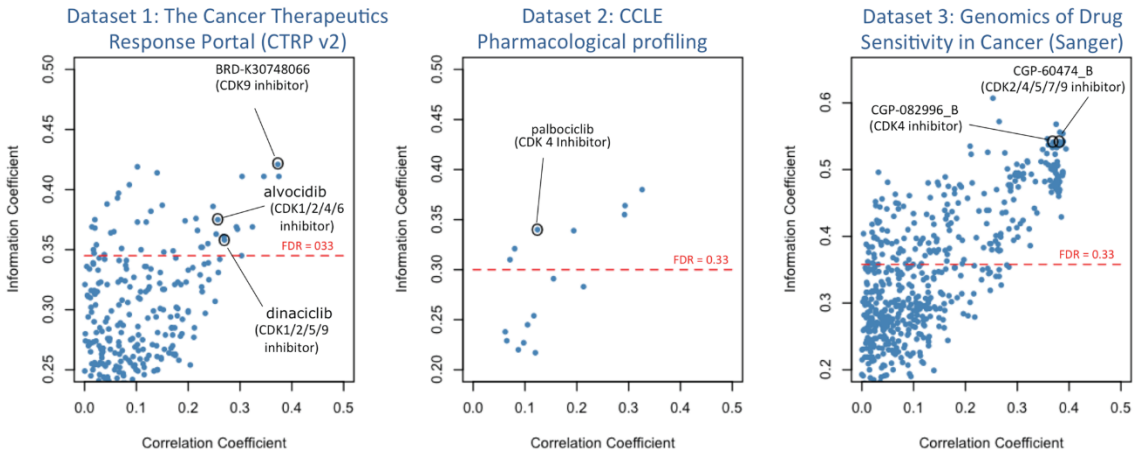

Figure 19: Top scoring compounds from each of the signature vs drug sensitivity comaprisons.

Top scoring compounds from each of the 3 signature vs. drug sensitivity comparisons. The y-axis is the Information coefficient (IC) and the x-axis the correlation coefficient. As can be seen in the Figure the CDK inhibitors are top hits in the 3 drug sensitivity datasets. The different scores in the x- and y-axis (correlation vs. information coefficients) are useful to appreciate how much of the relationship between the signature and a given drug is driven by a linear or non-linear correlation.

CURRICULUM VITAE

Contact Info

Home	Institutional
(949) 412-9643	(410) 502-5157
3021 N Calvert St, Apt 3	400 N Broadway, Smith 4001N
Baltimore MD 21218	Baltimore MD 21287
allison.hanaford@gmail.com	ahanaford@jhmi.edu

Education

2011-Present	John Hopkins School of Medicine, Pathobiology Graduate Program, Baltimore, MD, PhD (anticipated 2017)
2006-2011	California State University Fullerton (CSUF), BS Biological Science, Minor in Music, *Summa cum laude* and University Honors, (June 2011)

Awards and Honors

2016	Oral Presentation Award, Pathobiology Program Retreat, Johns Hopkins School of Medicine
2016	Scholar-in-Training Award, American Brain Tumor Association and American Association of Cancer Research
2016	Award for Excellence in Translational Research, Pathology Young Investigators Day, Johns Hopkins
2015	Award for Excellence in Translational Research, Pathology Young Investigators Day, Johns Hopkins
2014	Women in Cancer Research Scholar Award, American Association of Cancer Research
2014	Award for Excellence in Translational Research, Pathology Young Investigators Day, Johns Hopkins
2013	Award for Excellence in Translational Research, Pathology Young Investigators Day, Johns Hopkins
2012	Poster Award, Pathobiology Program Retreat, Johns Hopkins
2006-2011	Dean's List, CSUF
2008	General Chemistry Award, Chemistry Department, CSUF
2008	Merit Award, National Society of Collegiate Scholars

2008	Jewel Plummer Cobb Scholarship, College of Natural Sciences and Mathematics, CSUF
2006	President's Scholar, full tuition scholarship, highest award given to incoming freshmen in the California State University

Research Experience

2012-present	Johns Hopkins School of Medicine, Baltimore MD Mentors: Dr. Charles Eberhart and Dr. Eric Raabe Project: Developing genetically accurate models and investigating therapeutic modalities for aggressive medulloblastoma
2012	Johns Hopkins School of Medicine, Baltimore MD Mentor: Dr. Sanjay Jain Project: Gene expression profiling of the *Mycobacterium tuberculosis* PknD mutant following human brain microvascular endothelial cell invasion
2011	Johns Hopkins School of Medicine, Baltimore MD Mentor: Dr. Lee Martin Project: Adult onset neuro-degenerative disease genes and neonatal brain injury
2010	The Jackson Laboratory Summer Student Program, Bar Harbor ME Mentor: Leona Gagnon and Dr. Kenneth Johnson Project: Mapping and pathology of mouse mutations causing hearing loss

Publications

Hanaford AR, Archer TC, Price A, Kahlert UD, et al. DiSCoVERing innovative therapies for rare tumors: combining genetically accurate disease models with *in silico* analysis to identify novel therapeutic targets. Clin Cancer Res. 2016 Aug 22 (15): 3903-14.

Asnaghi L, Tripathy A, Yang Q, Kaur H, Hanaford A, Yu W, and Eberhart CG. Targeting Notch signaling as a novel therapy for retinoblastoma. Onocotarget. 2016 Oct 25 (43): 70028-44.

Suwala AK. Hanaford AR., Kahlert UD, Maciaczyk J. Clipping the wings of Glioblastoma: Modulation of WNT as a novel therapeutic strategy. J Neuropathol Exp Neurol. 2016 May 75 (5): 388-96

Martin, LJ, Samantha S, Hanaford A, Wong M. The mitochondrial permeability transition pore regulates Parkinson's disease development in mutant α-synuclein transgenic mice. Neurobiol Aging. 2013; 35(5):1132-52.

Patents and Inventions

61773189 "TARGETING GLUTAMINE METABOLISM IN BRAIN TUMORS." Initial patent application filed March 6, 2013; updated patent filed 3/6/2014; submitted for US patent protection 9/6/2015

Platform Presentations

2016	CNS Anticancer Drug Discovery and Development Conference, Scottsdale, AZ	Prodrugs of 6-diazo-5-oxo-norleucine improve oral absorption and brain penetration and demonstrate efficacy against orthotopic brain tumor xenografts
2016	17th International Symposium on Pediatric Neuro-oncology, Liverpool, UK	DiSCoVERing innovative therapies for medulloblastoma: combining genetically accurate disease models with *in silico* analysis to identify novel therapeutic targets.
2015	Pediatric Neuro-oncology Basic and Translational Research Conference, San Diego, CA	Pathway analysis of a human neural stem cell model of aggressive medulloblastoma reveals CDK inhibition as a potential therapeutic modality
2014	16th Internal Symposium on Pediatric Neuro-oncology, Singapore	Targeting Glutamine metabolism as a therapeutic strategy in MYC-driven medulloblastoma
2013	Pediatric Neuro-oncology Basic and Translational Research Conference, Ft Lauderdale, FL	A human neural stem cell model of medulloblastoma reveals glutamine metabolism as a potential therapeutic target

Other Oral Presentations

2016	Pathobiology Program Retreat, Johns Hopkins School of Medicine, Baltimore MD	DiSCoVERing innovative therapies: Combining genetically accurate disease models of medulloblastoma with advanced *in silico* analysis to identify novel therapeutic targets
2016	Brain Tumor Group Meeting, Johns Hopkins School of Medicine, Baltimore MD	DiSCoVERing innovative therapies: Combining genetically accurate disease models of medulloblastoma with advanced *in silico* analysis to identify novel therapeutic targets

2015	Society for Neuro-oncology Neuro-Tumor Club Dinner, American Association for Cancer Research, Annual Meeting 2015, Philadelphia PA	Pathway analysis of a human neural stem cell model of aggressive medulloblastoma reveals CDK inhibition as a potential therapeutic modality
2013	Society for Neuro-oncology Neuro-Tumor Club Dinner, American Association for Cancer Research Annual Meeting 2013, Washington DC	A human neural stem cell model of medulloblastoma reveals glutamine metabolism as a potential therapeutic target
2013	Pathology Grand Rounds, Johns Hopkins School of Medicine, Baltimore MD	A human neural stem cell model of medulloblastoma reveals glutamine metabolism as a potential therapeutic target
2013	Neuropathology Division Monthly Seminar, Johns Hopkins School of Medicine, Baltimore MD	Glutamine metabolism as a potential therapeutic target for treating MYC-driven medulloblastoma

Poster Presentations

2016	American Association for Cancer Research Annual Meeting 2016, New Orleans, LA	DiSCoVERing innovative therapies for rare tumors: combining genetically accurate disease models with *in silico* analysis to identify novel therapeutic targets
2016	Pathology Young Investigator's Day, Johns Hopkins School of Medicine, Baltimore MD	DiSCoVERing innovative therapies for rare tumors: combining genetically accurate disease models with *in silico* analysis to identify novel therapeutic targets
2015	Pathobiology Program Retreat, Johns Hopkins School of Medicine, Baltimore MD	Pathway analysis of a human neural stem cell model of medulloblastoma reveals CDK inhibition as a potential therapeutic modality
2015	Pathology Young Investigator's Day, Johns Hopkins School of Medicine, Baltimore MD	Pathway analysis of a human neural stem cell model of aggressive medulloblastoma reveals CDK inhibition as a potential therapeutic modality

2015	American Association for Cancer Research Annual Meeting 2015, Philadelphia, PA	Glutamine metabolic inhibitors suppress growth and tumorigenicity in MYC and MYCN-driven pediatric malignancies
2014	Pathology Young Investigator's Day, Johns Hopkins School of Medicine	Targeting Glutamine metabolism as a therapeutic strategy in MYC-driven medulloblastoma
2014	American Association for Cancer Research Annual Meeting 2014, San Diego, CA	Targeting Glutamine metabolism as a therapeutic strategy in MYC-driven medulloblastoma
2013	Pathobiology Program Retreat, Johns Hopkins School of Medicine, Baltimore MD	Targeting MYC-driven medulloblastoma using inhibitors of glutamine metabolism
2013	Pathology Young Investigator's Day, Johns Hopkins School of Medicine, Baltimore MD	Targeting MYC-driven medulloblastoma using inhibitors of glutamine metabolism
2013	American Association for Cancer Research Annual Meeting 2013, Washington DC	Targeting MYC-driven medulloblastoma using inhibitors of glutamine metabolism

Teaching Experience

2012-2016	Teaching Assistant	Introduction to Biomedical Sciences, Bloomberg School of Public Health
2012, 2014	Teaching Assistant	Pathology: Basic Mechanisms, Johns Hopkins School of Medicine

Leadership Experience

2013-2014	Chief Graduate Student	Pathobiology Program, Johns Hopkins School of Medicine, Baltimore MD
2015-present	Vice President, Membership	Baltimore Alumnae Chapter, Sigma Alpha Iota International Music Fraternity, Baltimore MD
2013-2014	Vice President, Ritual	Baltimore Alumnae Chapter, Sigma Alpha Iota International Music Fraternity, Baltimore MD
2007-2011	Treasurer	Lambda Chi Chapter, Sigma Alpha Iota International Music Fraternity, CSUF, Fullerton CA

Society Memberships
American Association of Cancer Research
Phi Kappa Phi
National Society of Collegiate Scholars
Golden Key International Honors Society